Fuzzy Logic Controlled Single - Stage Converter for Lithium-ion Battery Charger

By

AMMAR ISSA ISMAEL

A Dissertation Submitted in Partial Fulfillment of the Requirement
for the Degree of Master of Electrical Engineering
College of Graduate Studies
Universiti Tenaga Nasional

AUGUST 2013

DECLARATION

I hereby declare that this dissertation, submitted to Universiti Tenaga Nasional as a partial fulfillment of the requirement for the degree of Master of Electrical Engineering has not been submitted as exercise for a similar degree at any other university. I also certify that the work described here is my own except for excerpts and summaries whose sources are cited in the references.

This dissertation may be made available within the university library and may be photocopied or loaned to other libraries for the purpose of consultation.

15 JULY 2013 AMMAR ISSA ISMAEL

ABSTRACT

Recently, people are moving towards the use of electric vehicle transport compared to ordinary fuel consuming transportation. This is due to the increasing awareness to reduce the greenhouse gas emission generated from ordinary transportations. The main part of an electric vehicle is the battery and this battery requires charging as opposed to refueling in ordinary vehicles. Therefore, a home unit charger is important to make EV applicable at all places which have AC single phase electrical points. Typical Li-ion battery chargers consists of a two-stages converter topology, however this dissertation proposes a Lithium-ion battery charger for an electrical vehicle constructed from a single stage boost converter topology, namely a phase shift semi-bridgeless boost converter. The controller for the converter is designed using Sugeno fuzzy logic technique to manage the charging of a Lithium-ion battery load (dynamic load) depending on the battery state of charge to achieve constant current (CC) constant voltage (CV) charging strategy. The results presented in this thesis shows that the designed fuzzy logic controllers for the chosen single-stage converter topology is suitable for 400 V applications with low current ripple and it is capable of charging the lithium ion battery from 220 V until fully charged at 422 V. The designed battery charging system is ideally suited for automotive level I normal charging applications.

DEDICATION

To my parent, thank you for your unconditional support with my studies. I am honored to have you as my parent

To my beloved wife, who always has hidden strength and radiant beauty that has always been there through the hard times.

To my brothers and sisters, thank you for believing in me; for allowing me to further my studies. Please do not ever doubt my dedication and love for you.

ACKNOWLEDGMENT

All praises to Almighty ALLAH for his Divine Guidance and help towards completing this dissertation successfully. Our utmost respect to his last prophet Mohammad (peace and blessings of ALLAH be upon him) who was sent by ALLAH to be a great teacher of human kind.

I would like to this opportunity to thank my Supervisor Dr. **Ungku Anisa Bt. Ungku Amirulddin Al Amin** for guiding me throughout this Dissertation. It was an amazing learning experience to work under her guidance and also leads me in a positive attitude in my daily life.

I am also heartily thankful to my teacher, Dr. Mahmoud A A Younis, for his encouragement, guidance and support when I started my thesis.

Also I would like to thank Professor **Saad Mekhilef** and Madam **Sabarina Jaafar,** their emphasis on minute details have been instrumental in successfully completing this study. Their passion, patience, diligence and wisdom always influenced me from the past to the future..

I cannot find words to express my gratitude and love to my mother and my father. Words won't be enough to thank my mother for her inseparable support and prayers. May ALLAH keep her always under mercy. The mercy and Paradise with the prophet Mohammad to my father.

I want to thank my wife, who always supported me and encouraged me and she stood with me until I completed my study successfully. I'd like to thank my brothers and sisters for their unconditional love and support. I realize how lucky I am to have them. And I want thank my friends Khalid G. Mohammed and Yassen Mustafa Ahmed that they support me.

TABLE OF CONTENTS

LIST OF TABLES

LIST OF FIGURES

LIST OF ABBREVIATIONS

Ah	Ampere Hour
AIS	Automotive India Standards
ARAI	Automotive Research Association of India
ASDs	Adjustable-Speed Drives
BLIL	Bridgeless Interleaved Boost Topology
BMS	Battery Management System
BPNN	Back-Propagation Neural Network
CC	Constant Current
CO_2	Carbon Dioxide
CV	Constant Voltage
D	Duty Cycle
EV	Electrical Vehicle
fs	Frequency Sample
FLC	Fuzzy Logic Control
GHG	Global Greenhouse Gas
HN	High Negative
HP	High Positive
Li-ion	Lithium ion
LOLIMOT	Locally Linear Model Tree
N	Negative
NiMH	Nickel Metal Hydride
P	Positive
PFC	Power Factor Correction
PHEV	Plug-in Hybrid Electrical Vehicle
PWM	Pule Width Modulation
RL	Restive Load
RMS	Root Mean Square
SMPSs	Switch-Mode Power Supplies
SOC	State of Charge
SOH	State-of-Health

UPSs	Uninterrupted Power Supplies
Vin	Input Voltage
Vo	Output Voltage
ZCS	Zero Current Source
ZEBRA	Zero Emissions Batteries Research Activity
ZVS	Zero Voltage Source

CHAPTER 1

INTRODUCTION

1.1 Introduction

The greenhouse gas emission is the largest problem facing the world and greatly affects humans, animals and plants. One of the solutions to reduce CO_2 emission is through the use of electrical vehicles and plug-in hybrid electric vehicles. The electric vehicle is an optimum solution for urban mobility as it emits no exhaust fumes. Particularly in cities and in adverse climatic conditions, traffic-generated emissions are degrading air quality up to the point where the physical health of the population is directly threatened. Several cities have already had to apply repeatedly drastic traffic restrictions. The electric vehicle is also ideally suited to be integrated into new traffic management concepts, such as automatic rent-a-car systems and goods distribution centers, or small buses for city-center services. For all these reasons, an increasing number of cities and environmentally concerned companies have introduced electric vehicles in their fleets. Today, there is a clear necessity to generalize the support organized at the European level preparing so the step towards hydrogen electric vehicles[1].

For electric vehicle durability, storage remains a key point. The development of alternative battery systems shows the possibility of making a real technical and economic breakthrough in a short or medium term, consistent with an important market development. New battery types such as high-temperature batteries, Nickel-metal hydride (NiMH) batteries, and lithium-based (Li) batteries are already in the market or will be available in the coming years. Due to the high energy density (70 W h/kg for NiMH and 125 W h/kg for Li compared to 40 W h/kg for lead (Pb) and 60 W h/kg for Nickel Cadmium (NiCd)), NiMH and Li batteries will offer unprecedented

vehicle ranges, up to 250 km and even much more through the introduction of range extenders [1].

The more effective approach is valid for the design of the battery charger for which two charging situations can occur: normal charging conditions and residential charging. The time share between these two working conditions has surely an important impact on the resulting efficiency and the charger electronics will have to be designed accordingly, as well as the instrumentation and control hardware and software. No good electric vehicle can be developed without considering these working conditions. Many examples of wrong designs have been put on the road in the past. It is to be observed that an intelligent use of charging period on the mains can lead to substantial energy economy and CO_2 emission reduction without creating the necessity of implementing a large and costly new infrastructure for electricity transportation. Electric vehicles can be charged at night, when the main sources of electricity production are the base stations, which are different from the ‘‘average’’ power station, the latter also including old power plants and peak units. Furthermore the required additional electricity is small in comparison with the current use of electricity. For example, if 10% of the 5 million Belgian vehicles would be electric cars an additional electricity consumption of 1100 GW h is required on a total of 80,000 GW h (1.375%) [1]. The controller is very vital and important part in the charging system that provides easy and safety charging for the battery, there are many types of controller like PI, PID controller and also modern as controller fuzzy logic controller [2].

1.2 Fuzzy Logic Control in Battery Charger

The battery equalization control predicting issues is very complicate; the control issues can be reduced by applying the fuzzy logic control technique, the fuzzy logic control technique is good for predicting the nonlinear behavior of battery equalization, because the fact that it has more

adaptableness, robustness, and well efficiency for a nonlinear control system [2]. The rules base collects the control rules that label the knowledge and experience of the battery equalization control in the fuzzy set. The complicated and unpredictable mathematical model of the battery cell is not required to describe the cell balancing system in the Fuzzy Logic Control (FLC) design method [3].

1.3 Problem Statement

The battery in an electrical vehicle is very expansive and is an important component of the vehicle. The process of charging the battery must consider many issues pertaining to the battery such as starting current, time, state of charge at the beginning of the charging process and over-charging voltage problem. There has been many converter topologies proposed by previous researchers to charge a battery, some being single stage, others two stages, with some including Power Factor Correction (PFC). The common structure of choice for the Plug-in Hybrid Electrical Vehicle (PHEV) and Electrical Vehicle (EV) lithium ion batteries chargers are two-stage converters with an AC to DC converter followed by a DC to DC converter [4, 5]. In this work proposed Sugeno fuzzy logic control for a single-stage converter to charge Li-ion battery is employed which leads to reduced size of the converter and increases the system's performance for inductive, resistive and battery load. The designed home unit charger can be employed for EV applications because the design can be in any place which has an AC single phase electrical point present such as in houses and places of work.

1.4 Project Objectives

The objectives of this research are to:

a. Investigate PI controller to control the operation of the battery charger (single stage) for Li-ion battery.

b. Design a fuzzy logic controller to control the operation of the battery charger (single stage) for Li-ion battery.
c. Comparison on the performance results of PI and fuzzy logic controller (over-current/over-voltage and transient time response).

1.5 Scope of Project

The scope of this dissertation is constrained by examining PI controller to control charging process of Li-ion battery, and then design Sugeno fuzzy logic to control the process of charger the single-stage AC to DC converter supplied from a single phase utility available at a home unit for an electrical vehicle with a Li-ion type battery being charged at night. Also comparing between results of the two types of controls are conventional control (PI) and fuzzy logic control.

1.6 Research Methodology

The research conducted started with a literature review on the common types of batteries employed in electric vehicles as well as their characteristics, in addition review of previous research on converter topologies employed for battery charging in particular for Li-ion batteries was also conducted. Once a suitable converter topology had been determined from the literature review then explanation on the working principle of the battery charger and the fuzzy-logic controller to manage the battery charging was performed. The design was simulated in Matlab to verify that the designed battery charging was able to charge a battery to the desired voltage under different initial battery state-of-charge conditions.

1.7 Outline of the Dissertation

This dissertation is divided into five chapters. The first chapter provides a general introduction on the project, fuzzy logic control in battery charger, the problem statement, project objectives, the scope of project, research methodology and outline of the desertion.

The second chapter will present the literature review conducted pertaining to the project with regards to the types of battery and methods of charging the electrical vehicle battery, including the Battery Management System (BMS). A review of battery charger topologies is also presented as well as previous research on the use of fuzzy-logic to control battery chargers.

Detailed description of the designed fuzzy logic controlled battery charger is presented in chapter three of this dissertation. This includes explanation on the principle work phase shifted semi-bridgeless boost topology, construction of the triangle signal used to compare with the output of the fuzzy logic controller to obtain the pulse width modulation (PWM) signal, as well as the construction of Sugeno fuzzy logic controllers to provide the duty cycle of the MOSFET switches of the converter. The simulation results of PI controller and Sugeno fuzzy logic system are then provided in chapter four. The results presented are based on simulation a Li-ion battery load.

Finally, chapter five of the dissertation will provide the conclusions of the project together with recommendation for future work.

CHAPTER 2

LITERATURE REVIEW

2.1 Introduction

This chapter has been divided into three main parts, which discusses the types of battery electric vehicles and management system of batteries, battery charger topologies, then application of fuzzy logic to control battery charging.

Of late, transportation sector is a huge consumer of fossil fuels, and this substantially leads to global greenhouse gas (GHG) emissions [6]. It is noteworthy that, at the year 2005, 15% of global GHG emissions was influenced by the transport sector, of which 73% was contributed by road transport [7]. Hence, there has been increased interest towards the use of electric vehicles (EV). EV requires charging as opposed to refueling in conventional vehicles. Majority of EV charging can happen at residences overnight, especially in the car shed, where the EV can be connected to a convenience outlet for Level I (slow) charging. Generally, level II charging is outlined as the principal approach for both, private and public services and needs a 240V outlet (see table 2.1 for summary of charging levels). Future developments in charging techniques target Level I; semi-fast charging presents enough power and can be applied in a lot of circumstances. Generally, single-phase methods are employed for Levels I and II. On the other hand, Level III and dc fast charging are designed for industrial and general public applications, for instance, three-phase solutions generally suitable for businesses such as filling stations. Stations for public most probably utilize Level II or III chargers set up in parking lots, shopping malls, resorts, rest area, cinemas, eateries, etc.

EV battery chargers are usually categorized as, on-board or off-board based on unidirectional or bidirectional power flow. Unidirectional charging is a rational initial phase, for its capability of, reducing hardware needs, simplifying the problems

associated with interconnection, and to minimizing battery deterioration. A bidirectional charging system facilitates charge from the grid, where the battery energy can be returned back to the grid, and power stabilizes with sufficient power conversion. Common on-board chargers restrict high power, due to the limitations of weight, space and cost; however, they can be incorporated with the electric drive to avoid these challenges. On-board charger systems could be conductive or inductive; the conductive charging systems employ immediate contact between the connector and charge inlet, on the other hand, an inductive charger magnetically transmits power. This type of charger has been investigated for 1st and 2nd levels, and may be fixed or moving. Nevertheless, an off-board battery charger is less restricted by size and weight [8].

AC–DC conversion of electric power has been extensively used for a number of purposes such as, Adjustable-Speed Drives (ASDs), switch-mode power supplies (SMPSs), Uninterrupted Power Supplies (UPSs), and battery energy storage. Generally, AC–DC converters, also referred to as rectifiers, are formulated making use of diodes and thyristors, to offer uncontrolled and controlled dc power, with unidirectional and bidirectional power flow. However, it has a few disadvantages, which includes inadequate quality of power due to injected current harmonics; voltage distortions, poor power factor at input ac that main have ripple dc output at load end, low efficiency so requires ac and dc filters of large size. Elimination of harmonic components with the resultant increase in power factor (PF) could be obtained by utilizing either passive or active power factor correction (PFC) methods [9]. It is essential for a reliable battery charger to perform efficiently, possess high power density with lower energy loss, low cost, small in volume and weight. Its operation is dependent on components such as: converters, power semiconductor devices, capacitors, inductors, thermal systems etc., as well as the employed control and switching strategies. Furthermore, a charger must be compatible with the voltage and current levels of each and every country, and fulfill Electromagnetic Interference (EMI), electromagnetic compatibility, and safety standards [10].

Table 2.1: Charging Power Levels [8]

Power Level Types	Charger Location	Typical Use	Energy Supply Interface	Expected Power Level	Charging Time	Vehicle Technology
Level 1 Opportunity 120 Vac (US) 230 Vac (EU)	On-board 1-phase	Charging at home or office	Convenience outlet	1.4kW(12A) 1.9kW(20A)	4–11 h 11–36 h	PHEVs (5-15kWh) EVs (16-50kWh)
Level 2 (Primary) 240 Vac (US) 400 Vac (EU)	On-board 1- or 3-phase	Charging at private or public outlets	Dedicated EVSE	4kW (17A) 8kW (32 A) 19.2kW(80A	1–4 h 2–6 h 2–3 h	PHEVs (5-15 kWh) EVs (16-30kWh) EVs (3-50kWh
Level 3 (Fast) (208-600 Vac or Vdc)	Off-board 3-phase	Commercial, analogous to a filling station	Dedicated EVSE	50kW 100kW	0.4–1 h 0.2–0.5h	EVs (20-50kWh)

2.2 Battery Electric Vehicles (BEV)

2.2.1 History

Thomas Davenport in 1834 was the pioneer in developing BEV; interestingly, many years before the introduction of the first ICE vehicle. Furthermore, the first vehicle to exceed the 100 km/h hurdle was also a battery vehicle called the 'Jamais Contente' in which Camille Jenatzy had the privilege of driving it in 1899[11]. As opposed to the ICE vehicles, the BEVs were convenient, silent and clean. Nevertheless, as a result of the limitations in energy storage capabilities of the battery, BEVs had very limited range, and consequently, the ICE was getting better and better significantly. This led to the BEV nearly disappearing by the 1930s [12]. Nevertheless, due to the energy turmoil and oil deficiency in the 1970s, car manufacturers and policy makers began to reconsider the BEV, as it presented high energy efficiency and helped in diversifying energy resources, along with possessing zero local emissions, which leads to enhanced quality of air in cities [13].

2.2.2 Batteries

A battery is an electrochemical cell (also known as a Galvanic cell), which converts chemical energy into electrical energy; it includes an anode and a cathode, which are segregated by an electrolyte; an ionic conductor or an electronically insulating medium. The anodes produce electrons, which flow towards the cathode by means of the external circuit, at the same time, electro-neutrality is guaranteed by ion transportation over the electrolyte [13].

Nickel metal hydride (NiMH) and Lithium-ion (Li-ion) are two primary types of batteries for BEVs; of which, in most cases the NiMH batteries have been used as secondary energy sources in HEVs (e.g. Toyota Prius)where the NiMH batteries are combined with an internal combustion engine (ICE). On the other hand, the Li-ion batteries have generally been used as primary energy sources in BEVs, such as the Nissan Leaf and Mitsubishi iMiev ; powered by 12 ×4 cells (48 modules), which provides a capacity of 24 kWh, and takes up to 8 hours to become fully charged from a standard domestic outlet from zero state-of-charge (SOC), or requires 30 minutes to fully charge from a 3-phase AC supply [13].

Table 2.2 Characteristics of various types of battery [14].

Battery chemistry	Type: primary (P)secondary (S)	Cell potential (ΔV)/V	specific energy/Whkg−1		Useful energy density/ WhI^{-1}
			Theoretical	practical	
Alkaline zinc manganese dioxide (Zn/MnO2)	p	1.5	358	145	400
Lithium iodine (Li/I2)	p	2.8	560	245	900
Alkaline nickel cadmium (NiCd)	S	1.3	244	35	100
Nickel metal hydride (NiMH)	S	1.3	240	75	240
Lead acid (Pd/A)	S	2.1	252	35	70
Sodium sulphur (Na/S)	S	2.1	792	170	345
Sodium nickel chloride (Na/NiCl2)	S	2.6	787	115	190
Lithium-ion (Li-ion)	S	4.1	410	180	400

2.2.3 Types of Batteries of Electrical Vehicle

Nowadays, there are five categories of batteries in the market, which are appropriate for different kinds of vehicles. Table 2.2 illustrates the various categories of batteries and their associated features. The most common type of battery used in typical ICE vehicles is lead–acid battery. Basically this type is preferred when weight is of lowest concern; however, this type is not eco-friendly, as it leads to ecological issues either during, production or disposal process [15].

On the other hand, the nickel battery, for instance, nickel–zinc is more eco-friendly but less durable due to its short lifespan as opposed to the lead–acid batteries. Furthermore, heavy weight is a major issue of nickel–iron batteries, followed by high maintenance cost, and high self-discharge rate. Due to its memory effect, the nickel–cadmium (Ni–Cd) battery is not ideal for high charge/discharge rate applications such as in automobiles; however, it is more effective under strenuous working circumstances. Furthermore, it also contains toxic materials, and incurs high maintenance cost. It is noteworthy that, the Nickel– metal hydride (Ni–MH) is also one of the eco-friendly batteries. Ni–MH batteries possess nearly 50% higher self-discharge, as against the Ni–Cd battery. The longer charging time is also another disadvantage of this battery, as opposed to the lead–acid and Ni–Cd batteries, and moreover it generates a huge amount of heat during charging. Subsequently, Ni–MH battery needs more sophisticated charging algorithm and costly chargers, in spite of it being most extensively used in EV [16].

Zero emissions batteries research activity (ZEBRA) battery is composed of sodium nickel chloride (NaNiCl) possessing high temperature capabilities of up to 300 to350^{o} C. This requires the use of high temperature technology for the purpose of sustaining appropriate efficient operations. Furthermore, ZEBRA batteries have less life-cycle-cost as against the lead–acid batteries [17]and it has benefits such as, greater or similar energy density as the lithium battery, cheapest cost of any contemporary EV battery technologies, greater calendar life, durability and fail-proof cells , tolerant to overcharge and over-discharge. On the other hand, the main disadvantage of this battery is it's 90W energy loss while not in use [18]. Lithium battery is one of significant battery extensively studied by researchers, which will be explained further in the next sub-section. The zinc-air battery is another appealing battery, which has higher specific energy, and higher energy density when compared to a lithium battery. On the other hand, the main drawbacks are this battery is its reduced specific power, limited cycle life, and bulkiness [16]. At present, the lithium air battery is still in the research stage, and is not yet marketed. As the lithium-air batteries have a higher energy density compared to the zinc air battery, it might become the target for use in all future EVs.

2.2.4 Lithium-ion (Li-ion) Batteries

Of late, most electronic gadgets, such as smart phones, digital tablets, laptops, and electric vehicles, such as E-bikes, use Lithium-ion (Li-ion) batteries, and in the near future it will be used in electric cars as well. However, the use of high-performance Li-ion batteries have also raised concerns due to serious safety -issues, particularly in mobile computers[19]. As the terminal voltage of lithium based cells is 80% to 300% greater as against other widely used batteries, the cells using lithium provide a much higher energy density, both, gravimetric and volumetric, when compared to other non-exotic, rechargeable battery chemistries. Even though the amp-hour capacity of the different lithium cells is equivalent to NiMH and NiCd, the energy density is a lot higher as a result of the higher terminal voltage. This feature is the cardinal acumen for the appearance of lithium based batteries in EVs, of late [20]. Li-ion batteries decidedly represent the better market allotment of batteries for BEVs. Therefore, this type of battery is the preferred option for BEVs in the short term. Also, in the mid-term and possibly long-term they are believed to play an important role in BEVs [6].

A lithium battery is an effective energy storage device because of its portability, high specific energy, high specific power and high energy density. Moreover, lithium batteries do not have memory effect and do not contain toxic metals, such as lead, mercury or cadmium. Each lithium battery requires a safety circuit in every pack so as to ensure safe operation. The primary drawback is that, lithium battery needs higher manufacturing expense as against NiCad and Ni–MH battery packs. As illustrated in Table 2.3, in the lithium group of batteries, lithium metal is the costliest, but significantly less secured as against lithium-ion battery. Presently, the lithium–sulphur battery may provide a greater energy capacity with minimal weight amongst the lithium group of batteries; however, cycle life is a main disadvantage. Lithium-ion polymer batteries can conform to an extensive range of packaging shaped, are reliable and durable, however, it has a poor conductivity and lower power density. Lithium–iron phosphate leads in terms of battery choices due to its higher power density compared to other lithium batteries; owing to its higher discharge current. On top of that, lithium–iron phosphate batteries have outstanding

thermal capabilities and chemical stability, which offers better protection features as against lithium-ion batteries. The lithium–titanate battery possesses the benefit of having faster charging potential, as against other lithium–ion batteries, which are presently used by Mitsubishi's i-MiEV electric vehicles [15].

Table 2.3: The comparison of energy storage specifications based on type of energy storage device [15]

	Energy storage Type	Specific energy (Wh/kg)	Energy density (Wh/L)	Specific power (W/kg)	Life cycle	Energy efficiency (%)	Production cost ($/kWh)
1	Lead acid battery						
	Lead acid	35	100	180	1000	>80	60
	Advance lead acid	45	-	250	1500	-	200
	Valve regulated lead acid(VRLA)	50	-	150+	700+	-	150
	Metal foil lead acid	30	-	900	500+	-	-
2	Nickel battery						
	Nickel–iron	50-60	60	100-150	2000	75	150-200
	Nickel–zinc	75	140	170-260	300	76	100-200
	Nickel–cadmium (Ni–Cd)	50-80	300	200	2000	75	250-300
	Nickel–metal hydride(Ni–MH)	70-95	180-220	200-300	<3000	70	200-250
3	ZEBRA battery						
	Sodium–sulfur	150-240	-	150-230	800+	80	250-450
	Sodium–nickel chloride	90-120	160	155	1200+	80	230-345
4	Lithium battery						
	Lithium–iron sulphide(FeS)	150	-	300	1000+	80	110
	Lithium–iron phosphate(LiF	120	220	2000-4500	>2000	-	350

	ePO$_4$)						
	Lithium–iron polymer(LiPo)	130-225	200-250	260-450	>1200	-	150
	Lithium–iron	118-250	200-400	200-430	2000	>95	150
	Lithium–titanate (LiTiO/NiMnO2)	80-100	-	4000	1800	-	2000
5	Metal-air battery						
	Aluminum-air	220	-	60	-	-	-
	Zinc-air	460	-	80-140	200	60	90-120
	Zink-refuelable	460	1400	-	-	-	-
	Lithium-air	1800	-	-	-	-	-

2.3 Battery Management System (BMS)

A large volume of studies have been conducted in the field of electric vehicles, particularly on battery management systems (BMS). Normally, BMS comprises of State-of-Charge (SOC), State-of-Health (SOH) and cell balancing for the maintenance of batteries. This system provides reliability as it is able to present instant information about the condition of the battery and its power capacity. In tandem with battery management system, the battery charger for the primary battery is also an essential component for BEV. It is necessary for the battery charger to efficiently charge the battery wirh minimum charging time, since extensively long charge time is regarded as the weak point of the EV. So as to charge the main battery for EV, it is essential to have the off-line battery charger, to be competent of higher power system for high power density battery [21]. As a result of their higher energy density, greater nominal voltage, and absence of memory impact, Li-ion cells perform a vital part in electric vehicle (EV) applications. However, if not accurately dealt with, this battery can experience drastic reduction in efficiency, and probably generate hazardous conditions. Battery management systems (BMSs) are a useful means to handle these battery packages and enhance their performance.

Over two decades ago the researchers have been engaged with investigations on charging equalization, whereby in 1998, Nasser H. Kutkut [22] proposed a method for equalizing a battery series utilizing a modular non-dissipative current diverter. As illustrated in Figure 2.1, the proposed system retains each pair of battery modules at the similar charge level by redirecting the extra energy from the overcharged module to the weaker module in a non-dissipative manner. The equalizers are overlapped to guarantee balancing for the entire battery series. As opposed to earlier systems, which are based on a multi-winding transformer structure, the new system could be effortlessly incorporated with a series of batteries, as a result of its modular characteristics, where each equalizer is associated with a couple of modules.

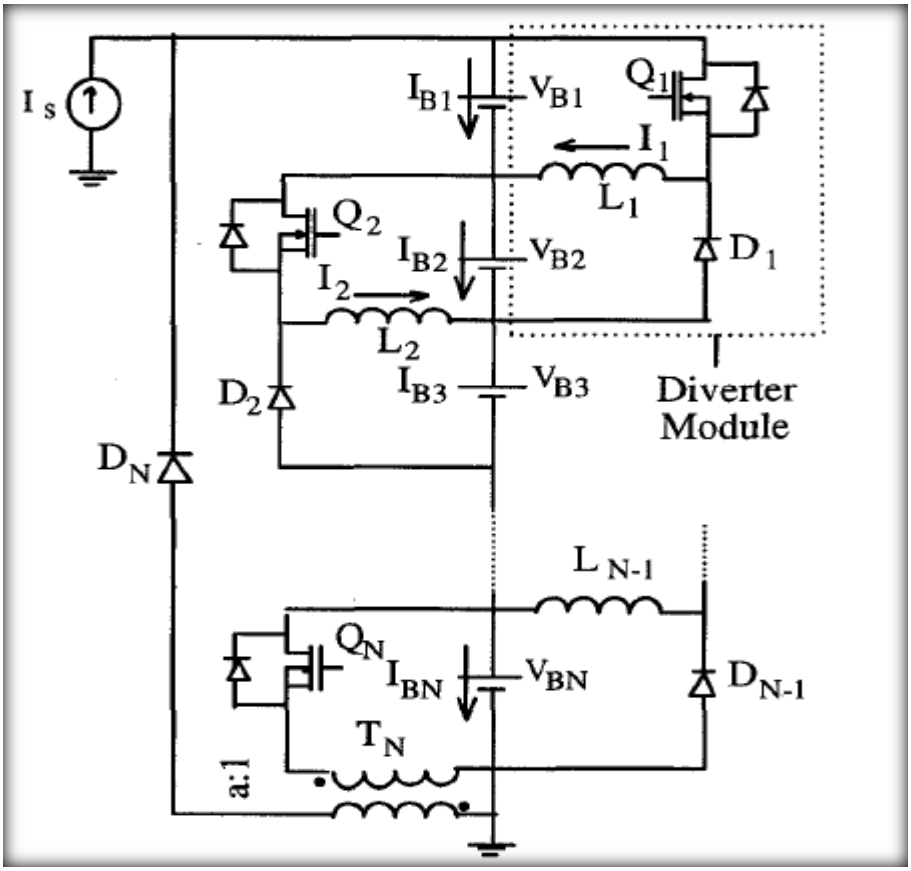

Figure 2.1: The proposed non dissipative current diverter structure [22]

Antonio Manenti et.al., [23] have proposed an novel BMS structure, which is specifically appropriate for light-EV applications, depending on the principle of redundant cell; namely a method that aggressively disconnects a cell in the battery pack for ideal balancing requirements. The suggested BMS is quite versatile, cost-effective, stable and space saving. Figure 2.2 illustrates the block diagram of the

proposed BMS structure, which comprises three main stages: the switch network, the data acquisition block, and the control unit. The switch network is the main part of the system, because it is crucial for both, security and performance concerns. Even though, at an initial glimpse, the structure and the operation modality of the circuit are basic (as seen in Figure 2.3), the setup exposed numerous challenging problems in the design layout and the management algorithm.

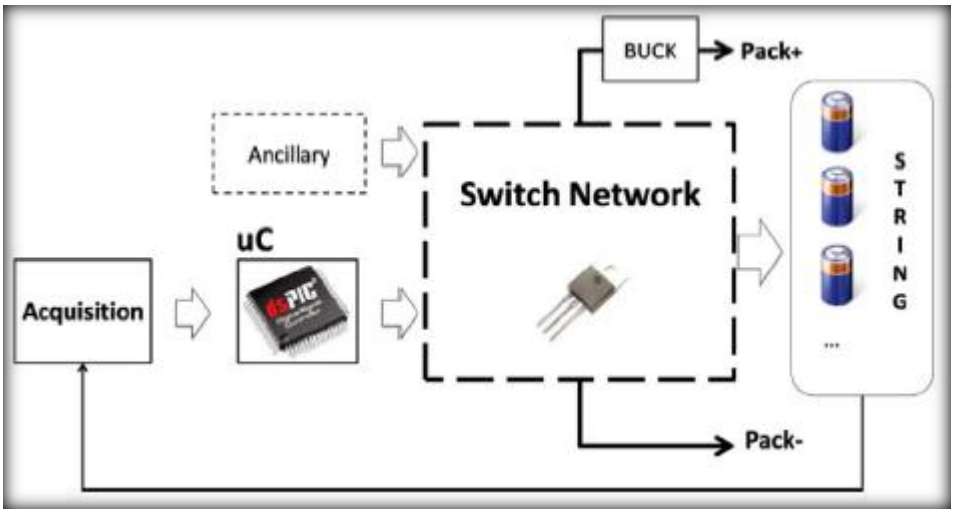

Figure 2.2: Block diagram of the proposed BMS architecture. The cores of the system are the data acquisition block ("Acquisition"), the control unit (the microcontroller "uC"), and the "Switch Network [23].

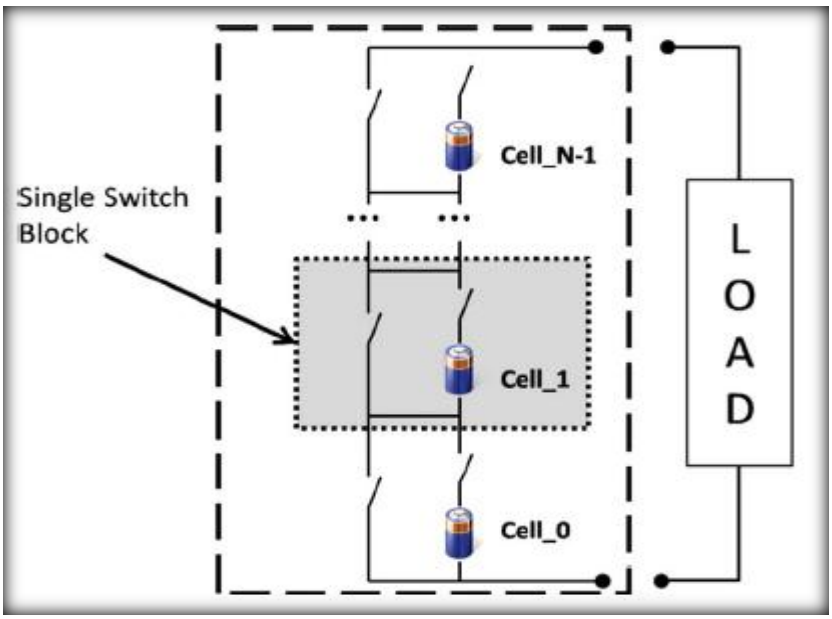

Figure 2.3: Basic representation of the switch network shown in Figure 2.2 [23]

Wu-Shun Jwo and Wei-Liang Chien [24] have proposed an equalization charger based on positive/negative pulse technology as illustrated in Figure 2.4. The positive pulse current is used to charge the entire battery strings while the negative pulse current will acquire some energy from the battery strings, which will be stored in the energy storage parts. Based on the energy distribution among the batteries, a transformer employs the energy from the energy storage parts to redistribute the energy in the batteries, which leads to the balance charging process. The proposed equalization charger comprises a DC-to-DC converter and a multi-winding transformer. This basic framework of the proposed equalization charger includes a straightforward circuitry, and hence becomes cost effective. The proposed equalization charger's performance was tested on a set of battery strings and was compared with a charging system without the equalization charger under the same operation conditions. The outcomes have revealed that the proposed equalization charger can accomplish the efficiency equalized charging presents a superior charging operation, and efficiently manages the temperature of the battery. This presents an efficient way to increase the life-span of battery strings. With the equalization charger, it is possible to charge batteries equally, increase the performance of batteries, and administer their increasing temperature, and extend the life of the battery string.

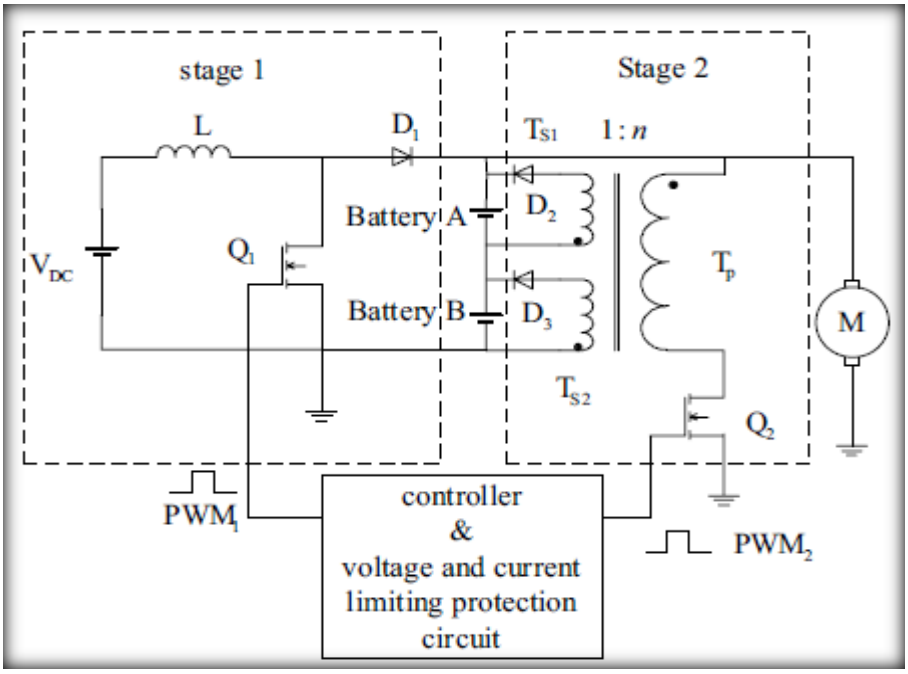

Figure 2.4: The equalization charger block diagram [24]

M. Brandl et.al., [25] have proposed an innovative BMS, which includes a built-in active charge equalizer. The battery system utilizes 96 serially connected Li-ion cells with the capacity of 50 Ah, for accomplishing the expected voltage level of up to 400 V. The cells are segregated into modules of four cells. The battery pack comprises of 24 modules, each of them comprising an electronic circuit for cell monitoring and control as shown in Figure 2.5.

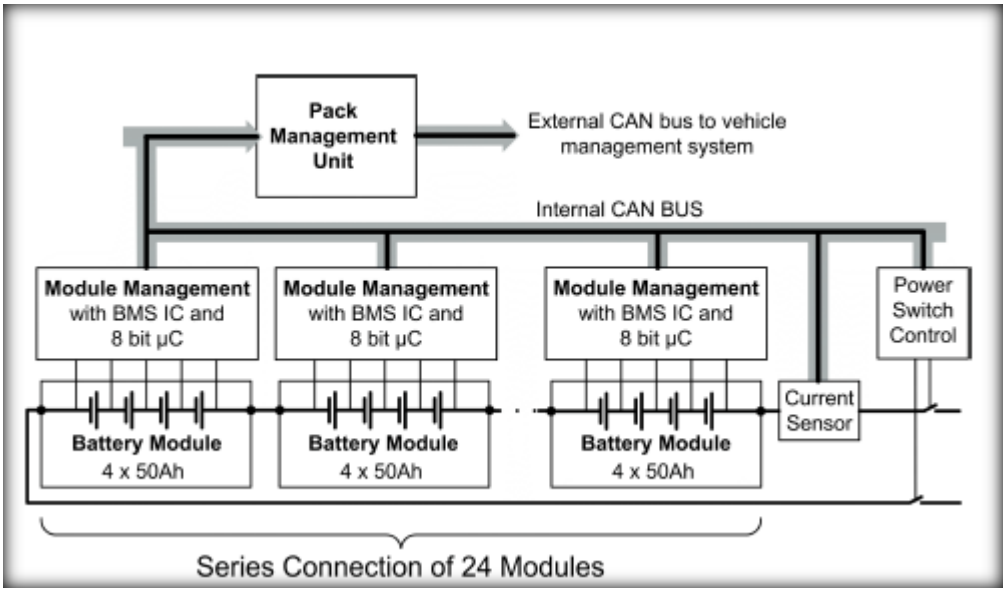

Figure 2.5: Battery system overview [25]

2.4 Battery Charger Topologies

There are two kinds of battery chargers for EV; off-board (stand-alone) and on-board (built-in) chargers. An on-board battery charger has to be lightweight, have high energy density, compact in size, and competent in delivering high power, with high efficiency to maximize the distance encompassed by the EV per charging. A range of power architectures, circuit topologies and control techniques have been developed for PHEV battery chargers. Nevertheless, as a result of large low frequency ripple in the output current, the single-stage AC-DC power conversion architecture was previously found to be ideal only for lead acid batteries. On the other hand, two-stage AC-DC/DC-DC power conversion offers built-in low frequency ripple rejection.

Consequently, the two-stage approach was recommended for PHEV battery chargers, where the power rating is comparatively higher, and lithium-ion batteries, which require low voltage ripple, are employed as the primary energy storage system [5]. Figure 2.6 illustrates a basic scheme of a universal input two-stage battery charger used for PHEVs [5].

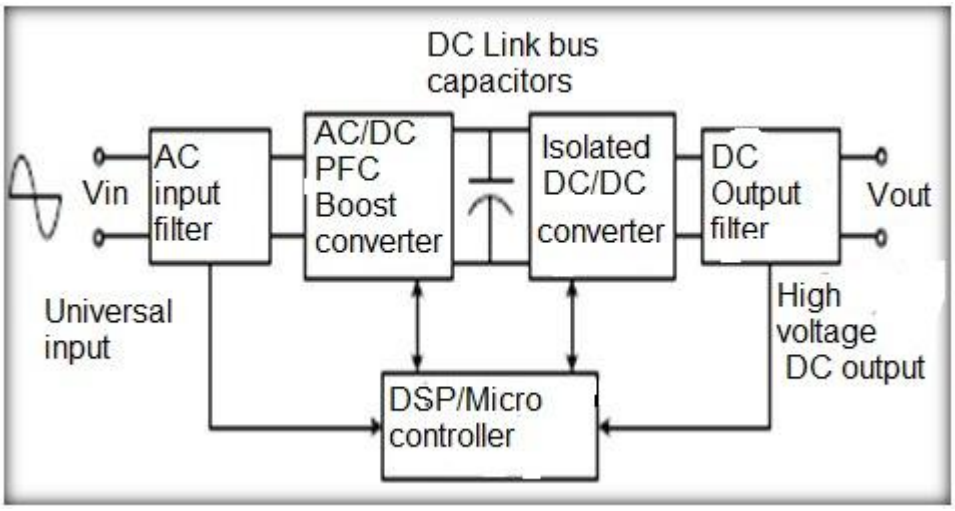

Figure 2.6: Simplified block diagram of a universal battery charger [5].

2.4.1 AC/DC Converter for Electrical Vehicle

2.4.1.1 Conventional Boost Converter

The most popular AC/DC converter topology used in PFC applications, is the conventional boost topology, which employs a dedicated diode bridge to rectify the AC input voltage to DC and complemented by the boost section as seen in Figure 2.7. In this topology, the output capacitor ripple current is very high and it represents the difference between the diode current and the dc output current. Moreover, when there is an increase in the power level, the diode bridge losses considerably reduces the converter's efficiency as shown in Figure 2.9, therefore, creating issues in managing the heat dissipation in limited area. Due to these restrictions, this topology is suitable for a low to medium power range up to approximately 1kW. For power levels higher than 1kW, generally, designers use parallel semiconductors which can deliver higher output power, moreover, the inductor volume also turns into a challenging design issue at high power [26].

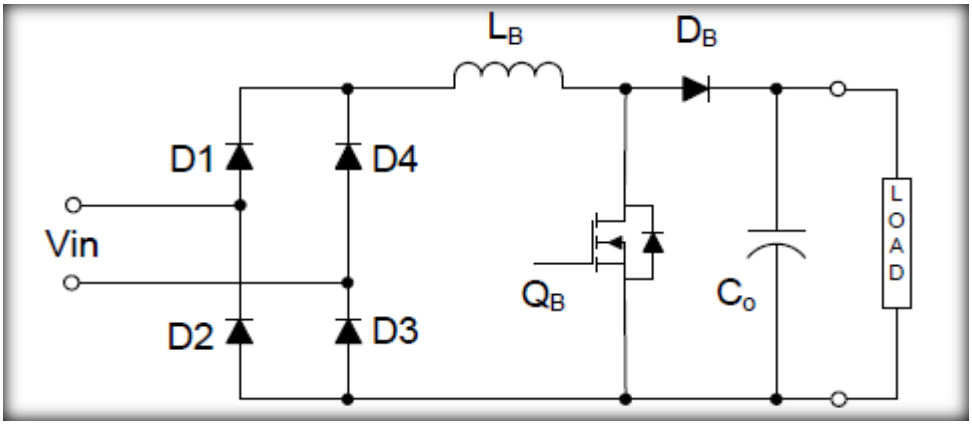

Figure 2.7: Conventional PFC boost converter [26]

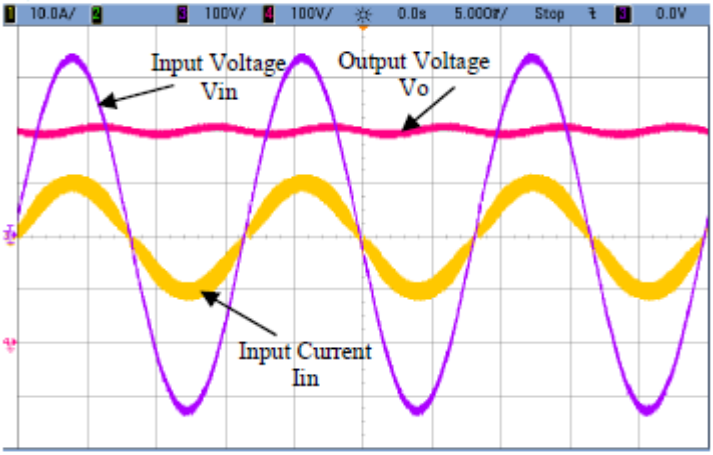

Figure 2.8: Input current, input voltage and output voltage of a conventional boost converter at Vin = 240 V. Y-axis scales: Iin 10 A/div, Vin 100 V/div and Vo 100 V/div [27]

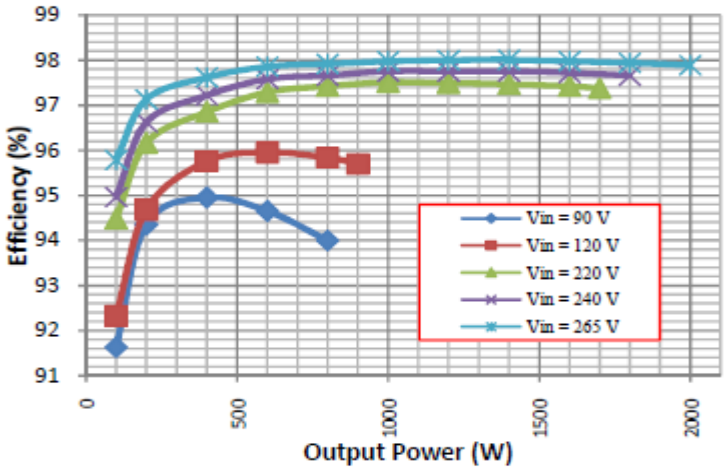

Figure 2.9: Efficiency versus output power at different input voltages for a conventional boost converter [27]

2.4.1.2 Single-Stage AC to DC Power Factor Correction Charger

Ningliang Mi et.al. (2003) have proposed a single stage AC-DC topology with power factor correction for battery charger applications [28]. The ideal features for a battery charger such as, low cost, rapid charging, charge profile programmability, high efficiency and reliability are completely accomplished by using the proposed solution. Furthermore, its multiphase operation configuration offers effortless power scaling. Moreover, the proposed approach was reported to be superior to traditional ferro-resonant regulation, which is extensively employed in EV charger applications. Particularly, it is appropriate for and high power applications with low cost requirements. The practicality and realistic value of the proposed technique were validated by the outcomes of the experiments from a 1 kW product prototype.

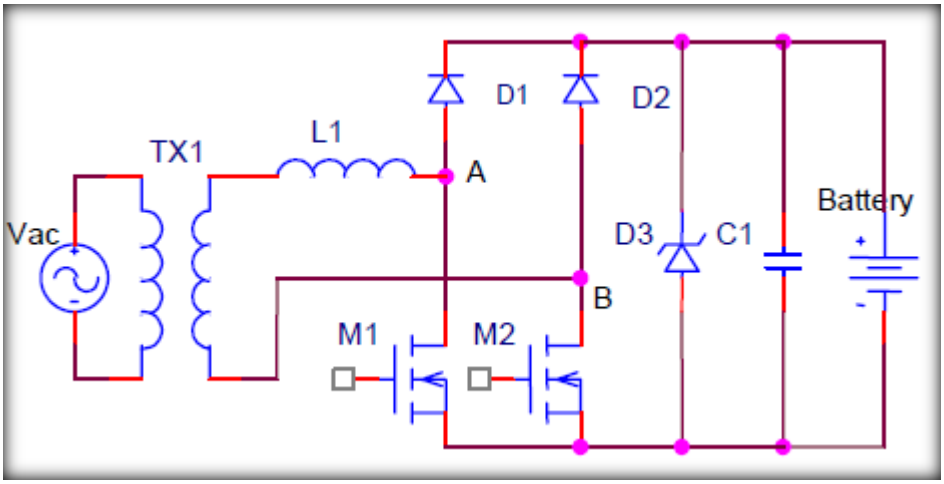

Figure 2.10: Single stage power factor correction battery charger proposed by Ningliang Mi et.al. [28]

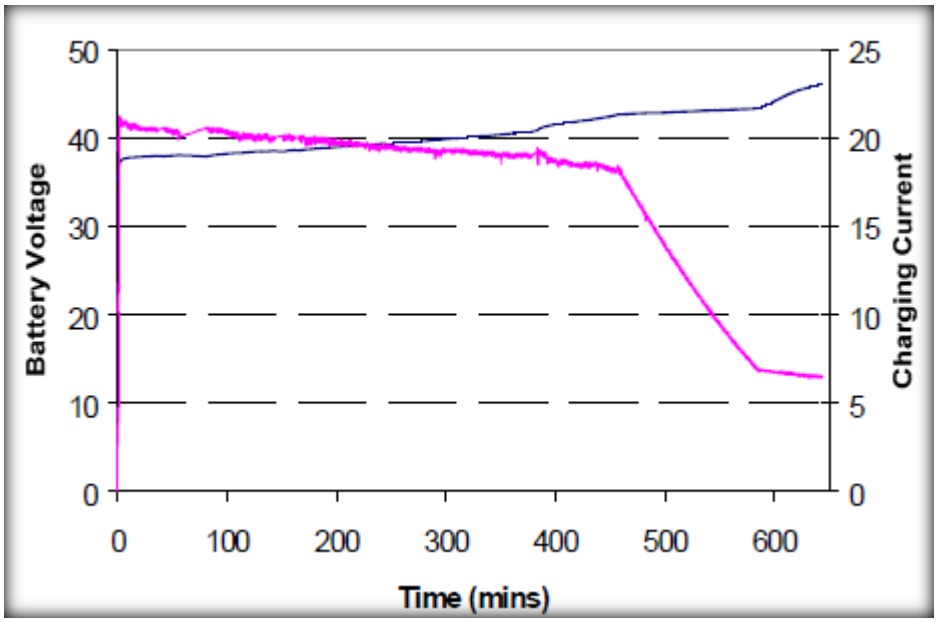

Figure 2.11: Implemented charger profile for 36V lead acid battery bank [28]

Figure 2.10 depicts the proposed single-stage charger topology and Figure 2.11 illustrates the battery voltage and charging current obtained by the researchers. In this technique, an LF line transformer was employed to ensure safety isolation and to step down the line voltage. Subsequently, a unity power factor rectifier [6] was used to charge the battery with rectified sinusoidal waveform current. Due to the availability of step down line transformer, the traditional two-stage topology (consisting of PFC plus DC-DC converter), was not required. A single-stage two-switch-type power factor rectifier might be implemented for battery charger application to accomplish higher performance.

Advantages of the proposed approach are as follows:

1. Unit input power factor.
2. AC boost inductor contributes to EMI reduction.
3. Very low conduction losses because the current always flows through only two semiconductors.

2.4.1.3 Bridgeless Boost Converter

The bridgeless boost converter topology eliminated the requirement of the rectifier input bridge; however it sustains the classic boost topology as shown in Figure 2.12.

It is an appealing option compared to the previous converters explained because it can use employed for applications above 1 kW, in particular where the power density and performance are essential. The bridgeless boost converter resolves the problem of temperature management in the input rectifier diode bridge, however it presents enhanced EMI [26].

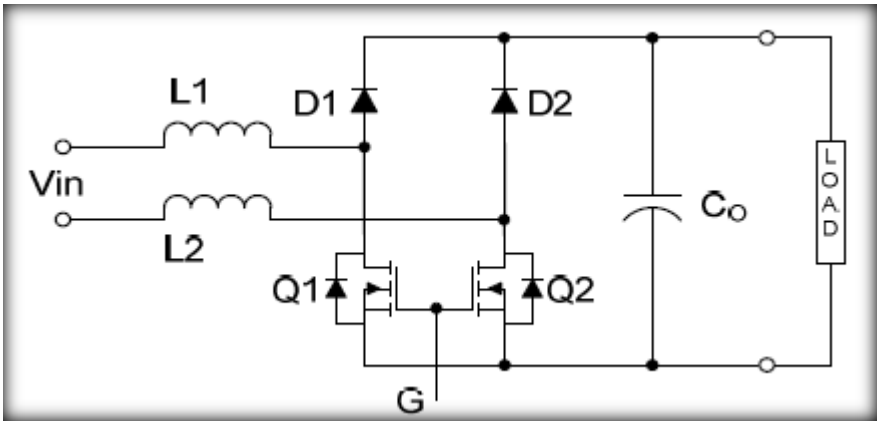

Figure 2.12: Bridgeless PFC boost topology [26]

2.4.1.4 Interleaved Boost Converter

The inter-leaved boost converter shown in Figure 2.13 consists of two-boost converters operating 180° out of phase. The input current is the sum of the two inductor currents. Since the ripple currents of the inductors are out of phase, they are likely to cancel one another and decrease the input ripple current due to the boost switching action. The inter-leaved boost converter has the benefit of paralleled semiconductors. Moreover, by switching 180° out of phase, it enhances the effective switching frequency by two times leading to smaller input current ripple, so the input EMI filter size can be reduced as shown in Figure 2.14. This converter also has less output capacitor high frequency ripple, however, the challenge of heat dissipation management for the input diode bridge rectifiers still prevails as depicted in Figure 2.15 [29].

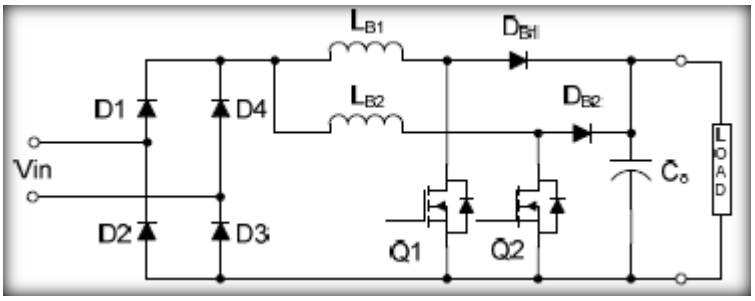

Figure 2.13: Interleaved PFC boost topology [29]

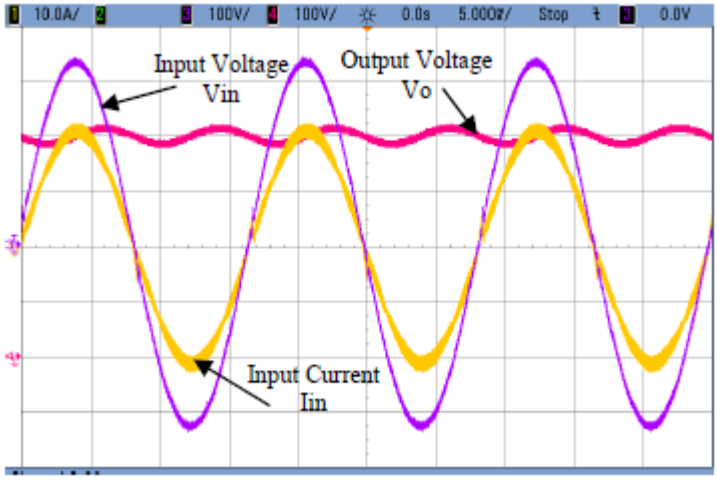

Figure 2.14: Input current, input voltage and output voltage of an interleaved boost converter at Vin = 240 V. Y-axis scales: Iin 10 A/div, Vin 100 V/div and Vo 100 V/div [27]

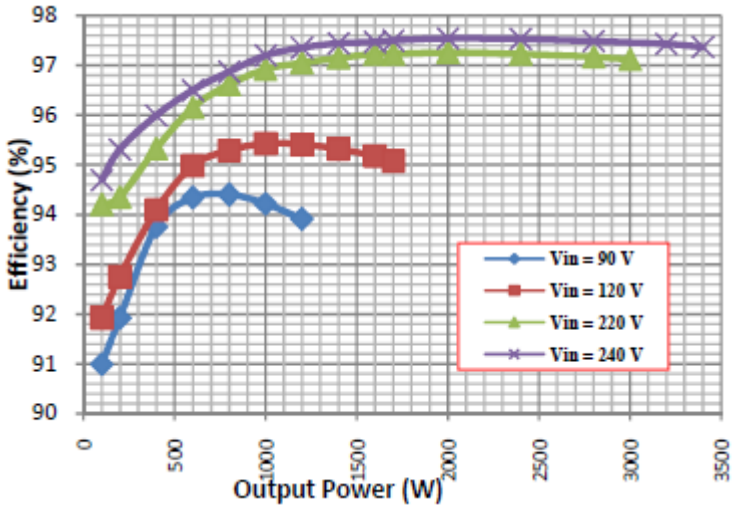

Figure 2.15: Efficiency versus output power at different input voltages for an interleaved boost converter [27]

2.4.1.5 Bridgeless Interleaved Boost Topology (BLIL)

The bridgeless inter-leaved (BLIL) PFC converter was proposed to enhance the total efficiency of the AC-DC PFC converter, whilst keeping all the benefits of interleaved boost converter (see Figures 2.16 to 2.18). This converter presents two more MOSFETs and two more fast diodes, instead of the four slow diodes employed in the input bridge of the interleaved boost PFC converter discussed previously [29].

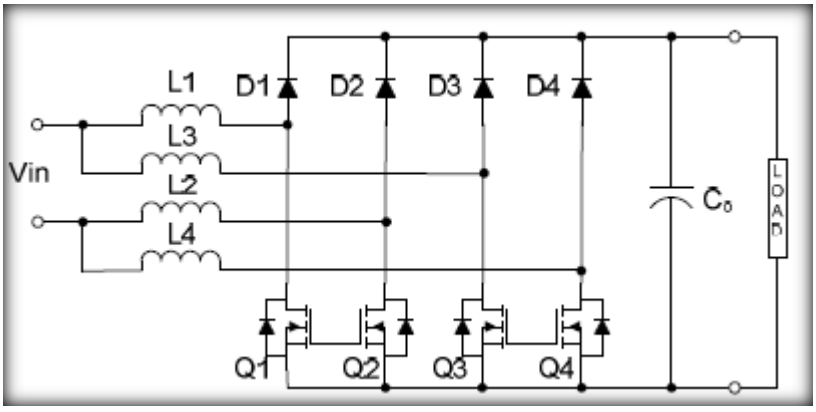

Figure 2.16: Bridgeless interleaved (BLIL) PFC boost converter [29]

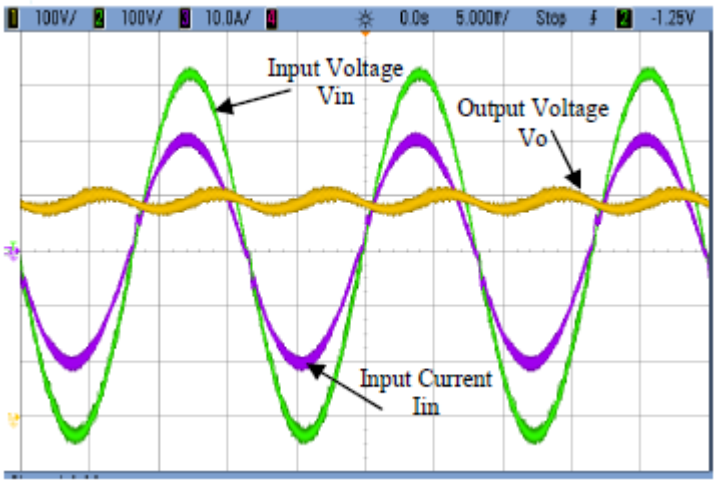

Figure 2.17: Input current, input voltage and output voltage of a bridgeless interleaved boost converter at Vin = 240 V. Y-axis scales: Iin 10 A/div, Vin 100 V/div and Vo 100 V/div [27]

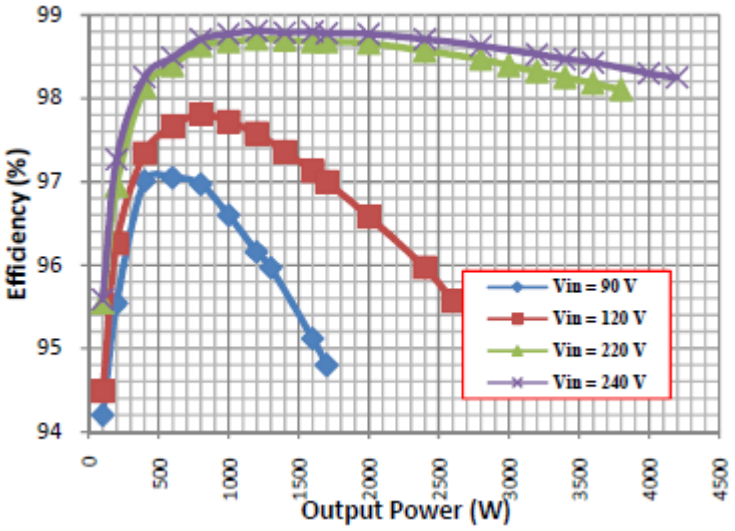

Figure 2.18: Efficiency versus output power at different input voltages for a bridgeless interleaved boost converter [27]

2.4.1.6 Phase Shifted Semi-Bridgeless Boost Topology

The phase-shifted semi-bridgeless topology shown in Figure 2.19 has been proposed as a solution to deal with the issues specified for the conventional boost, bridgeless boost and interleaved boost topologies explained earlier. This topology attributes high efficiency at light loads and low lines, which is significant to decrease the size of the charger, charging time, lower the volume and expense of electricity drawn from the utility; reduced component count, which minimizes the charger cost; and reduces EMI. The converter is essentially appropriate for automotive Level I residential charging applications in North America, where the standard supply is limited to 120V and 1.44kVA [4].

The proposed topology presents two additional slow diodes (Da and Db) to the bridgeless setup to connect the ground of the PFC with the input line. Nevertheless, the current does not always return by means of these diodes, so their related conduction losses are low. This happens since the inductors provide low impedance at the line frequency, hence, a huge part of the current flows through the FET intrinsic body diodes. Furthermore, the gating signals for FETs are 180° out of phase [4].

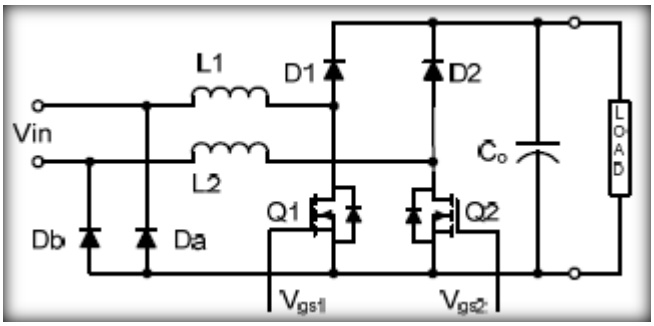

Figure 2.19: Phase shifted semi-bridgeless PFC boost topology [4]

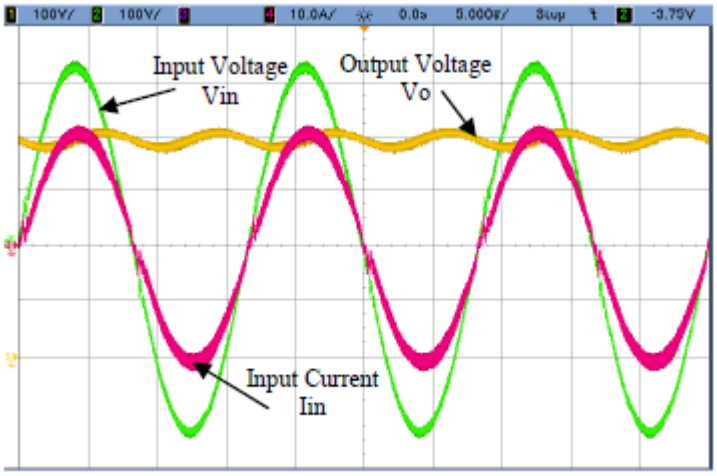

Figure 2.20: Input current, input voltage and output voltage of a phase shifted semi-bridgeless boost converter at Vin = 240 V. Y-axis scales: Iin 10 A/div, Vin 100 V/div and Vo 100 V/div [27]

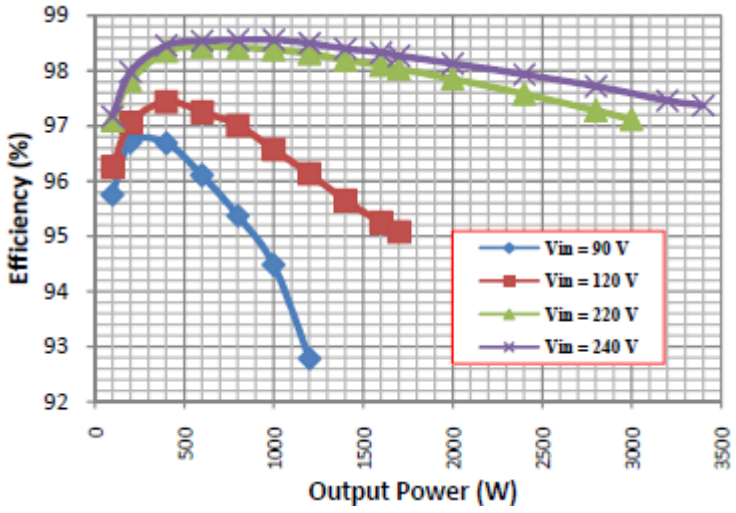

Figure 2.21: Efficiency versus output power at different input voltages for a phase shifted semi-bridgeless boost converter [27]

2.4.1.7 Bridgeless Interleaved Resonant Boost Converter

Infineon Technologies have introduced the bridgeless interleaved resonant topology functioning in Battery Continuous Mode **(**BCM) [30], especially for front end ac-dc stage of Level II on-board chargers (see Figure 2.22). Compared to the bridgeless interleaved boost converter, it supplements the four fast diodes with four slow diodes; nevertheless it needs two high side drivers for MOSFETs – Q1 and Q2, along with two low-side drivers for Q3 and Q4. The other disadvantages with this topology are the requirement of a minimum of two sets of current sensors, two snubbers and a complex digital control scheme [27].

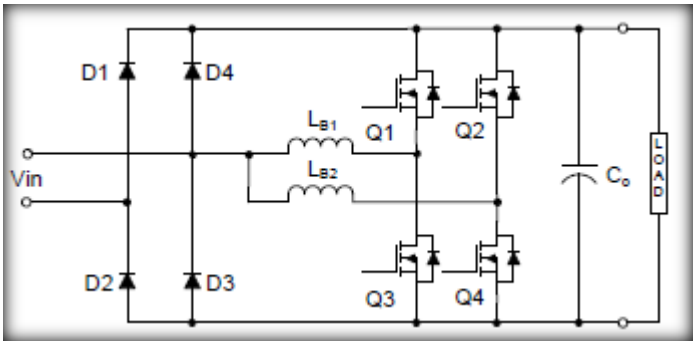

Figure 2.22: Bridgeless interleaved resonant PFC boost converter [27].

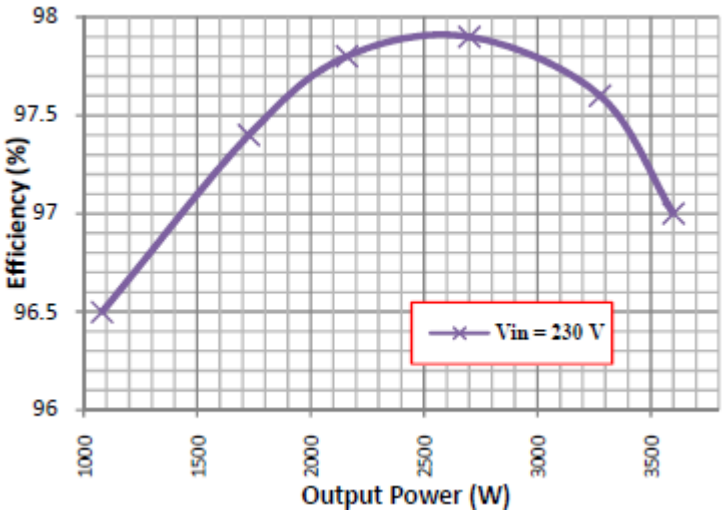

Figure 2.23: Efficiency versus output power at 230 V input voltages for a bridgeless interleaved resonant boost converter by Infineon Technologies AG [30]

2.4.1.8 Topology Comparison

Of late, Fariborz Musavi et.al, (2011) have compared the conventional Boost Converter, Phase Shifted Semi-Bridgeless Boost, Interleaved Boost Converter topology, Bridgeless Interleaved Boost topology, and Bridgeless Interleaved Resonant Boost Converter. The Figure 2.24 depicts the efficiency assessed as a function of output power for all five topologies examined within the following working circumstances [27]: fs = 70 kHz, Vin = 240 V and Vo = 400 V. All prototype units use similar semiconductor and magnetic devices in order to ensure accurate comparison of performance. Much more significantly, performances of all topologies were evaluated at 230V input. Table 2.4 and Table 2.5 illustrates the summary and evaluation of all topologies considered for the front end ac-dc stage of a PHEV battery charger. The phase shifted semi-bridgeless PFC converter was found to be the topology of choice for Level I chargers, and the bridgeless interleaved PFC converter was concluded as an optimal topology for Level II chargers.

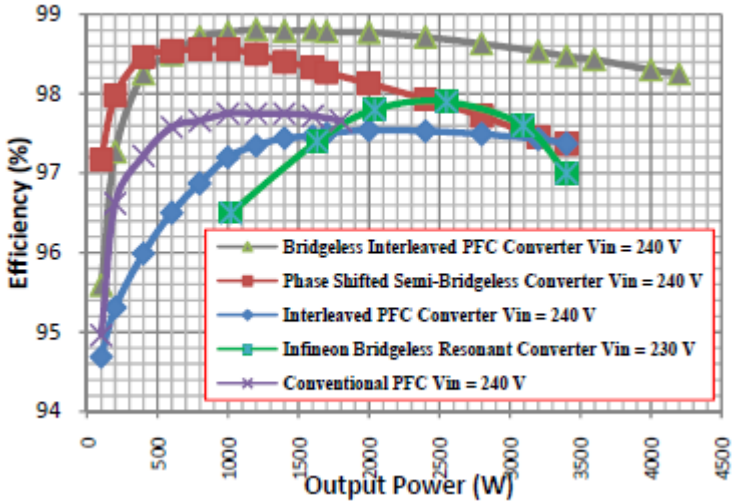

Figure 2.24**:** Efficiency versus output power for different PFC boost Converters [27]

Table 2.4:Performance comparison between five types of PFC converter [27]

Topology	conventional PFC boost converter	Phase shifted semi-Bridgeless PFC boost	interleaved PFC boost converter	bridgeless interleaved PFC boost converter	bridgeless interleaved resonant PFC boost converter
Power Rating	< 1000 W	< 3500W	< 3500W	> 5000W	> 5000W
EMI / Noise	Poor	Fair	Fair	Best	Best
Capacitor Ripple	High	Medium	Low	Low	Low
Input Ripple	High	Medium	Low	Low	Low
Magnetic size	Large	Medium	Small	Small	Small
Driver	2LS	2LS	2LS	2LS	2LS+2HS
Efficiency	poor	Best	Fair	Best	Fair
Cost	Low	Medium	Medium	High	Highest

Table 2.5: Comparison between four types of topologies for boost converter [29]

Topology	Conventional PFC	Bridgeless PFC	Interleaved PFC	BLIL PFC
Power Rating	< 1000 W	< 2000W	< 3000W	> 3000W
EMI / Noise	Fair	Poor	Best	Fair
Capacitor Ripple	High	High	low	Low
Input Main Ripple	High	High	Low	low
Magnetic Size	Large	Medium	Small	small
Efficiency	poor	fair	fair	best

2.4.2 DC/DC Converters for Electric Vehicles

Miro MilanoviE et.al, [31] have proposed a double-buck and boost converter framework, appropriate for battery charger in electrical vehicle application (see Figure 2.25). It is very useful to use inverter elements for battery charging process. Various DC-to-DC converter components can be structured from the inverter semiconductor components. In case of the induction motor electrical drive application, the necessary inductors could be from the windings of motor. These kinds of merged converter should also fulfill the unity power factor function. By

making use of the double buck circuit, the present high harmonic distortion might be either, prevented or considerably minimized. The boost converter created from the inverter components allows the energy transfer from the mains to the load, during the entire mains voltage half period. This combined converter will not require any additional semiconductor or inductor components apart from the diode bridge. As indicted by the figure, the circuit is very big converter, which increases the cost, and reduces the efficiency of the system.

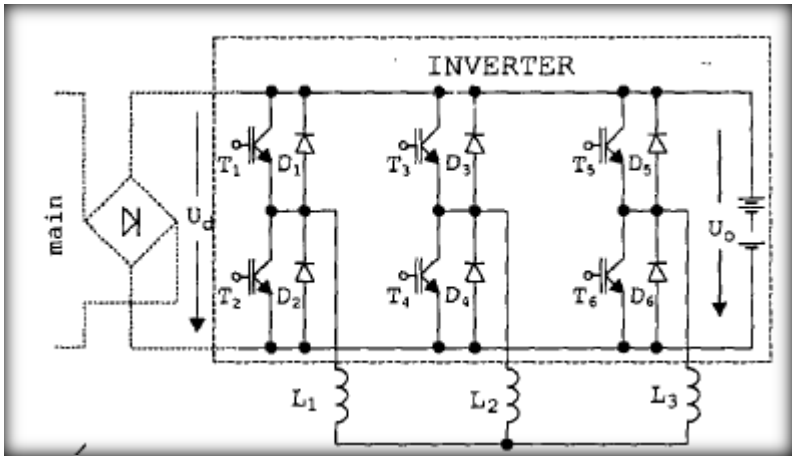

Figure 2.25: Inverter of Electrical vehicle [31]

Majid Pahlevaninezhad et.al [32] have presented a load adaptive control approach, for ideally controlling the volume of reactive current necessary to ensure zero-voltage switching (ZVS) of the converter switches (see figure 2.26). The proposed DC/DC converter is utilized as a battery charger for an electric vehicle (EV). As this application needs a broad range of load variations, the converter needs to be capable of retaining ZVS from full-load to no-load conditions. The converter utilizes an asymmetric auxiliary circuit to supply the reactive current for the full-bridge semiconductor switches, which assures ZVS at turn-on periods. The proposed control scheme is capable of determining the ideal value of the reactive current supplied by the auxiliary circuit, for minimizing extra conduction losses in the power MOSFETs apart from the losses in the auxiliary circuit. In the proposed strategy, the peak value of the reactive current is controlled through the switching frequency to ensure that there is sufficient current to charge and discharge the snubber capacitors during the dead time. Experimental results for a 2-kW DC/DC converter indicate an enhancement in efficiency of the converter.

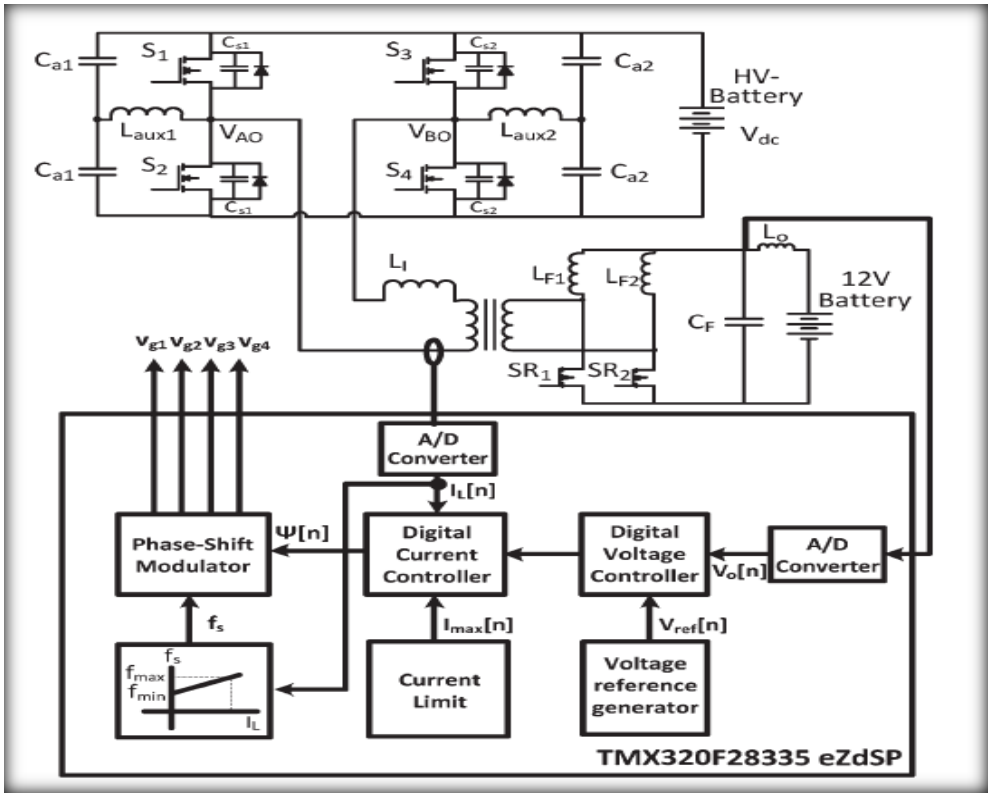

Figure 2.26: circuit proposed and Closed-loop control system block diagram [32]

Furthermore, Shunxiang Li and KwangHee Nam [33] have conducted comprehensive evaluation and circuit implementation of a ZVS high output current and higher power density converter, with a dynamic clamping circuit, ripple current reduced filter, and transformer isolation. For the purpose of minimizing the voltage stress of the main switch in the converter, an active clamping circuit is utilized to deliver ZVS for both, main switch and maxillary switch; and furthermore, the clamping capacitor is also utilized to reuse the power saved in the leakage inductor, and magnetizing inductor of both of the two isolation transformers. Four filter inductors are implemented in the circuit to minimize the current ripple of the output side, and the utilization of transformer presents galvanic isolation for security. Two transformers, which are serially connected (see figure 2.27) in primary side and similar in secondary side are employed to increase the turn proportion of the transformer, for guaranteeing the switch operation under a more constant switching duty proportion.

The advantages of the proposed converter have been included:

1. ZVS or ZCS transition without low switching loss
2. Two transformer topology which can avoid extremely small duty ration under light load situation
3. The energy stored in the leakage inductance and magnetizing inductance is recycled

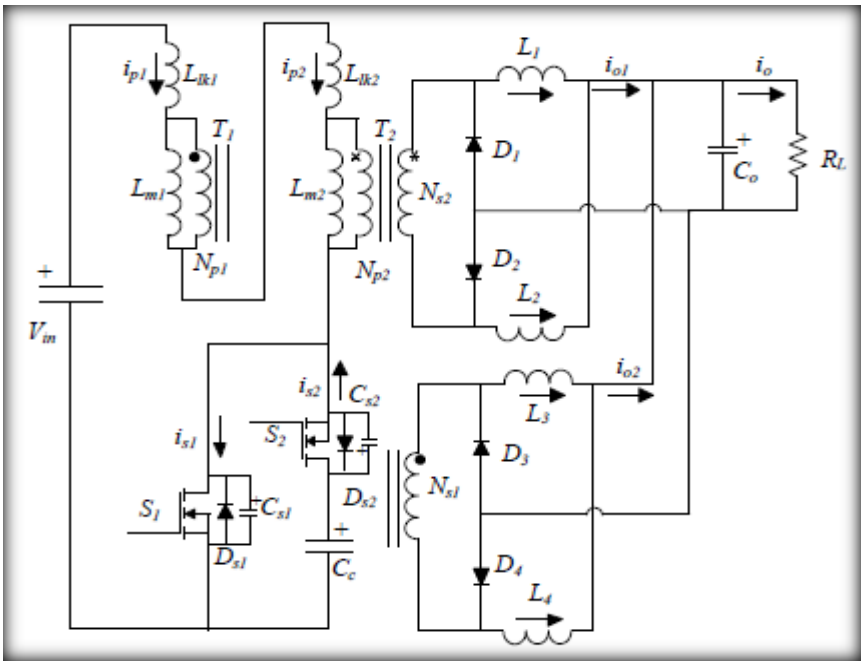

Figure 2.27: Configuration of the converter [33]

In 2012, Rong-Jong Wai, and Kun-Huai Jheng [34] have developed a high-efficiency single-input multiple-output (SIMO) dc–dc converter demonstrated in Figure 2.28. The proposed converter is capable of boosting the voltage of a low-voltage input power source to an adjustable high-voltage dc bus, and middle-voltage output terminals. The high-voltage dc bus can be used as the primary energy for a high-voltage dc load, or the front terminal of a DC–AC inverter. In addition, the middle-voltage output terminals can supply energy for independent middle-voltage dc loads or for charging auxiliary power sources (such as battery modules). Rong-Jong Wai, and Kun-Huai Jheng [34] have employed a coupled-inductor based dc–dc converter system, which employs just one power switch with the attributes of voltage clamping and soft switching, and the equivalent device specifications are thoroughly designed. Consequently, the goals of high-efficiency power conversion, high step-up ratio, and

numerous output voltages with various levels could be acquired. Several experimental outcomes based on a one kilowatt-level prototype were provided to confirm the efficiency of the proposed SIMO DC–DC converter in practical applications.

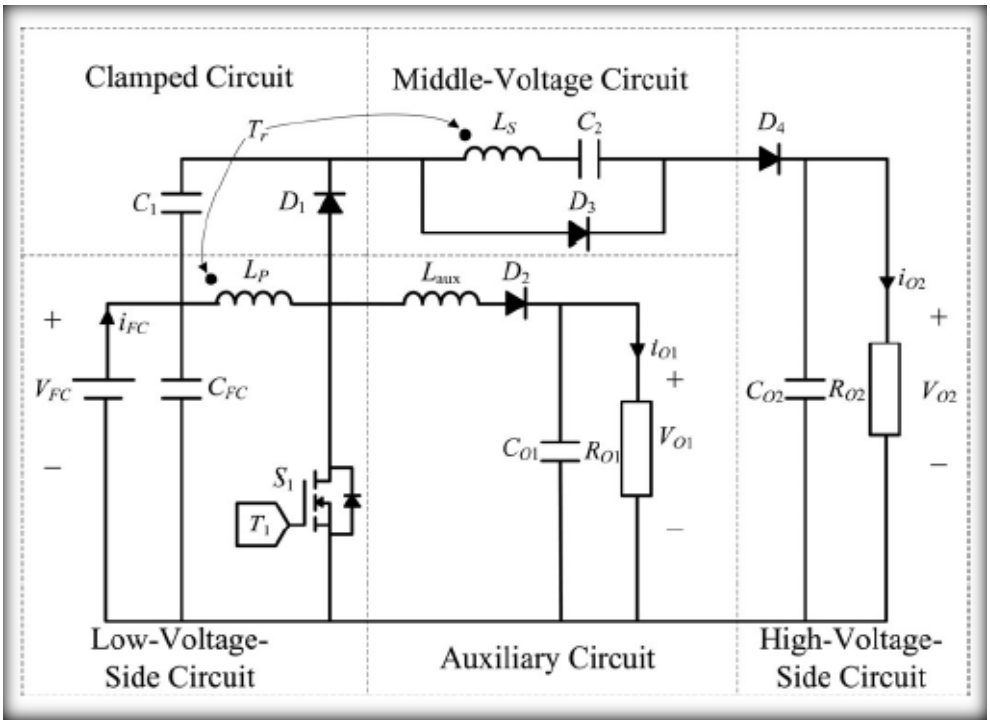

Figure 2.28: System configuration of high-efficiency single-input multiple-output (SIMO) converter [34]

2.5 Charging of Battery

Chandrasekar et.al., [35] have effectively developed a 350W offline battery charger and executed in the field trial. The 3WHEV has been tested at Automotive Research Association of India (ARAI) for Automotive India Standards (AIS) standards, and this charger has also passed the tests required by standards. The cost evaluation has been made and was identified to be very cost-effective, as compared to the line frequency isolated chargers, and it also fulfilled the requirement of charger costs to be within 1.5% of the total cost of the vehicle. The Figures 2.29 and 2.30 respectively indicate the results of theoretical matching performance and the charger output voltage, throughout a typical charging operation.

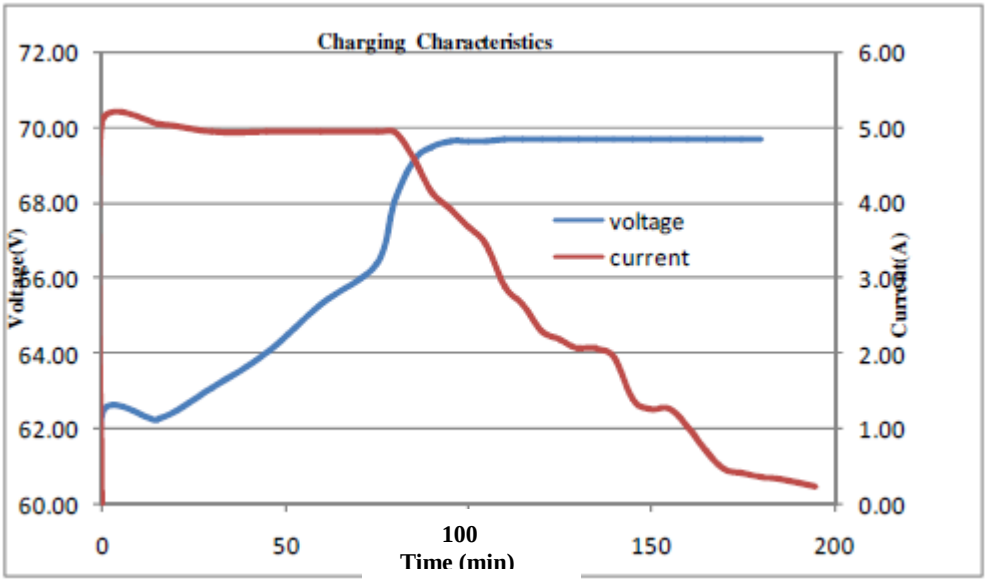

Figure 2.29: Step charging characteristics of the battery charger module [35]

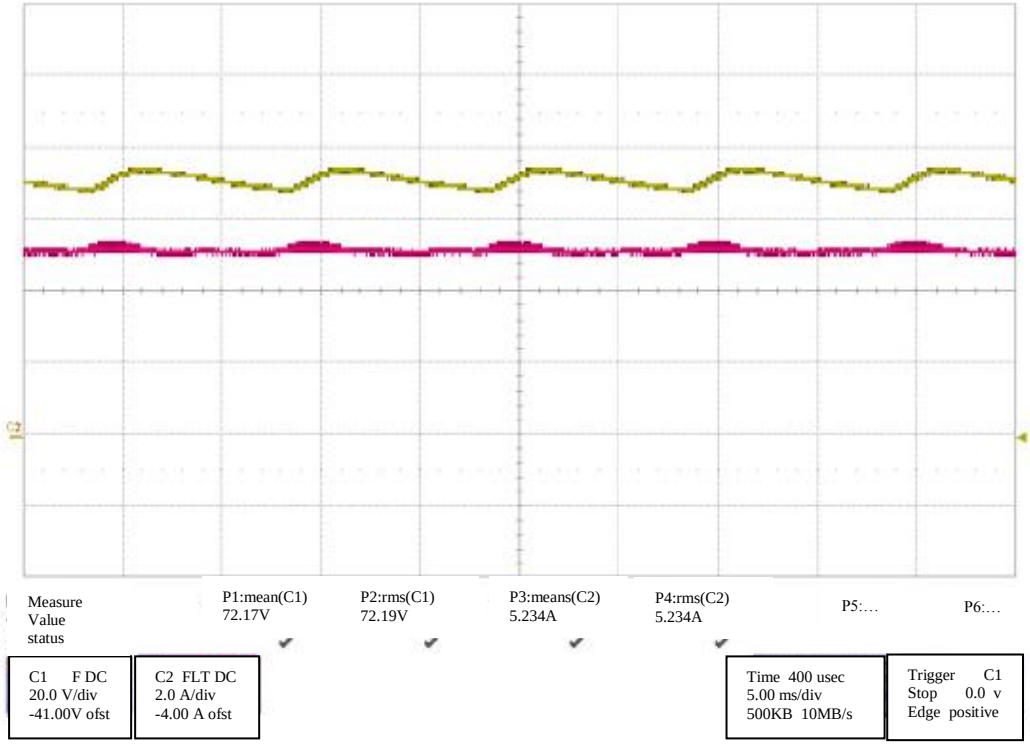

Figure 2.30: Typical Output Voltage and Current of the charger module [35]

Ming-Shi Huang et.al, [36] have proposed a novel electrolytic capacitor-less and single-stage controlled three-phase battery charger with electrical isolation as seen in Figure 2.31, for providing broad range of output voltage for EV applications. Furthermore, a novel control technique for the charger has been designed to

minimize the current and voltage ripples during battery charging, and improve the power factor as against traditionally controlled single-stage rectifier. Through the use of ZCS and ZVS under light-load conditions and single-stage switching structure for the proposed charger, the efficiency was found to be enhanced. Experimental results derived from the DSP-based controlled charger have been presented. The charger rating is 4 kW, and output voltage is from 50V to 400V. It is noteworthy that, the output current and voltage ripples are substantially minimized, without any electrolytic capacitor in the proposed charger. It has also been proven that, the efficiency and power factor are more than 0.94 even during 25% rated load from 300V to 400V output voltage. These test results consequently validate the performance of the proposed topology and control approaches.

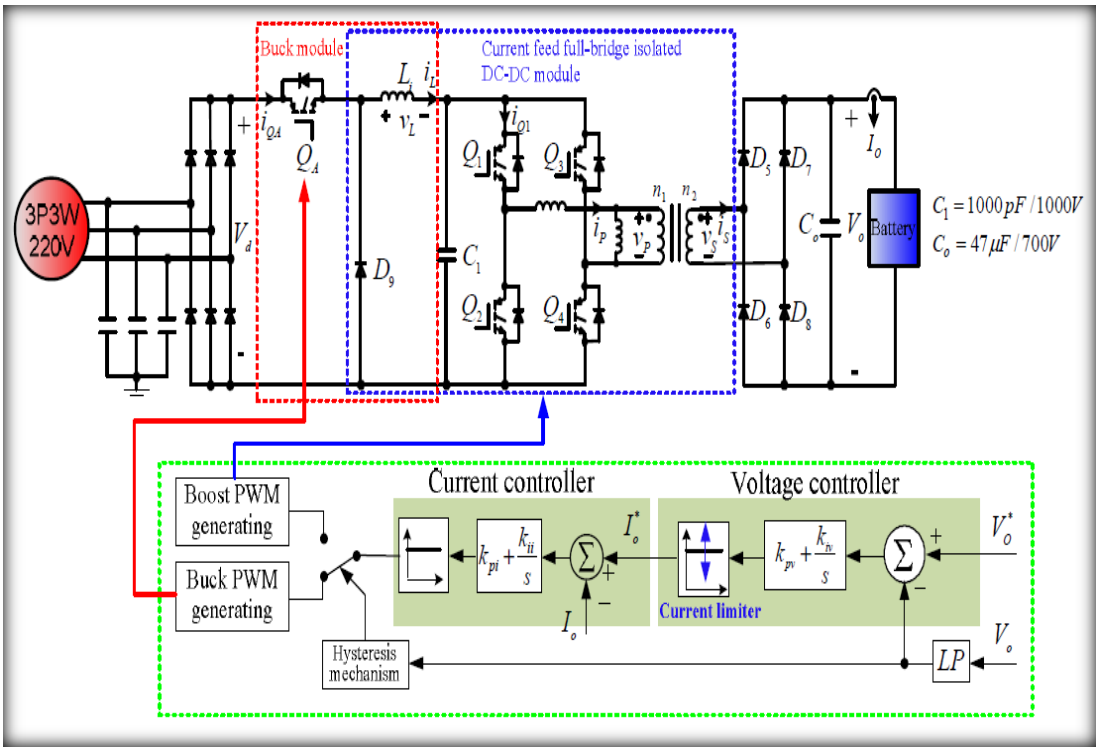

Figure 2.31: The proposed circuit topology and control schemes for battery charger [36]

2.6 Smart Charging of Battery

H.Makkonen et.al, [37] have stated that an intelligent charger is capable of minimizing the shortcomings of the distribution system. The charging system has

also capabilities of discharging the batteries and providing backup power in the event of a distribution network failure. With the intelligent charging and discharging, the effects of electric cars on the distribution network, and ventures associated with them can be effectively reduced.

As shown in Figure 2.32, voltage control loop and current control loop with PI regulators are employed in the charging control diagram. These two loops are used to realize three stage charging (constant current charge, constant voltage charge and floating charging) for conventional lead-acid battery and avoid overcharge. *V*BH is the upper voltage limit of the battery during charging, which corresponds to 95% state-of-charge (SOC). In [36], *V*BH is set at 54V. *I*B_limit is the maximum charging current of the battery, which is usually equal to 0.1C-0.15C. In [36], the battery capacity is 230Ah, thus *I*B_limit is set at 23A. Figure 2.33 shows the simulated charging process, where the initial SOC is 40%. These simulation results exhibit three stages battery charging clearly. It is also apparent that the battery has been charged efficiently without overcharge [38].

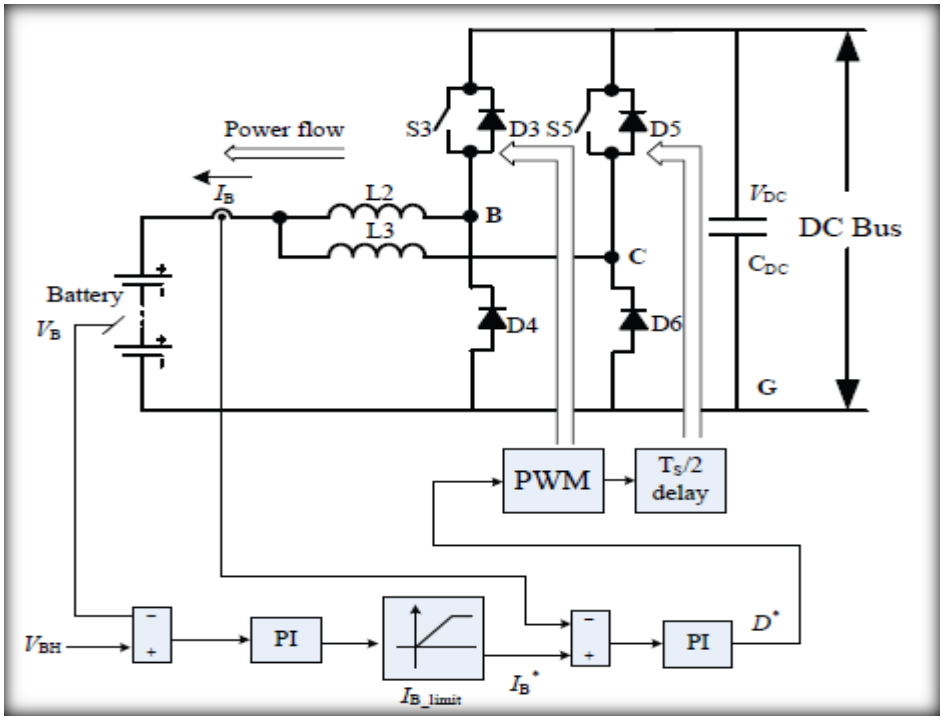

Figure 2.32: Control diagram of battery converter at the grid-connected mode [38]

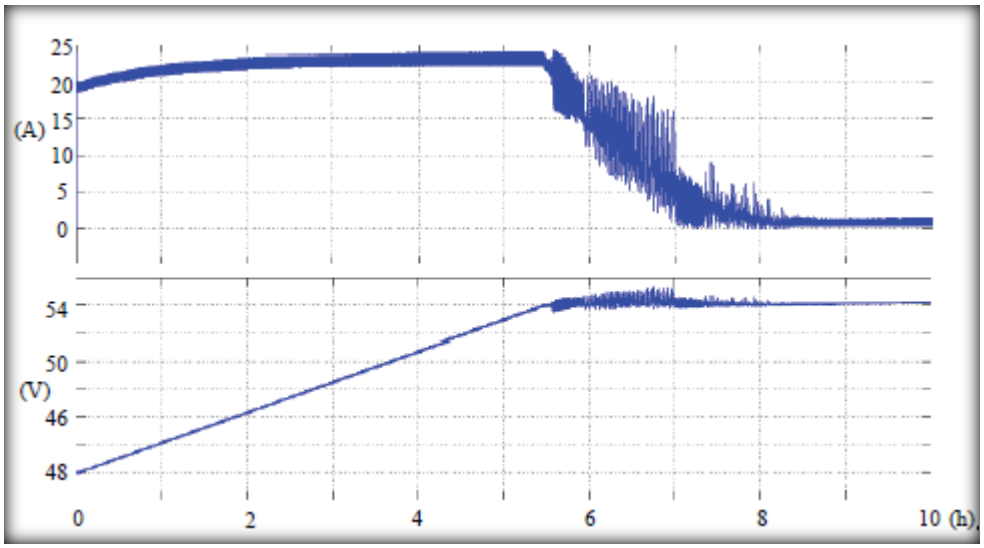

Figure 2.33: Voltage and charge current of the battery at the grid-connected mode [38]

A highly performance two-stage smart battery charger has been proposed for off-road and urban electric vehicles in [38]. The proposed charger has been examined and its functionality features are provided. The charger minimizes both, low and high frequency current ripple on the battery, therefore improving battery life devoid of afflicting the volume of the charger. The outcomes of the experiments and simulation of a prototype unit which converts universal AC input to 58 V DC at 650 W showed accomplishment in attaining peak efficiency of 93.2% at input of 240 V confirmed the validity of the concept (see Figure 2.34). The charger power factor has also been provided for the entire load power range at 120 V and 240 V input. The power factor is higher than 0.99 from half load to full load [39].

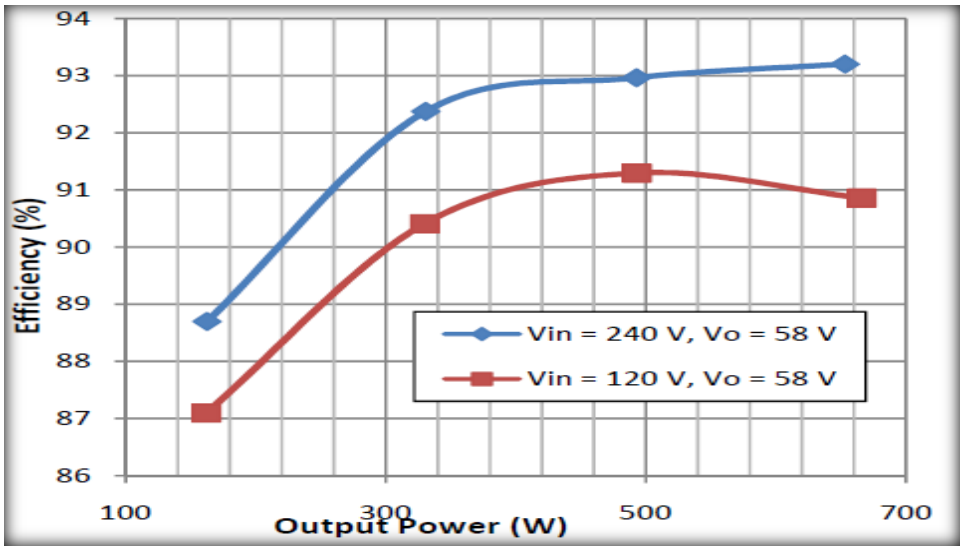

Figure 2.34: Overall charger efficiency as a function of output power at 58 V output [39]

The development of battery charger has been presented by the authors of [40] for charging sequence of Li-ion batteries. It examines the fundamental principles of Li-ion battery charging such as, the charging method, cell balancing, charging control, performance tracking, protection, and also the design limitations. According to the experimental outcomes presented [40], it is proven that, constant current/constant-voltage-based battery charger with charge shunting cell balancing technique, provides very fast charging time. The usage of diverse charging/balancing time, depending on the variation between the maximum and the minimum voltage, whilst charging in constant-current charging mode has assured that all the batteries are well-balanced in the end. Consequently, this allows preservation of the performance and capacity of the series-connected Li-ion batteries, along with its life-cycle. The design of Li-ion battery charger as illustrated in Figure 2.35, comprises of an 8-bit micro-controller, which is linked to the constant-current/constant-voltage source sensors and analog-to-digital converter. This facilitates in charging the batteries quicker, by implementing higher digital converters. The typical charging and discharging profile, illustrating the relationship between the battery's voltage and current as apparent in Figure 3.36 [40].

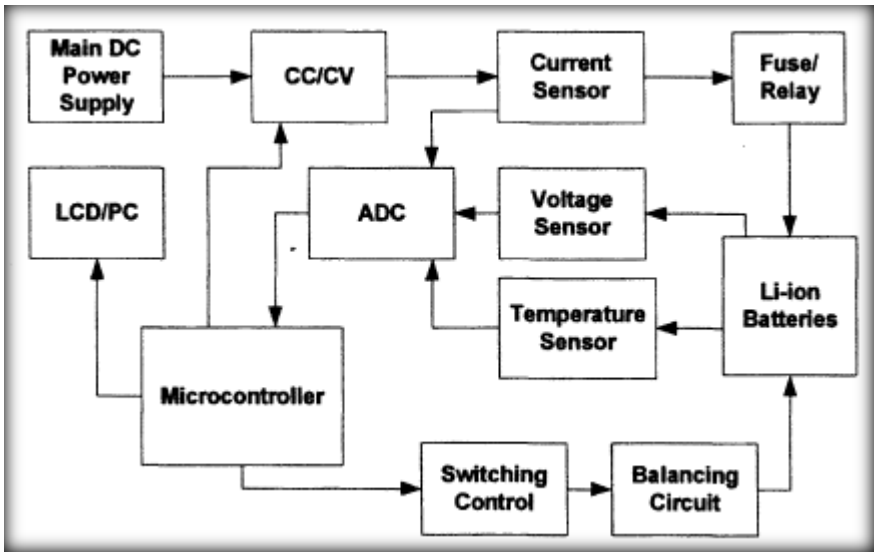

Figure 2.35: Block diagram of Li-ion battery charger [40].

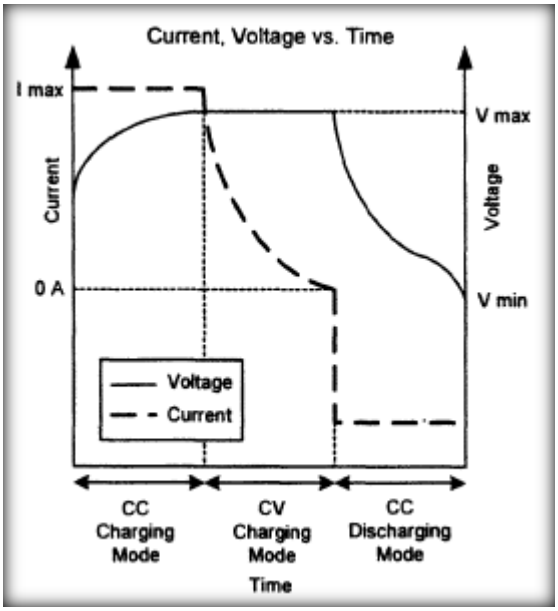

Figure 2.36: Typical Li-ion battery charge and discharge profile [40].

2.7 Constant Current Constant Voltage Battery Charging Methods

The battery charging strategy is crucial for the development of the charger, it is also needed to minimize the charging time and avoid overcharging.

Jung-Song Moon et.al., [21] have proposed the enhanced CC-CV charging as shown in Figure 2.37. In their study, the charging began at 20% SOC, and the termination time was established at 90% SOC, which protects the battery from over-discharging and overcharging. The rated capacity of lead-acid battery employed in the study is 80Ah. Therefore, in CC mode, the battery was charged safely by 8A (0.1C). In CV mode, if the current reduces to 0.5A, the battery charging was terminated. The Figure 2.42 indicates the battery terminal voltage and the SOC estimated by the proposed approach. In the traditional CC-CV charging method, the charging time is prolonged, since the CV mode requires longer time relating to the electro-chemical characteristics of the battery during the CV mode. In contrast, the enhanced CC-CV algorithm shows that, CC time becomes prolonged and CV time is reduced as apparent in Figure 2.38. Overall, the enhanced CC-CV algorithm proposed decreases the total charge time and offers the details of estimated SOC. Therefore, the termination time can also be established through the SOC.

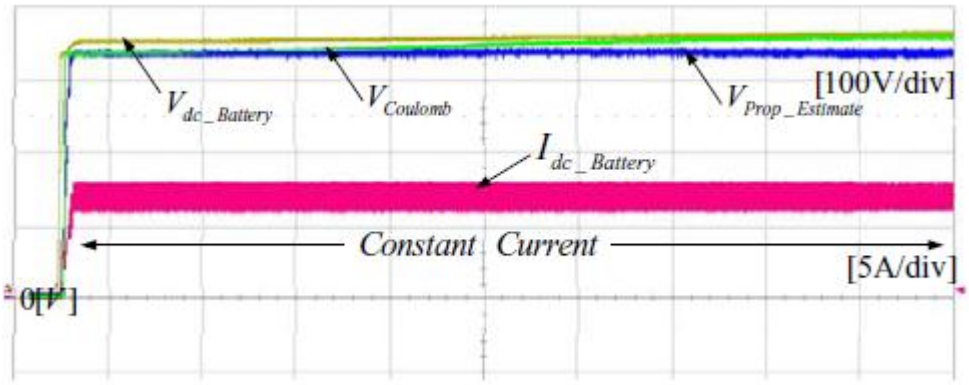

(a)

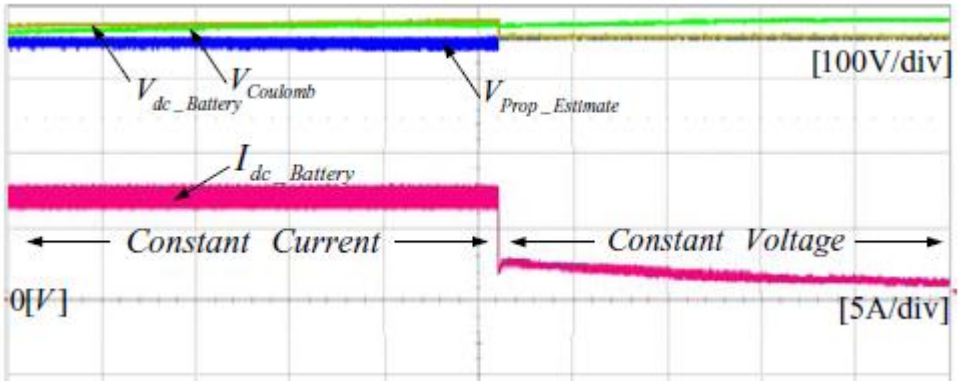

(b)

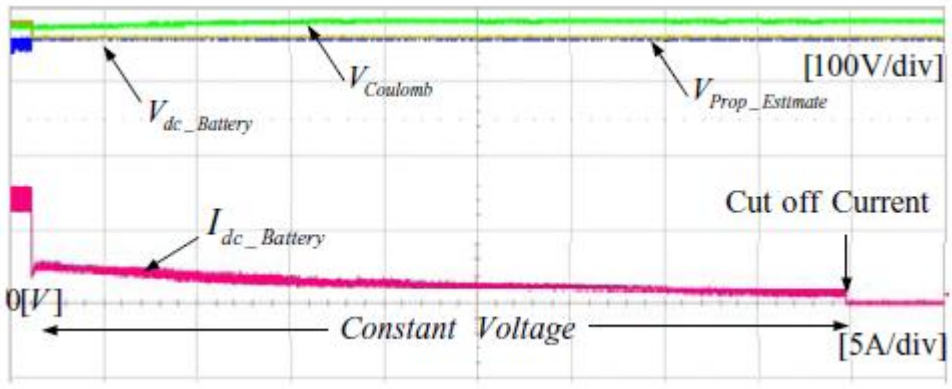

(c)

Figure 2.37: Improved CC-CV charge profiles. (a) CC charge region, (b) transition region, (c) CV charge region [21]

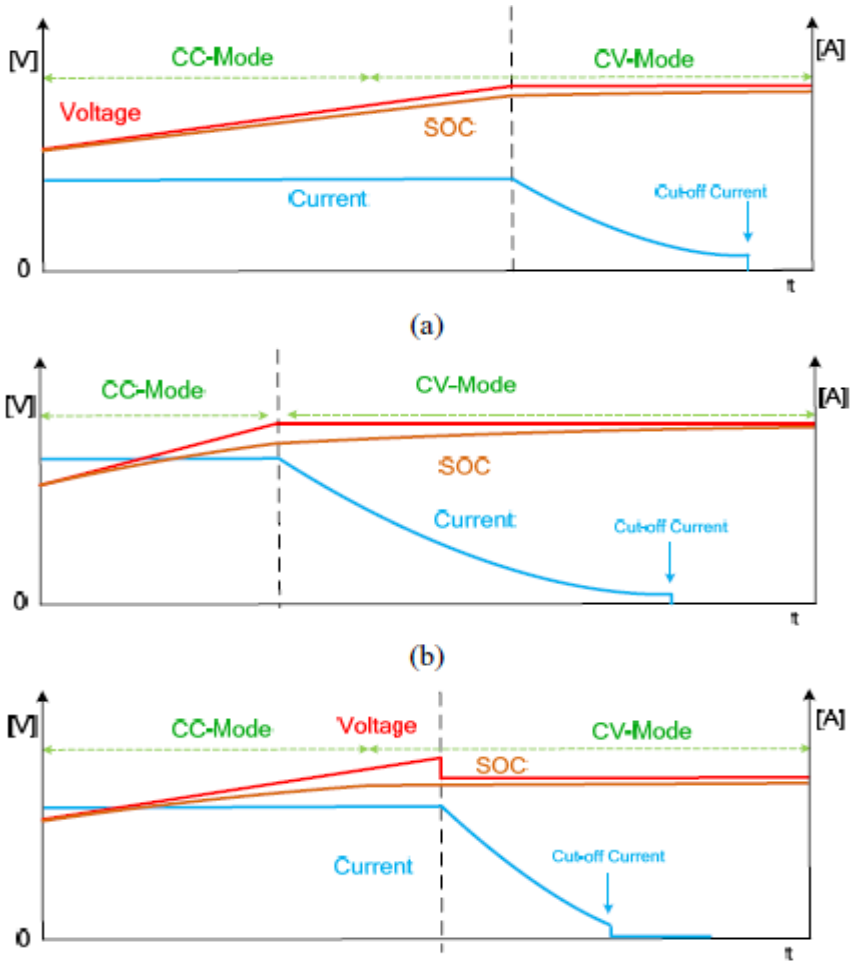

(c)

Figure 2.38: CC-CV charging algorithm. (a) Slow charge based on the terminal voltage, (b) fast charge based on the terminal voltage, (c) proposed charging based on the SOC [21]

2.8 Fuzzy-Controlled Battery Charge System

Fuzzy logic controller proposed in [41] get these features; during charging the temperature slows down which increases charger efficiency, charging is made faster, no stop errors occur through charging. therefore the fuzzy logic control has many features for example that the software implementation of complex systems is not computer intensive, then by apply cost effective microcontrollers to interpret complex signals. Also the line power qualify and transport maximum permissible output power can improve by proposed [42] the fuzzy control algorithm implemented with Digital Signal Processor (DSP). But absorbed the conventional battery charger has practices an extremely distorted current harmonic waveform and low power factor. By using the intelligent charging system (DSP fuzzy logic control) fund [43] the data collection, calculation and peripheral circuit control are achieved for the battery charging standing. It is built via the battery protection cell voltage and voltage difference among the batteries that used as the input variable to shorten the charging and equalizing time and guarantee that the battery will be operated within the safety voltage range.

Figure 2.39 illustrates a fuzzy-controlled active state-of-charge controller (FC-ASCC) for enhance the charging of a lithium–ion (Li–ion) battery proposed by [44]. The proposed FC-ASCC has been developed to substitute the common constant-voltage charging mode, based on sense and charge modes. A fuzzy-controlled (FC) algorithm has been developed with the expected charger functionality to increase charging speed and to maintain the charge procedure in a proposed safe-charge area (SCA). A modeling work has been carried out for examining and explaining the Li–ion battery in charging process. A three-dimensional Y-mesh diagram for outlining the charging trajectories of the proposed FC charger is simulated. A prototype of a Li–ion battery charger with FC-ASCC has been simulated and realized to evaluate the charging performance predicted. Figure 2.40 illustrates that the charging speed of the proposed FC charger, as against the standard charger, improves by about 23%, and the charger can operate safely within the SCA [44]

.

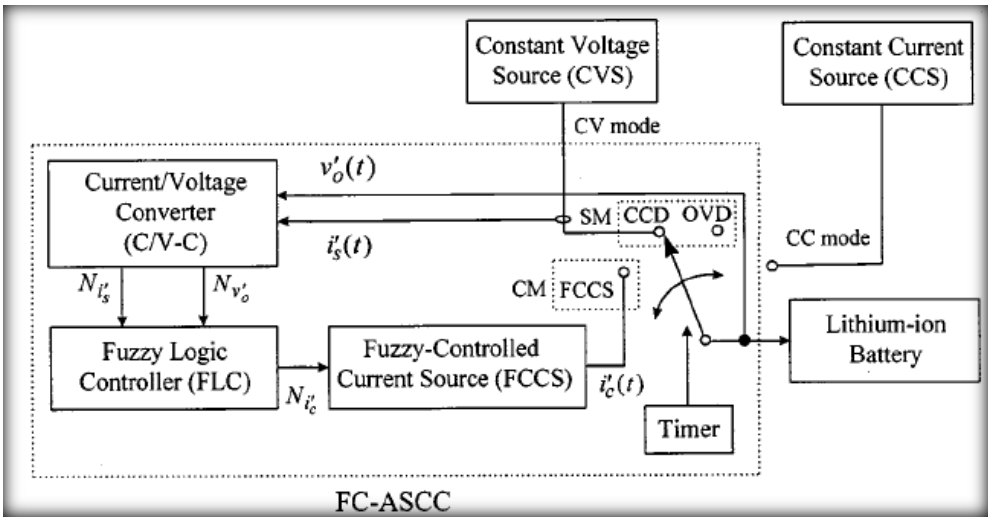

Figure 2.39: Configuration of the proposed FC charging system [44].

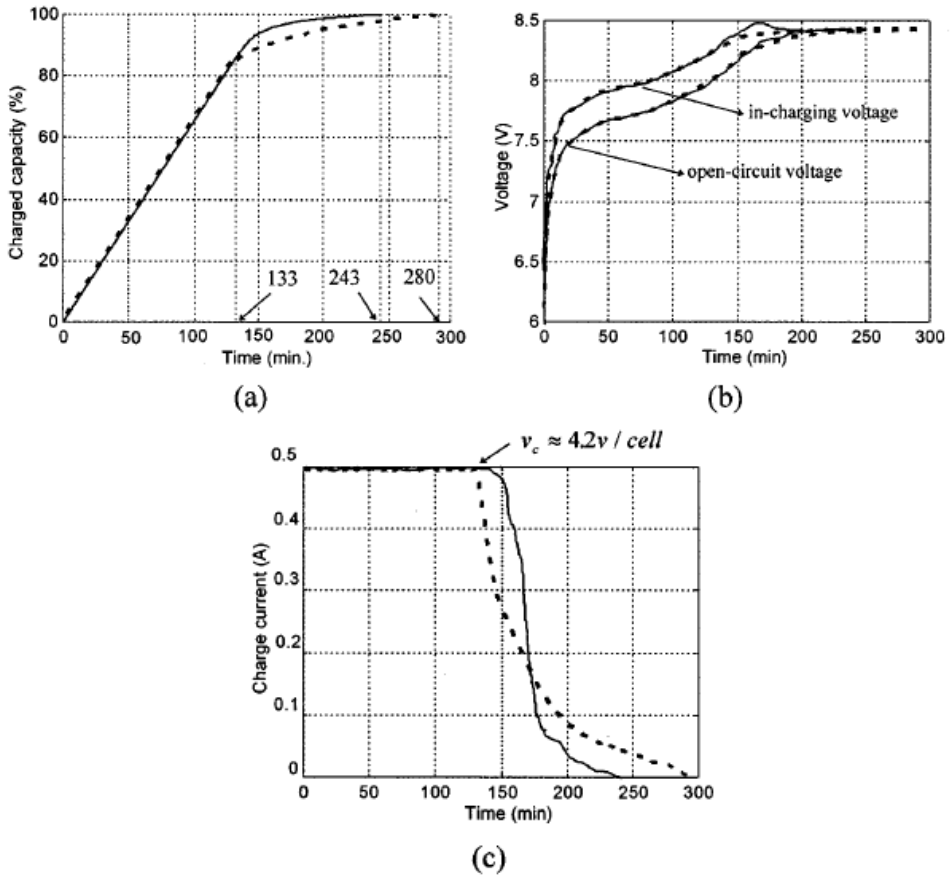

Figure 2.40: Charging performance of the general (- - -) and proposed FC (—) charging systems. (a) Remanent capacity versus charging time. (b) Detected open-circuit Voltage v_o (t) and the in-charging voltage v_c (t). (c) Charging trajectories of the deduced i_c (t) [44]

A DSP-based Probabilistic Fuzzy Neural Network (PFNN) controller, to manage a two-stage ac–dc charger has been proposed by[45].The charger comprises an AC–DC boost converter, with power factor correction and a phase-shift full bridge dc–dc converter. Additionally, the designed charger employs a constant-current and constant-voltage (CC–CV) charging technique to charge the lithium-ion battery packs. To enhance the transient voltage regulation during load variation, a PFNN controller has been proposed to substitute the conventional proportional–integral controller. Additionally, the discontinuous charging voltage and current during the conversion between the CC and CV charging modes could also be considerably minimized through the use of the proposed PFNN controller. Furthermore, the control performance of the proposed PFNN control system for CC–CV charging has been validated through experimental outcomes. The control scheme of the PSFB dc–dc converter is shown in Figure 2.41; over-voltage or over-current might happen, which would damage the life-cycle of the battery packs due to the discontinuous control attempt. To resolve the above mentioned complications, a PFNN management system for the CC–CV charging strategy has been illustrated in Figure 2.42, where a PFNN controller has been proposed for both, the CC and CV charging modes. Figure 2.43 illustrates the experimental outcomes of the two-stage converter [45].

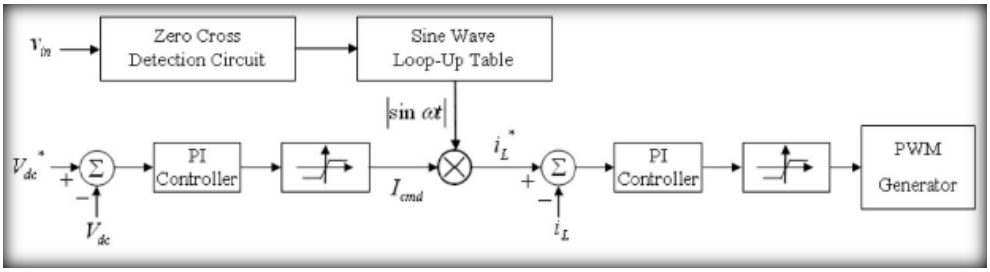

Figure 2.41: Control scheme of PFC ac–dc converter [45].

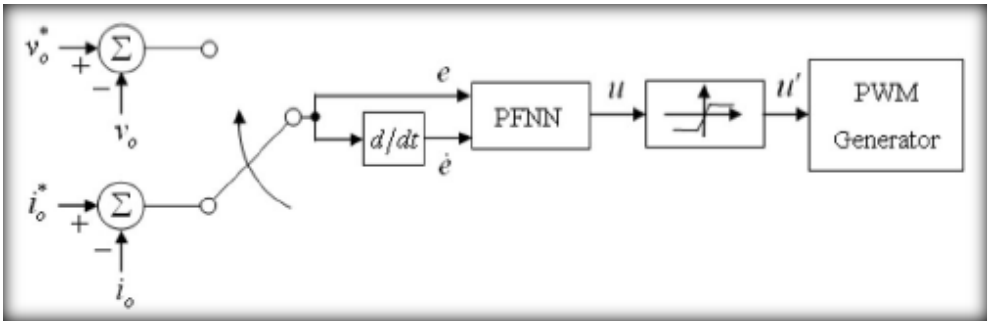

Figure 2.42: PFNN control block of charger [45].

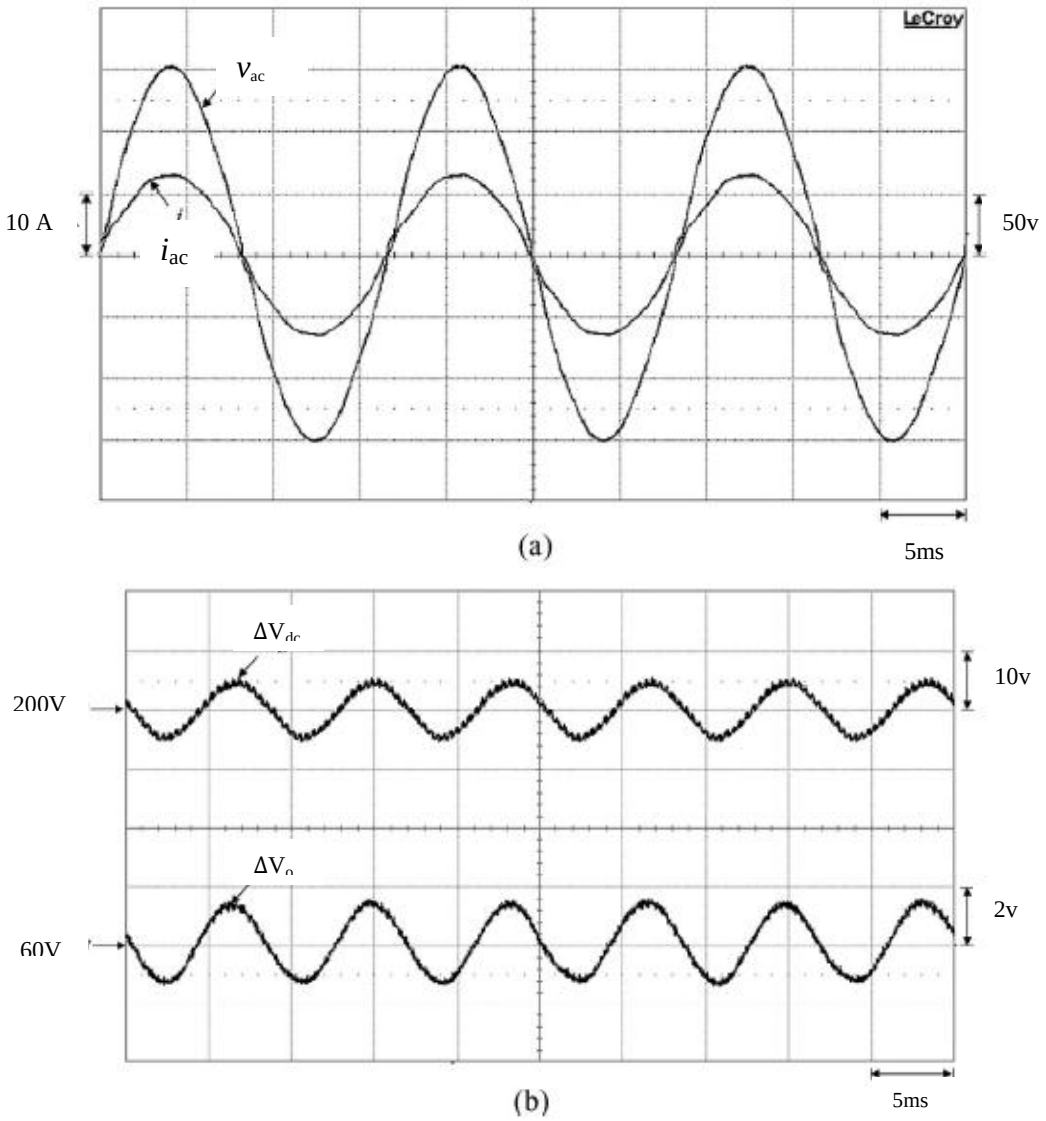

Figure 2.43: Experimental results using PI voltage controller at rated load 800 W of the two-stage converter. (a) Grid voltage and input cu rrent v_{ac} and i_{ac}. (b) DC-link voltage ripples and the output voltage ripples ΔV_{dc} and Δv_o [45].

In order to overcome the state of charge (SOC) estimation issue for lead-acid batteries in HEV, the online state of charge estimation has been conducted utilizing a local linear model tree (LOLIMOT), which is a nero-fuzzy network. The training data of LOLIMOT includes assessed voltage, current, and SOC data in various temperatures, in which current and temperature are utilized as inputs, and SOC is utilized as output. Outcomes of the LOLIMOT SOC estimator has been compared with ANFIS SOC estimator, and based on error and number of neuron in the

LOLIMOT SOC estimator, it was reported that the LOMILIT SOC estimator was abel to perform better, as against the ANFIS estimator. Whilst ANFIS is a soft computing approach based on adaptive neuro-fuzzy inference system, it has been employed to approximate SOC within various working conditions such as, constant current discharging (CCD) and random current discharging (RCD) [46].

2.9 Summary

Electric vehicle (EV) and plug-in hybrid electric vehicle (PHEV) have minimized fuel utilization and greenhouse emissions; consequently there has been rising attention in those technologies. The latest advancements in Lithium-ion batteries have resulted in an excellent expectation regarding efficiency and value for prospective application in EV. In contrast with other rechargeable batteries, Li-ion batteries possess higher energy density, higher voltage, fast charging prospect, higher discharge rate, extensive operating temperature range, exceptional charge-discharge cycle service life, and long self-life. Battery management system (BMS) has been considered as a very significant system, which plays an important role in ensuring the safety of the battery. The BMS generally consists of State-of-Charge (SOC), State-of-Health (SOH), and cell balancing for the preservation of the battery. A lot of studies have investigated equalization of voltage and charging of the battery, furthermore, the SOC estimation is a significant concern, and therefore, several techniques have been introduced. For the purpose of designing the charger it is essential to have an AC to DC topology converter, to enable charging of dc battery from the utility, for Li-ion batteries an additional DC to DC isolation converter is required. Furthermore, this chapter has shown that the application of fuzzy logic for battery charging system is an attractive prospect due to its modern technique and abilities to work with similar or better performance than analogue controllers.

CHAPTER 3

DESIGN OF FUZZY LOGIC CONTROLLED BATTERY CHARGER

3.1 Introduction

A number of methods can be used to control the charging of a battery for an EV, in this project a fuzzy logic control scheme was chosen, which is practical and does not employ complex classic mathematics in the design process. Furthermore, the use fuzzy logic can be easily implemented in Matlab, which is the chosen simulation environment for this project. The previous chapter had explained many types of topologies that using to convert from AC to DC voltage, so in this chapter will explain principle of working phase shifted semi-bridgeless boost topology converter which leads to understanding of the functionality of the topology, and the constrains of building fuzzy logic input and output rules to control the converter. In this dissertation the design of Sugeno fuzzy logic control scheme for phase shift semi bridgeless boost topology will be presented to charging Li-ion battery.

3.2 Simulation Program

Generally, two ways are used to construct model, the first is through practical or experimental method, which connects components of a circuit, and then using an oscilloscope to record the output and input figures, and results. The other method is through simulation, by using different types of software programs, dealing with the circuits proposed, for example Matlab and PSCAD. Matlab is a very famous program and has been used in very wide applications, including power electronic applications. In this dissertation, Matlab is used to simulate the designed fuzzy logic controller to control the phase-shifted semi-bridgeless boost converter. The Figure 3.1 explain methodology flowchart.

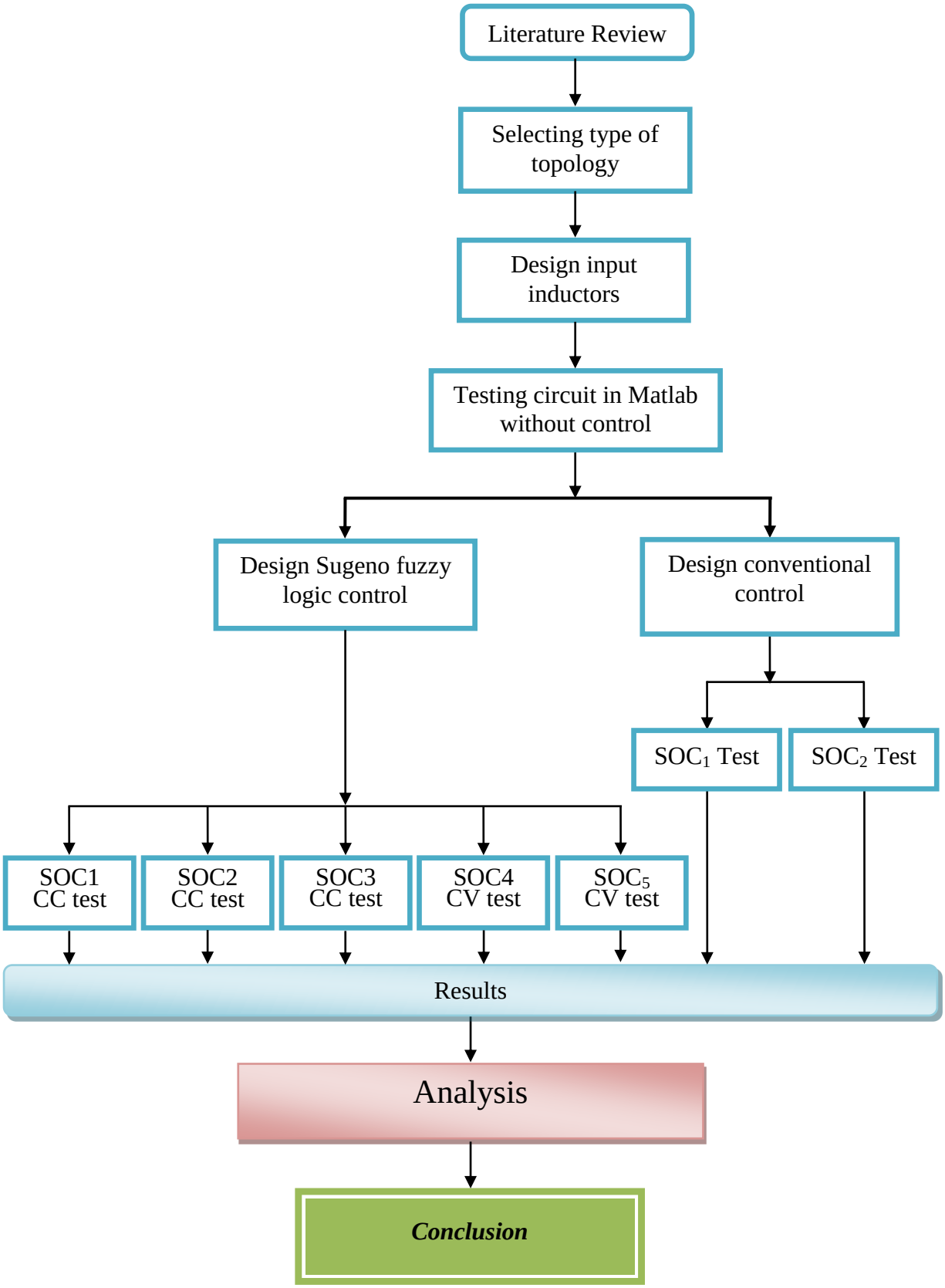

Figure 3.1: Methodology Flowchart

3.3 Operation Principle of the Phase Shifted Semi-Bridgeless Boost Topology

The phase shifted semi-bridgeless topology shown in Figure 3.2 has been proposed at reference [4] as a solution to address the problems of the conventional boost, bridgeless boost and interleaved boost topologies. As mentioned in chapter two , this topology has high efficiency features at light loads and low lines, which is critical to minimize the charger size, charging time, and the amount and cost of electricity drawn from the utility; the component count, which reduces the charger cost; and reduced EMI. The converter is ideally suited for automotive Level I, residential charging applications.

The topology introduces two more slow diodes (Da and Db) to the bridgeless configuration to link the ground of the PFC to the input line. However, the current does not always return through these diodes, so their associated conduction losses are low. This occurs, since the inductors exhibit low impedance at the line frequency, a large portion of the current flows through the FET intrinsic body diodes. Furthermore, the gating signals for FETs, are 180° out of phase.

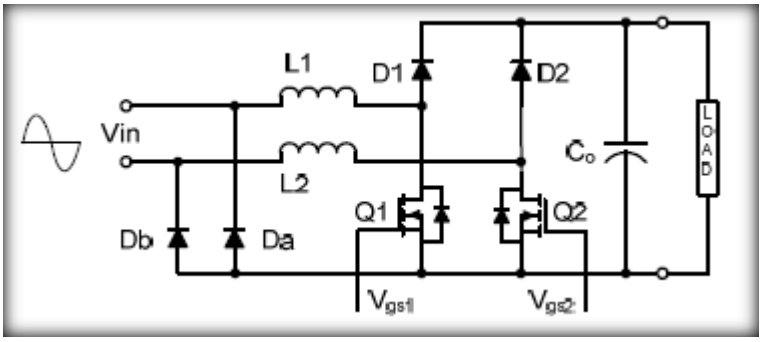

Figure 3.2: Phase shifted semi-bridgeless PFC boost topology [4]

To analyze the circuit operation, the input line cycle has been separated into the positive and negative half-cycles, as explained in the following sub-sections 1 and 2. In addition, the detailed circuit operation depends on the duty cycle. Positive half-cycle operation analysis is provided for D > 0.5 and D< 0.5 in sub-sections 3 and 4.

3.3.1 Positive Half-Cycle Operation

Based on Figure 3.1, during the positive half-cycle, when the AC input voltage is positive, the Q1 turns on and current flows through L1 and Q1, and continues through Q2 and then L2 before returning to the line. Thus, storing energy in L1 and L2. During the return process, part of the current will flow through the body diode of Q2 and partially, through Db back to the input.

3.3.2 Negative Half-Cycle Operation

Based on Figure 3.1, during the negative half-cycle, when the AC input voltage is negative, the Q2 turns on and current flows through L2 and Q2, and continues through Q1 and then L1 before returning to the line, hence storing energy in L2 and L1. When Q2 turns off, the energy stored in L2 and L1 is released as current flows through D2, through the load, and returns split between the body diode of Q1 and Da back to the input.

3.3.3 Describe Positive Half-Cycle Operation and Analysis for D > 0.5

The operation of the proposed converter depends on the duty cycle employed. During any half-cycle, the converter duty cycle is either, greater than 0.5 ($D > 0.5$) or smaller than 0.5 ($D < 0.5$). The three operation conditions of the proposed converter are provided in Figure 3.2, Figure 3.3 and Figure 3.4 for duty cycles larger than 0.5 during the positive half-cycle. The first operating condition is as illustrated in Figure 3.3 when Q1 and Q2 are ON, the input current passes through L1 and L2 to store energy in the inductors, with some current passing through Db to source. At the same time, the capacitor bank discharges into the load. When Q1 is ON and Q2 is OFF with body diode of Q2 conducting, the inductor L1will store most of the energy through Q1, and some energy is stored in L2 through the body diode of Q2. At the same time, the capacitor bank discharges through the load as illustrated in Figure 3.4. The third operating condition is as shown in Figure 3.5, when Q1 is OFF and Q2 is ON. The energy from the source is released to the load through D1, and returns to the source through Db, with some of the current returning to the source through Q2 and L2. Based on the positive half cycle operation, it can be seen that for the negative

half cycle, similar operation will occur, but instead of Db conducting current, the diode Da will conduct and D2 will release the energy to the load when Q2 is OFF and Q1 is ON.

.

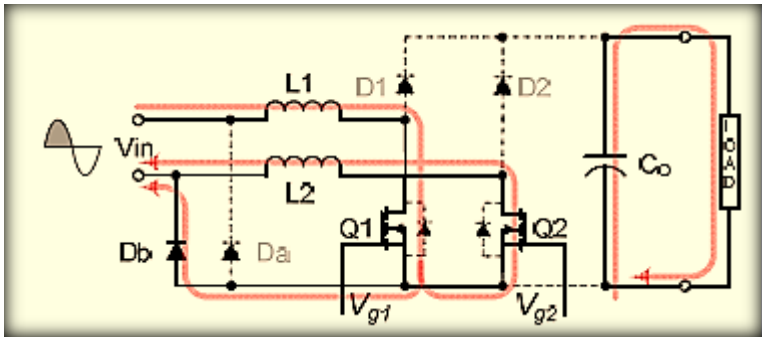

Figure 3.3: Positive-half cycle operation with D > 0.5: Q1 and Q2 are both ON

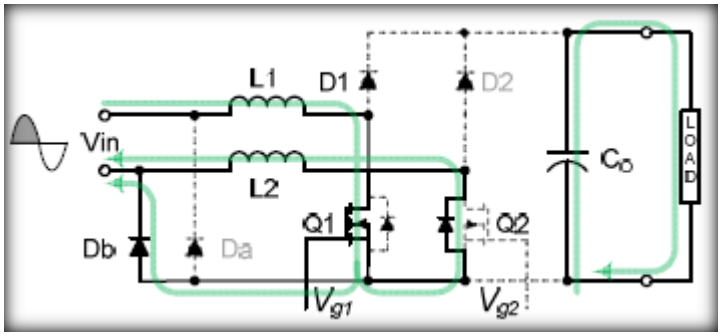

Figure 3.4: Positive-half cycle operation with D > 0.5: Q1 ON and body diode of Q2 conducting

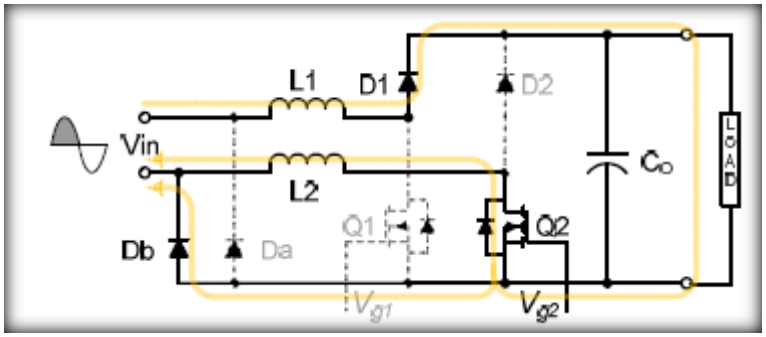

Figure 3.5: Positive-half cycle operation with D > 0.5: Q1 OFF and Q2 ON

3.3.4 Describe Positive Half-Cycle Operation and Analysis for D < 0.5

The three unique operating interval circuits of the proposed converter for duty cycles smaller than 0.5 during the positive half-cycle. The waveforms of the proposed converter during these conditions are shown in Figure 3.5. The intervals of operation are explained as follows.

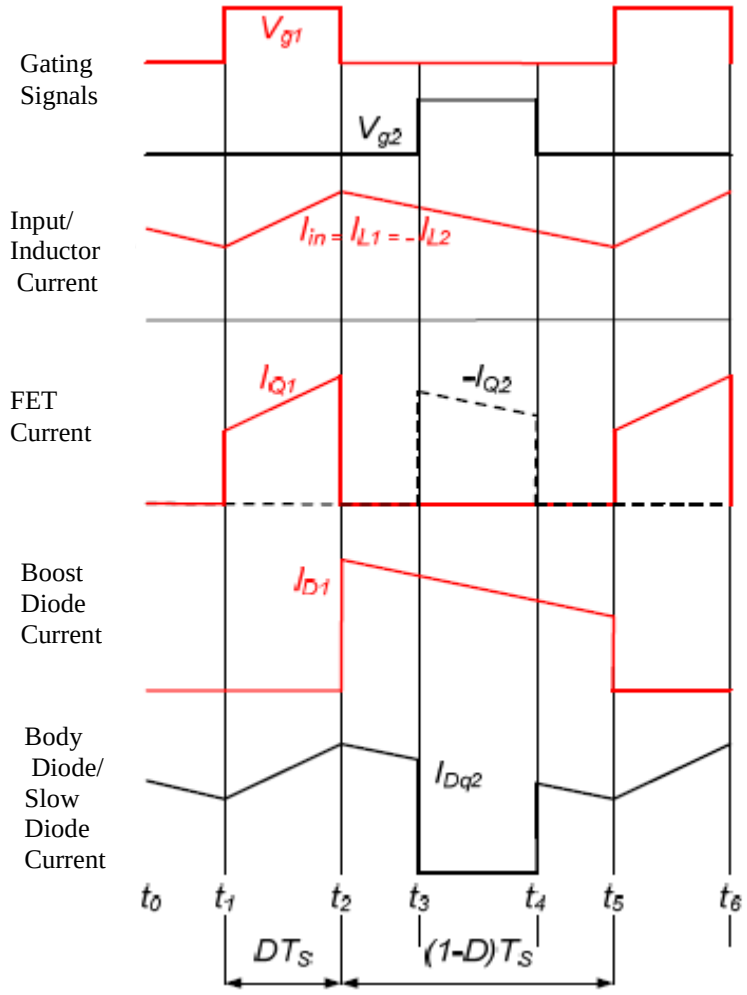

Figure 3.6: At D < 0.5 of boost converter steady state for Phase shifted semi-bridgeless [4]

Interval 1 [t0-t1]: At t0, Q1/ Q2 are off, as shown in Figure 3.6. During this interval, the energy stored in L1 and L2 are released to the output through L1, D1, body diode of Q2 and L2. The ripple currents in D1 and body diode of Q2 are the same as the ripple currents in L1 and L2.

Interval 2 [t1-t2]: At t1, Q1 is on and Q2 is off. During this interval, the current in series inductances L1 and L2 continues to increase linearly and store the energy in these inductors. The energy stored in Co provides energy to the load. The ripple currents in Q1 and the body diode of Q2 are the same as the current in series inductances L1 and L2.

Interval 3 [t2-t3]: At t2, Q1/Q2 are off again, and interval 1 is repeated, as shown in Fig. 9. During this interval, the current in series inductances L1 and L2 increases linearly and stores the energy in these inductors. The ripple currents in D1 and body diode of Q2 are the same as the ripple current in series inductances L1 and L2.

Interval 4 [t3-t4]: At t3, Q1 is off and Q2. During this interval, the energy stored in L1 and L2 is released to the output through L1, D1, Q2 and L2. The ripple currents in D1 and Q2 are the same as the ripple currents in L1 and L2. Also, during the negative-half cycle, similar operation will occur when Q1 and Q2 are both ON, body diode of Q1 will conduct (when Q1 OFF) and Q2 is ON in the negative half cycle.

Determining the values of inductors L1 and L2 depends on the amount of current ripple present at the load. Since the charging of the Li-ion battery is very sensitive towards current ripple [5], therefore the converter was designed by setting $\Delta I = 0.2$ (current ripple is less than 1.5 % for charger that can charge lithium-ion batteries, meaning less than 1.5% from current charging [47]). The values of L1 are determined using equation (3-1) for D < 0.5 and equation (3-2) for D > 0.5. The value of L2 is made equal to L1.

$$L1 = L2 \geq \frac{1}{2*\Delta}(Vo - Vin)(0.5 - D) * Ts \quad \text{..... (3-1)}$$

$$L1 = L2 \geq \frac{1}{2*\Delta}(Vo - Vin)(1 - D) * Ts \quad \text{..... (3-2)}$$

Thus, by using these two equations, Table 3.1 below presents the different values of L1 and L2 calculated at different values of duty cycle, D. From Table 3.1, the most suitable value for L1 and L2 was found to be 9mH due to it occurring repeatedly when D is 0.1 and 0.6. However, from the simulation conducted, it was found that 10 mH was the most the suitable value for L1 and L2 for the designed fuzzy logic controlled battery charger.

Table 3.1: Calculated values of L1 and L2 for different duty cycle

D	L1,L2
0.1	9 mH
0.2	6.75 mH
0.3	4.5 mH
0.4	2.25 mH
0.49	2.25 mH
0.51	11 mH
0.6	9 mH
0.7	6.74 mH
0.75	3.6 mH

3.4 Construction Triangle Signal

The triangle signal is used in the PWM system to generate the switching signals of the MOSFET by comparing the value of the triangle signal (20 KHz) with output values of the fuzzy logic control. If the triangle signal value is less than the fuzzy logic controller output value, then the switching signal becomes one, but if triangle signal value is bigger than the fuzzy logic controller output value, then the switching signal becomes zero.

Three methods were considered in this project to generate the triangle signal as explained below.

3.4.1 Discrete Virtual PLL

The discrete virtual PLL block connects the 'sin','asin' and 'Abs' blocks with the gain block as shown in Figure 3.7. The frequency of the discrete virtual PLL block is set to be half of the desired converter switching frequency. For this project, the desired converter switching frequency is 20 KHz. The problem encountered when employing this method in the project is due to the requirement of the discrete time solver for the discrete virtual PLL block which makes the simulation very slow. Hence, this method was not adopted in this project.

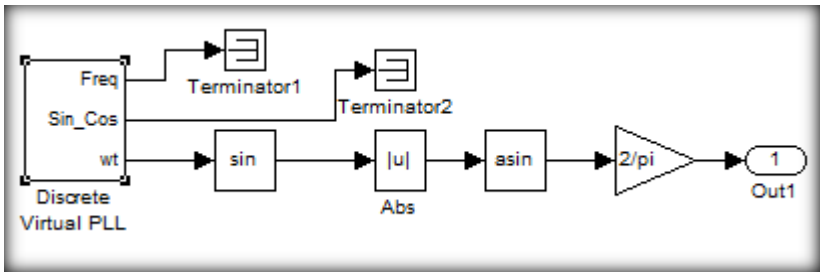

Figure 3.7: Discrete virtual PLL

3.4.2 By Coding Written in M-File

This method is effective for generating the triangle signal (see Figure 3.8) through the use of the function shown blow. This function was programmed into 'Embedded Matlab Function' block and connected with Quantizer block, used to change time interval step which is less than the periodic time. The end time depends on the end time of the simulation. Although this function is able to generate the triangle signal, this method caused all the current and voltage signals to have a discrete behavior as illustrated in Figure 3.9. Hence, this method was not adopted for this project

```
function y = fcn(t)
Amp=1;
Period=2.857e-5;
y =abs(2*Amp/pi*asin(sin(2*pi*t/Period*19900)));
```

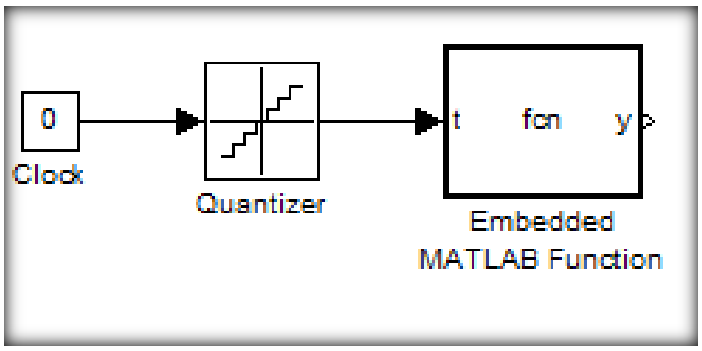

Figure 3.8: Embedded Matlab function to generate a triangle signal.

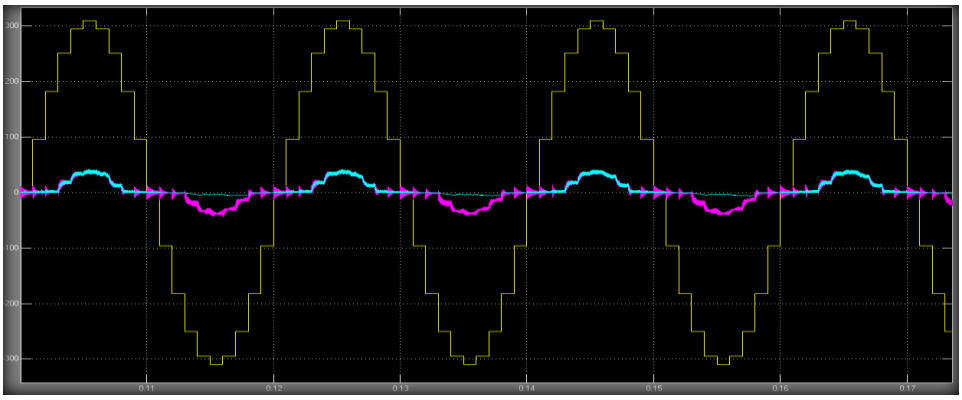

Figure 3.9: Input current, input voltage and inductor current.

3.4.3 Pulse Generator and Integrator

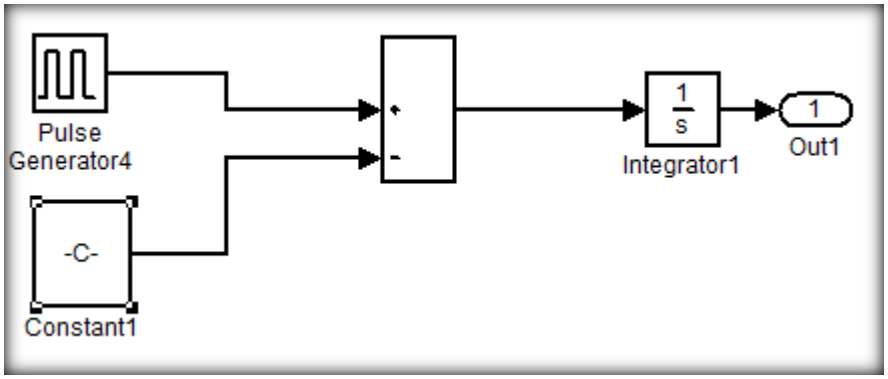

Figure 3.10 (a): Group of blocks to generate triangle signal for Vg1

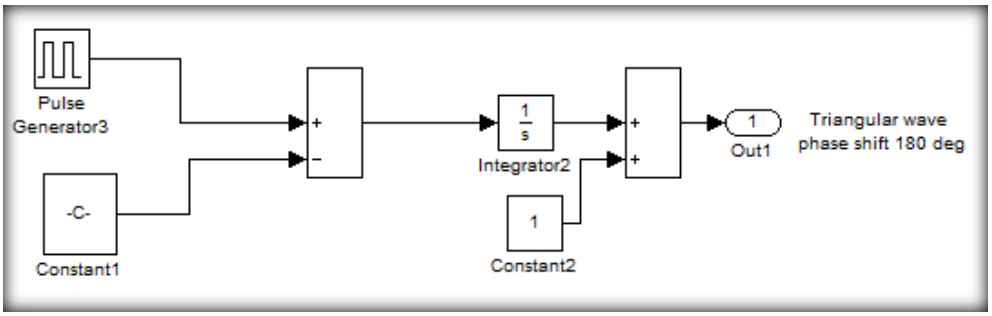

Figure 3.10 (b): Group of blocks to generate triangle signal for Vg2

Figures 3.10 (a) and (b) shows the use of a pulse generator subtracted from constant value (equal to 2*1/(1/fs)) and an integrator to generate the triangle signal with a peak value of 1 and fs represent the frequency has value equal to 20 KHz. However, for Vg2 the triangle signal was added to a constant value of 1.Also, the pulse

generator phase shift (1/(2*fs)) in Figure 3.10(b) adjusted time periodic (frequency) at pulse generator with amplitude (4*1/(1/fs)), so the outputs of fuzzy logic need to be adjusted to (0-1).This solution to generate the triangle signal was found to operate perfect in this project due to its ability to supply triangle signal (as show in Figure 3.11 below) under continuous time solver conditions with no effect on the input and output signals of the converter. Hence, this method was adopted for this project.

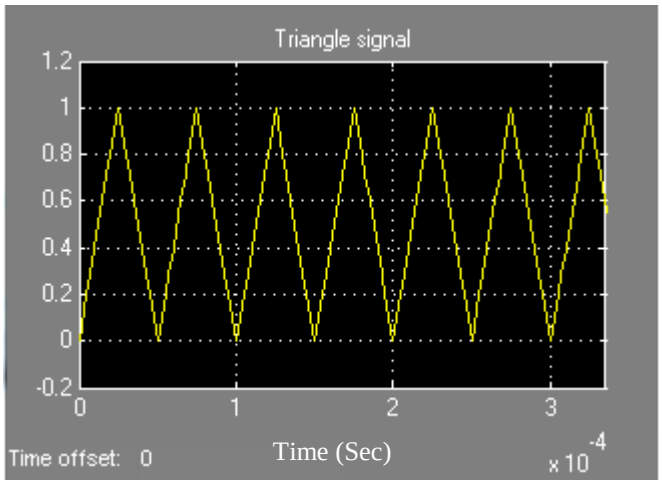

Figure 3.11: triangle signal

3.5 Design of Fuzzy Logic Controller to Control the Duty Cycle of Phase Shifted Semi-Bridgeless Boost Converter

The following is the required procedure to design a fuzzy logic control system:

1. Set the input membership functions.
2. Set the output membership functions.
3. Set the fuzzy rules.
4. Determine the intersection or Union method.
5. Determine the implication method.
6. Determine the aggregation method
7. Determine the defuzzification method

In fuzzy logic control system, there are two methods to aggregate the output of the fuzzy logic control which are the Mamdani and Sugeno methods. In the Mamdani method, the output fuzzy logic is independent of the input to the fuzzy logic system with the output being determined by functions such as'trimp', 'trapmf', 'gbellmf', 'gaussmf' and etc. In contrast, the Sugeno method has two types of outputs; constant

value and linear function; which are dependent on the input to the fuzzy logic system.

For this project, proposed Sugeno fuzzy logic controller will be designed to control the phase shifted semi-bridgeless converter to charge a Li-ion battery.

3.6 Sugeno Fuzzy Logic Control

The Sugeno fuzzy logic controller is designed to control the phase shifted semi-bridgeless converter topology for charging of a Li-ion battery load. In this designed controller, the Sugeno method in fuzzy logic is employed instead of the Mamdani method. This is because as the battery load voltage must be charged up to the desired voltage. In this case, the proposed method charges the 108 cell Li-ion battery from 220V (where 220V corresponds to 2.037V /cell) up to 422V (where 422V corresponds to 3.9V/ cell). In order to achieve this, the duty cycle must be changed depending on the initial SOC of battery level to keep charging current constant during the battery charging process. Therefore, the duty cycle depends on the SOC of the battery. For this reason, the Sugeno method is employed to control the battery charging, because in the Sugeno method the output of the fuzzy system is dependent on the input of the fuzzy system. For the battery charging case, there are two inputs to the fuzzy logic control system battery voltage (Vb), and state of charge (SOC) of the battery. With one output is duty cycle.

Vg1 generated by compared 20 KHz frequency triangle (refer to Figure 3.10 (a), and Figure 3.11) wave with output fuzzy logic , and Vg2 generated by compared 180 phase shift 20 KHz frequency triangle(refer to Figure 3.10 (b)) wave also with output fuzzy logic, which become input to gates pulses of MOSFITS.

3.6.1 Input 1: Battery Voltage

The first input of the fuzzy logic controller is the measured battery voltage. This input has two membership functions which are 'charge' and 'full', using the tramp functions as illustrated in Figure 3.12 below.

Charge (a) is between 0 to 400 (trapmf fun.).

$$\text{So, charge (a)} = \begin{cases} \frac{a}{10} & 0 \le a \le 10 \\ 1 & 10 < a \le 380 \\ \frac{a-400}{-20} & 380 \le a \le 400 \end{cases}$$

full (a) function is between 400 to 450

$$\text{So, full (a)} = \begin{cases} \frac{a-400}{20} & 400 \le a \le 420 \\ 1 & 420 < a \le 450 \end{cases}$$

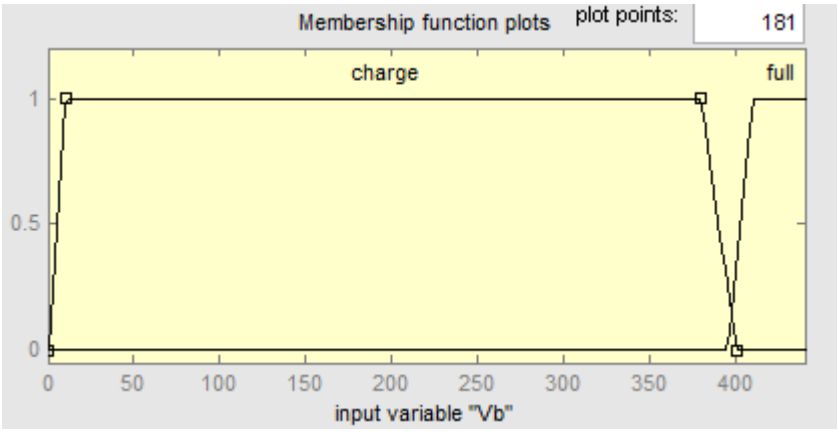

Figure 3.12: Input membership function of battery voltage

3.6.2 Input 2: State of Charge of Battery

The second input to the fuzzy logic controller is the battery SOC, which is a variable value ranging from 0 to 100% based on the observation conducted, the duty cycle and charging current are related to each other, depending on value of battery voltage. For this project, the 220 V initial voltage of battery is the same as input supply RMS voltage. Therefore, the converter does not have to boost the voltage, due to input voltage being same as output voltage at the start of the simulation and the duty cycle is adjusted close to zero. As the simulation progresses, the duty cycle is increased in

two stages: linearly with times and nonlinear with time. Therefore, twenty membership functions have been distributed from 10 to 100, close to each other from first membership function until 18th membership function, as shown in Figure 3.13 below.

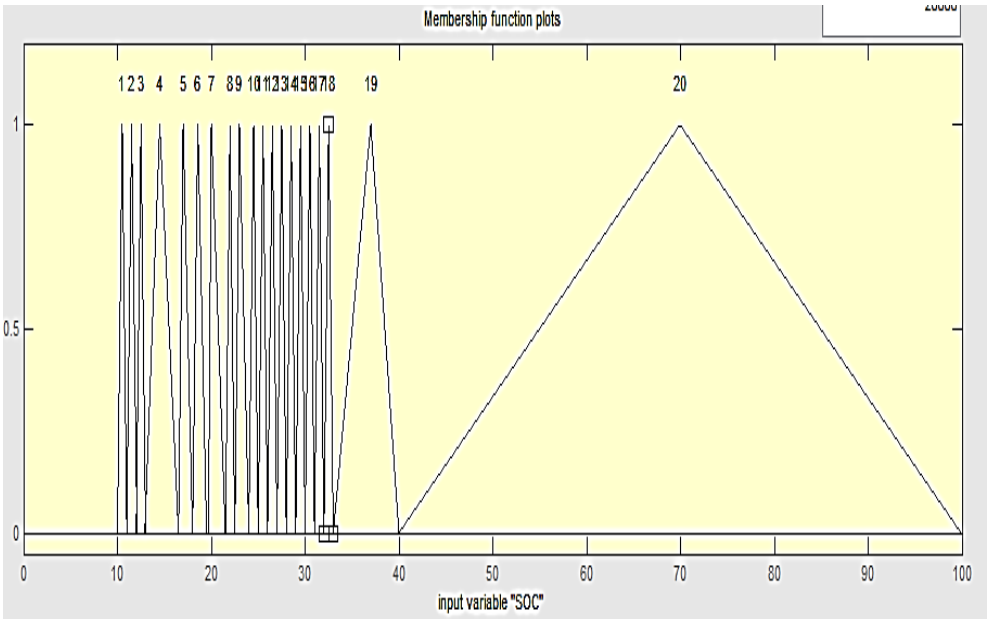

Figure 3.13: Membership function of SOC

3.6.3 Duty Cycle (Output of Fuzzy Logic)

As mentioned, the output of the Sugeno fuzzy logic controller designed in this project depends on the SOC of the battery. Therefore, the output membership function is linear function and is adjusted relative to the value of SOC and independent to the battery voltage. In the Sugeno method, the linear function can be adjusted through three constant parameters a, b and c depending on equation (3-3) below:

D (output of Sugeno fuzzy logic) = a*x1+b*x2+c ……. (3-3)

Where:-

x1 is first input of fuzzy logic, x2 is second input of fuzzy logic

a, b and c are constant values.

In our case put a = 0, so b and c are adjusted depending on the levels of battery SOC according to table 3.2. The rules for the fuzzy logic controller for battery charging can be obtained in Appendix A.

Table 3.2: Values of b and c parameter with respect to output membership functions of the designed Sugeno fuzzy logic controller

Membership functions of output	values of b	Values of c
1	0.0015	0
2	0.0175	0
3	0.031	0
4	0.03	0
5	0.033	0
6	0.035	0
7	0.032	0
8	0.028	0
9	0.024	0
10	0.025	0
11	0.0219	0
12	0.0218	0
13	0	0.42
14	0.034	0
15	0	0.4

3.7 Summary

This chapter had described the functionality of the phase shifted semi bridgeless boost converter topology, in which the circuit contains two MOSFETS and four diodes, with two inductances and a capacitor bank. The method to generate the PWM switching signals for the MOSFETS, by comparing a triangle signal with the output from the fuzzy logic controller was also presented. Finally, the design of Sugeno fuzzy logic controller for the phase shifted semi-bridgeless boost converter, Sugeno method employed to charge a Li-ion battery with two inputs; battery voltage and battery state of charge. For the Li-ion battery charging application, the fuzzy logic controller was designed to perform constant current (CC) and constant voltage (CV) charging strategies whereby constant current charging is adopted from the start of the charging process until the battery reaches close to the desired voltage before transferring to the constant voltage charging in which the charging current decreases to zero and the charging process is terminated. Simulation of the designed controllers will be presented in the next chapter.

CHAPTER 4

RESULTS AND DISSCUSION

4.1 Introduction

In this chapter the simulation results of the phase shifted semi-bridgeless boost converter topology controlled using the designed fuzzy logic controllers will be presented. Firstly, the simulation results for PI controlled boost converter system to charge a Lithium-ion battery is presentd. Secondly, the simulation results for the fuzzy-logic controlled boost converter system to charge a Lithium-ion battery is presented. The Lithium-ion battery chosen for the simultion is constructed from 108 Lithium-ion cells, with each cell having a charging voltage of 3.7V and a discharging voltage of 2.5V. Figure 4.1 illustrates the NCR18650A battery characteristic [48, 49] of the chosen battery.

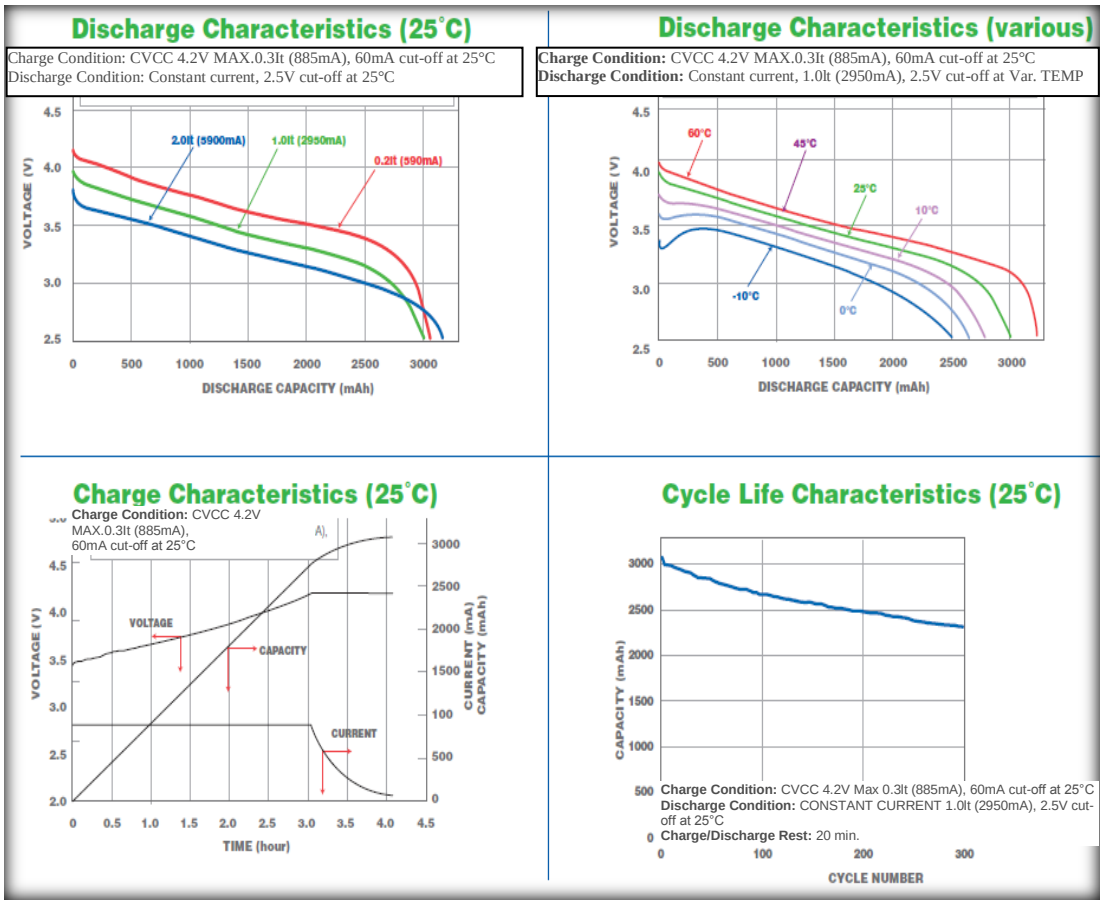

Figure 4.1: Discharge, charge and cycle life characteristics of the Lithium-ion battery chosen for the simulation [48, 49]

State-of-charge (SOC) estimation is one of the most important issues in battery applications. Accurate SOC estimation of the battery power can avoid unpredicted system interruption and prevent the batteries from being over-charged and over-discharged, which may cause permanent damage to the internal structure of batteries. The coulomb counting method is practical for state-of-charge (SOC) estimation of lithium-ion batteries with high charging and discharging efficiencies. The charging and discharging characteristics are examined and reveal that the coulomb counting method is convenient and accurate for estimating the SOC of lithium-ion batteries. The coulomb counting method calculates the remaining capacity simply by accumulating the charge transferred in or out of the battery. This method, requiring long time monitoring and memorizing, was thought to be impractical for real-time SOC estimation but critical in verifying the accuracy of estimated results from other methods. Nevertheless, the recent applications of battery power in many portable

devices and electric vehicles [50]. But in this dissertation we get SOC direct from battery measurements in simulation.

4.2 Lithium-ion Battery Load Charging Results (active load)

In order to simulate the application of the designed Sugeno fuzzy-logic controlled phase shifted semi-bridgeless boost converter to charge a lithium-ion battery, the battery parameters as shown in Figure 4.2 must be entered into the battery model in Matlab , the values of parameters are relative to the number of cells connected in series and in parallel. In this dissertion the Li-ion battery used is based on the NCR18650A battery with characteristics showed previously in Figure 4.1.

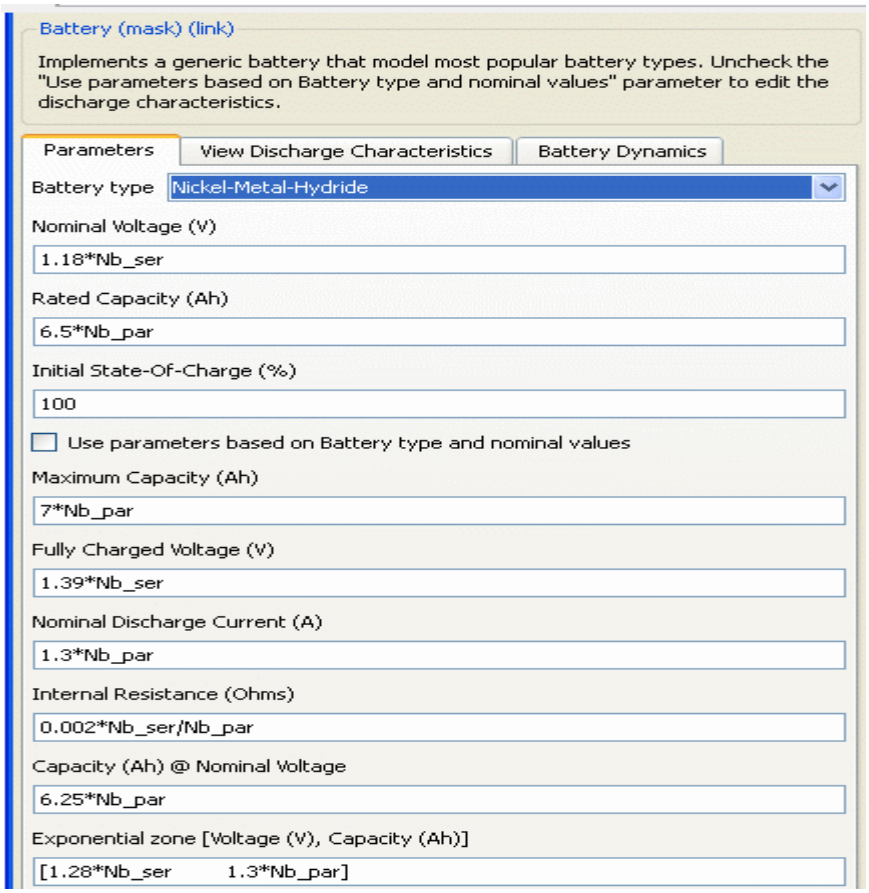

Figure 4.2: Sample of battery parameters to be entered in Matlab.

For the battery proposed in this dissertation, the battery type is Li-ion and the nominal battery voltage is 399.6V during discharge mode, and 270V during charging

mode. Hence, all battery parameters as shown in Figure 4.2 were adjusted in Matlab using the values shown below for the Li-ion battery which will be simulated.

Nb_ser (number of cells in series) = 108

Nb_par (number of cells in parallel) = 21

Nominal voltage per cell = 3.7V (Li-ion battery) (referring to figure 4.1)

Nominal voltage terminal = 3.7 * 108 = 399.6V

Rated capacity (Ah) = 5.95*21 = 125Ah

Initial SOC % = variable

Maximum capacity = 7*21 = 147Ah

Fully charged voltage 3.91* 108 = 422.28V

Nominal discharge current = 2.95*21 = 61.95A

Internal resistance = 0.002*108/21 = 0.01028 ohm

Capacity (Ah) @ nominal voltage = 5.7* 21 = 119.7

Exponential zone = [3.8*108 2.95*21] = [410.4 61.95]

For charging mode same adjustment except

Nominal voltage terminal = 2.5 * 108 = 270V

Internal resistance = 0.002*108/21 = 0.01028

Capacity (Ah) @ nominal voltage = 5.7* 21 = 119.7

Exponential zone = [3.8*108 2.95*21] = [410.4 61.95]

For charging mode same adjustment except

Nominal voltage terminal = 2.5 * 108 = 270V

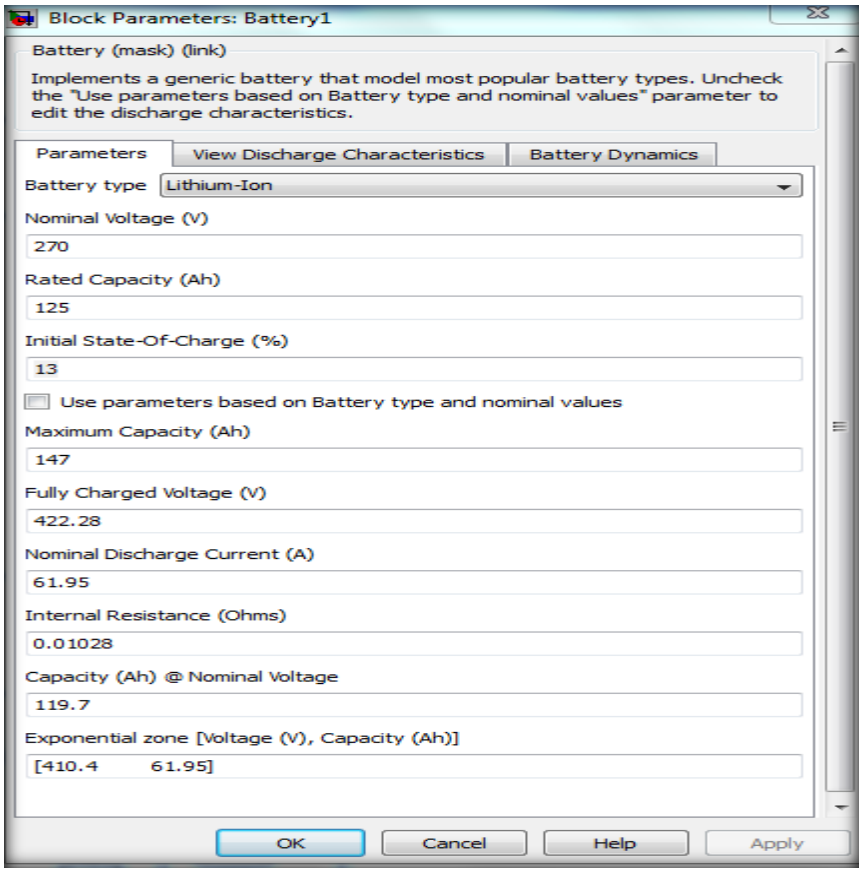

Figure 4.3: Lithium-Ion battery parameter employed in the simulations.

4.3 Charging of the Proposed Li-ion Battery Directly from a DC Source

The circuit shown in figure 4.4 was employed to simulate the Lithium-ion battery directly from a DC source through a 2 ohm resistor. Hence, this battery needs to charge until the battery voltage reaches 399.6V. Results shown in Figure 4.5 shows the charging profile of the battery for the case of 10% SOC starting battery which corresponds to a starting battery voltage of 207.61V and starting current of 96.1A. Figure 4.6 shows the charging profile with initial battery SOC of 20%, corresponding to initial battery voltage of 360.2V and starting current of 28.3A. The results from the third case simulated are illustrated in Figure 4.7 for the condition of 30% initial battery SOC whereby the battery voltage starts charging from 388.42V with 5.37A starting current. These results indicate that when the initial battery SOC increases, the starting current decreases. Furthermore, as observed in the results, the battery becomes fully charged (reaching a voltage of 399.6V) within 4 hours in all cases

except for the third case in which charging is complete within 3 hours and 45 minutes due to the higher initial battery SOC. At the end of the charging process, the current decreases to zero. But in Sugeno system observed the simulation in Matlab can not run for long time due to using fuzzy logic control with the converter topology.

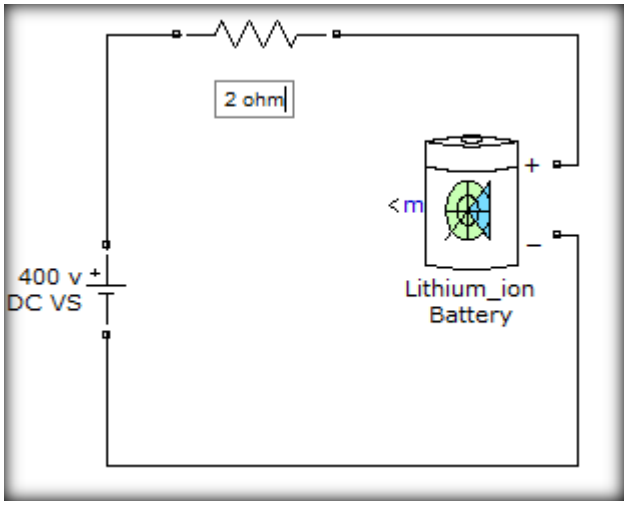

Figure 4.4: Simulation circuit to charge the Li-ion battery directly from a DC source.

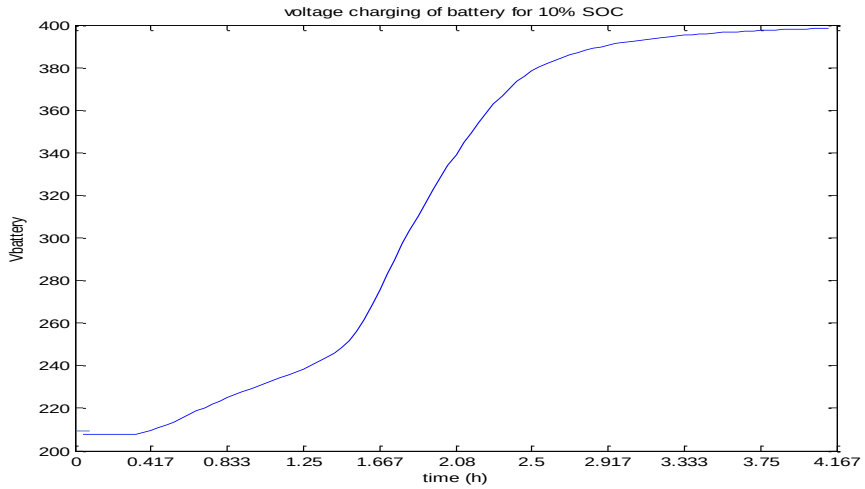

Figure 4.5 (a): Battery voltage charging profile for initial battery SOC of 10%.

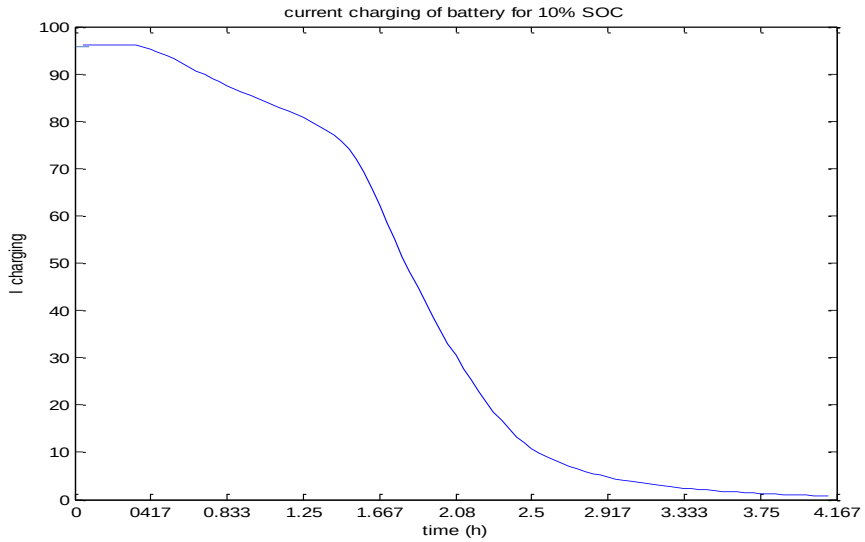

Figure 4.5 (b): Charging current for initial battery SOC of 10%.

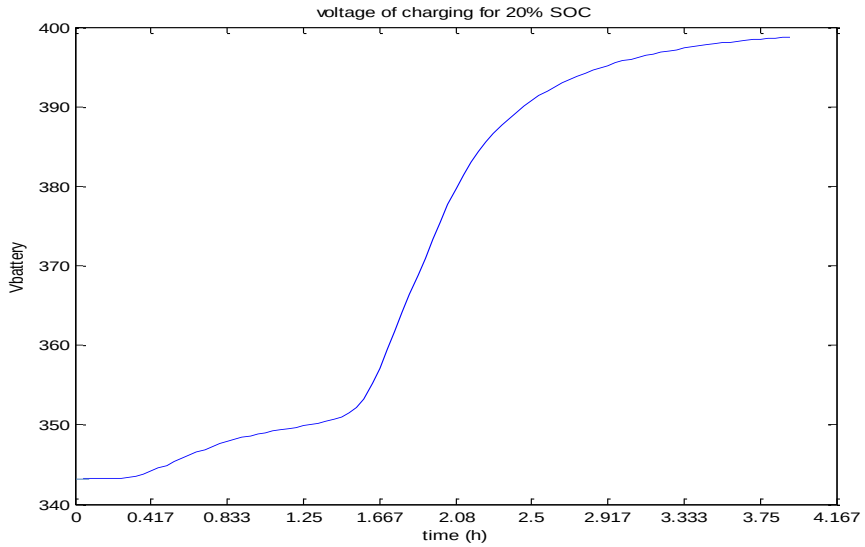

Figure 4.6 (a): Battery voltage when charging directly from a DC source with initial battery SOC of 20%.

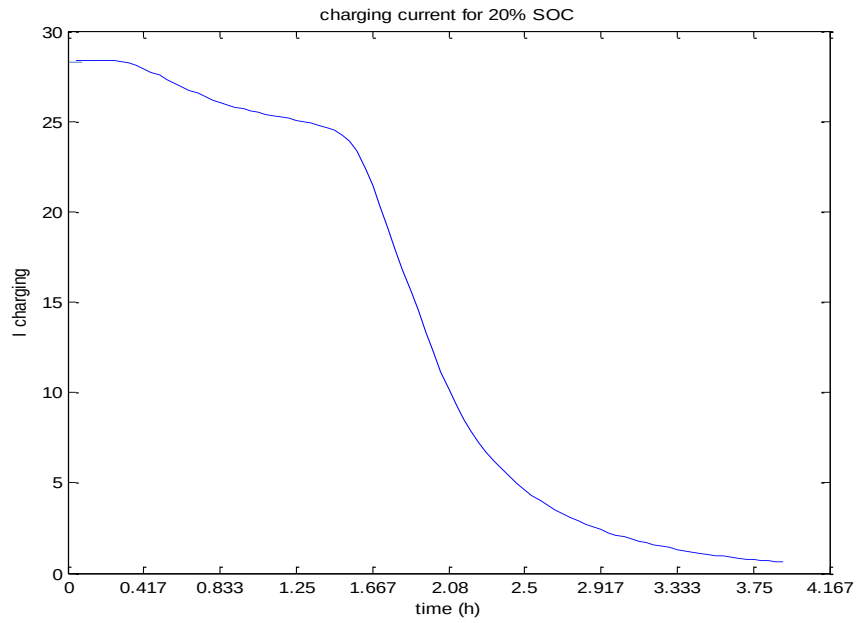

Figure 4.6 (b): Current behavour during charging process with initial battery SOC of 20%.

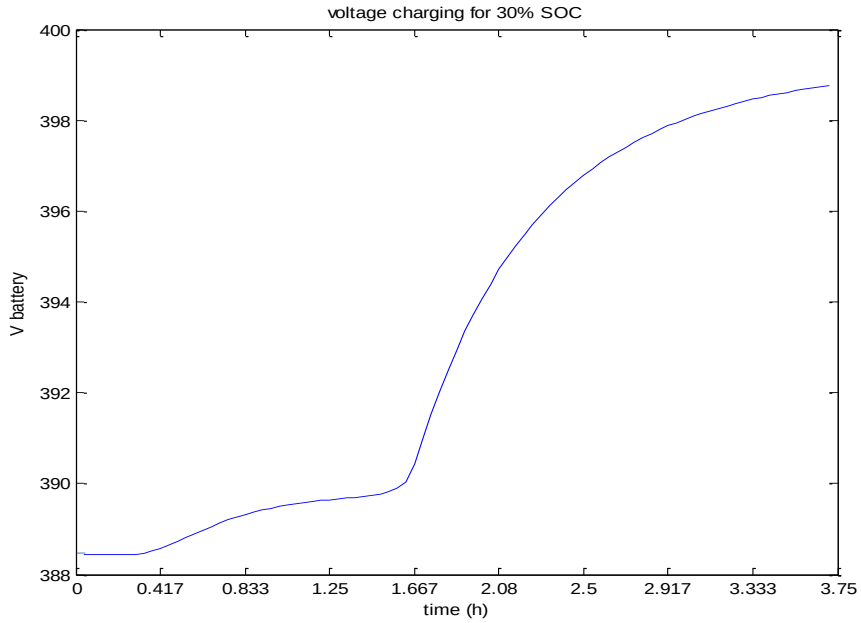

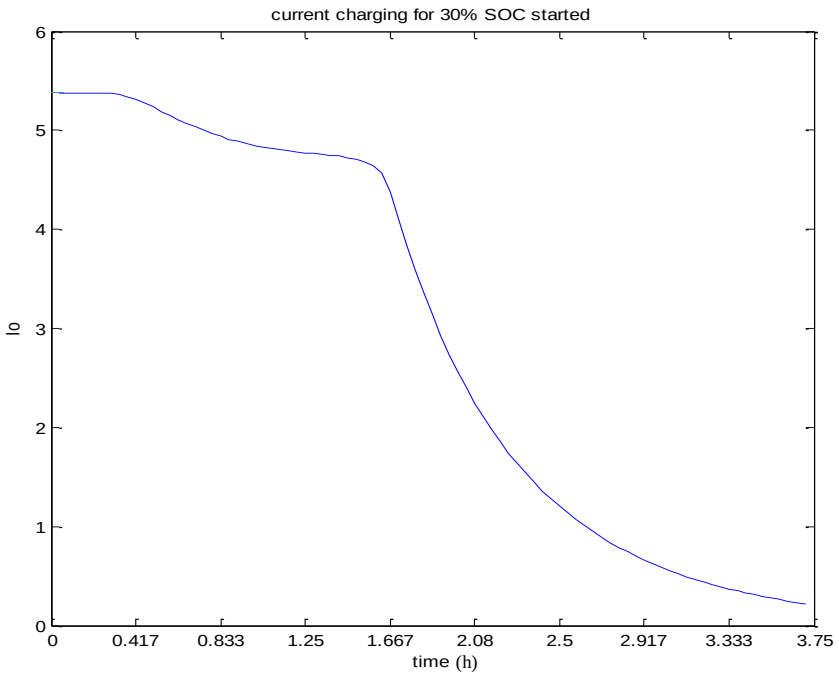

Figure 4.7 (a): Battery voltage charging profile for initial battery SOC of 30%.
Figure 4.7 (b): Charging current for initial battery SOC of 30%.

4.4 Charging of the Proposed Li-ion from a Single-Phase AC Source Through a Fuzzy-Logic Controlled Phase Shifted Semi-Bridgeless Boost Converter

The same Li-ion battery explained previously can be charged from a single-phase AC supply through the phase shifted semi-bridgeless boost converter designed previously in Section 3.3. In order to reduce the ripple voltage at the load, an inductance was added in series with the battery. In addition, a diode is also added in series with the battery to make sure the battery does not discharge through the boost converter as shown in Figure 4.8. In this dissertation, the converter is tested in two controller PI (conventional control) and Sugeno fuzzy logic control for compering between them. The highlighted circle in Figure 4.8 designed in two ways as illustrated in Figure 4.9 and Figure 4.10. In PI controller using feedback of SOC to control the charging, but for sugeno controller has the battery voltage and battery SOC feedback that measured and given as input to the designed Sugeno fuzzy logic controller which controls the switching of the MOSFETs in the boost converter as explained in Section 3.6. The fuzzy-logic controller, shown in Figure 4.10, operates

such that at any initial battery SOC, the duty cycle during the start of the charging process is 20% of the duty cycle determined by the fuzzy logic system. This is implemented using the relay switch shown in Figure 4.10.

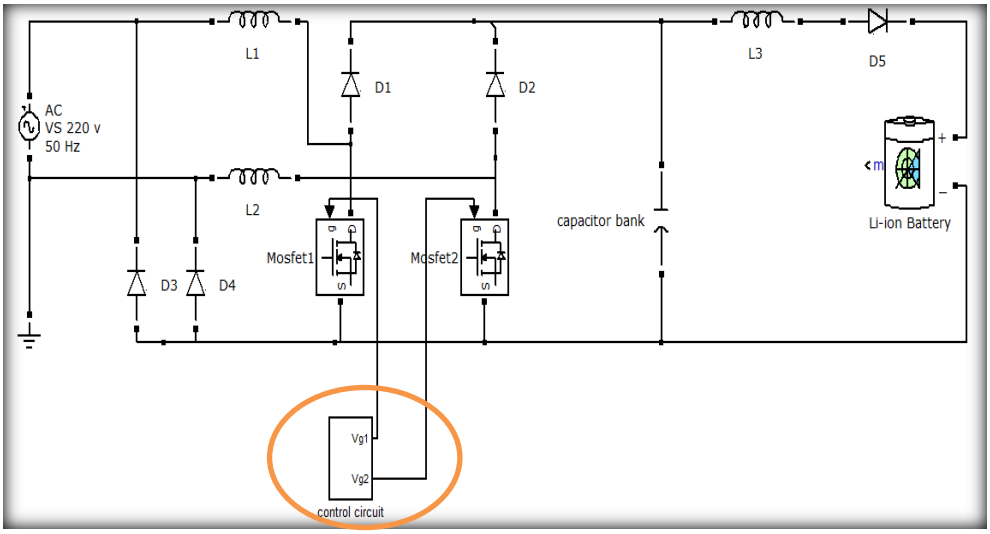

Figure 4.8: phase shifted semi-bridgeless boost converter circuit employed for charging of a Li-ion battery.

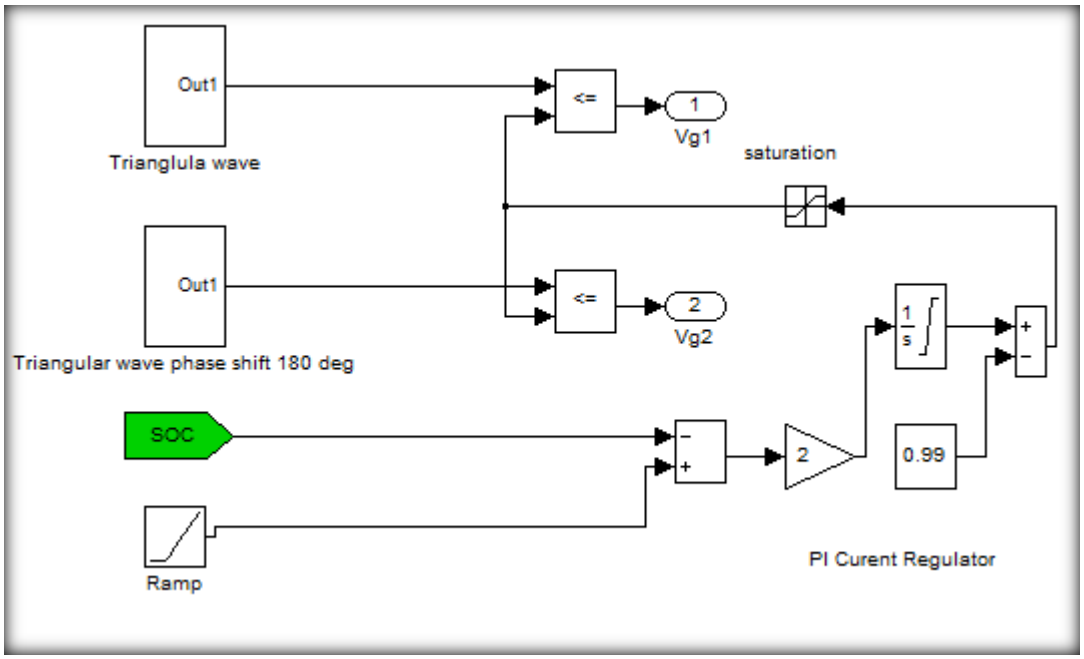

Figure 4.9: The designed PI controller as conventional control which determines the switching duty cycle of the boost converter to charge a Li-ion battery load.

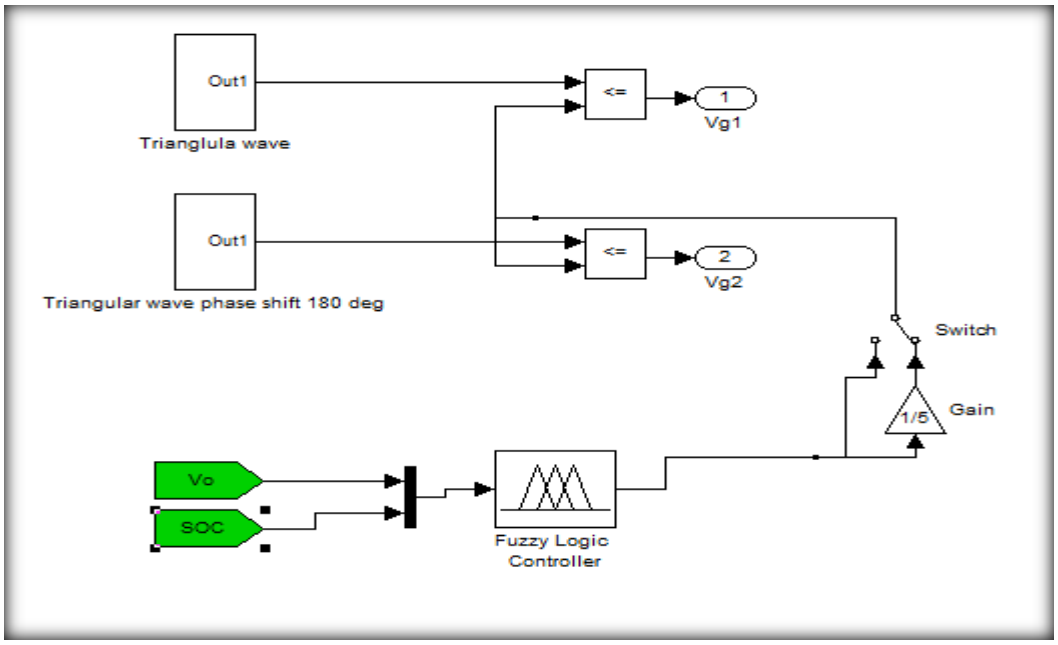

Figure 4.10: The designed fuzzy-logic controller which determines the switching duty cycle of the boost converter to charge a Li-ion battery load.

4.5 PI Conventional Control

PI controller is a conventional controller as shown up in Figure 4.9, PI result is compared with Sugeno fuzzy logic control. This controller needs two extra sources Ramp source and constant source. By comparing between SOC and Ramp function then input to integral function with subtracted from 0.99 constant value, after that have to compare with two triangle signals to create Vg1 and Vg2 pulse with modulations. When SOC increase, the duty cycle has increased because extra energy need to allow of current continue with constant current. The simulation results for PI controller are shown in item 4.7 below.

4.6 Sugeno Fuzzy Logic Control

As mentions the way of control duty cycle in Sugeno fuzzy logic need feedback battery voltage and SOC that become as inputs to fuzzy logic, then by fuzzy rules can get good results for the simulation. The fuzzy-logic controlled boost converter was employed to charge the Li-ion battery with an initial SOC of 10.5% which corresponds to a 220V initial battery voltage under constant current condition until the battery voltage reaches 395V. Once the battery voltage charges up to 395V, the fuzzy-logic controller will shift to constant voltage charging strategy whereby the charging current will be reduced to zero until the charging process is stopped at 422V. The results of Sugeno fuzzy logic control shows in item 4.7 results comparing between PI and fuzzy logic controller below.

4.7 Results comparing between PI (conventional) and Sugeno fuzzy logic controller

From input current in Figure 4.11 below showed (at PI controller) over current is 170A meaning 4.25 times from steady state of input current that draw high starting current with 0.04 sec transit time, but absorbed from Figure 4.12 (for Sugeno Controller) the input over current reduced (with respect to conventional control) to 110A that represent 2.75 times of steady state of input current for very short transit time 0.02 sec

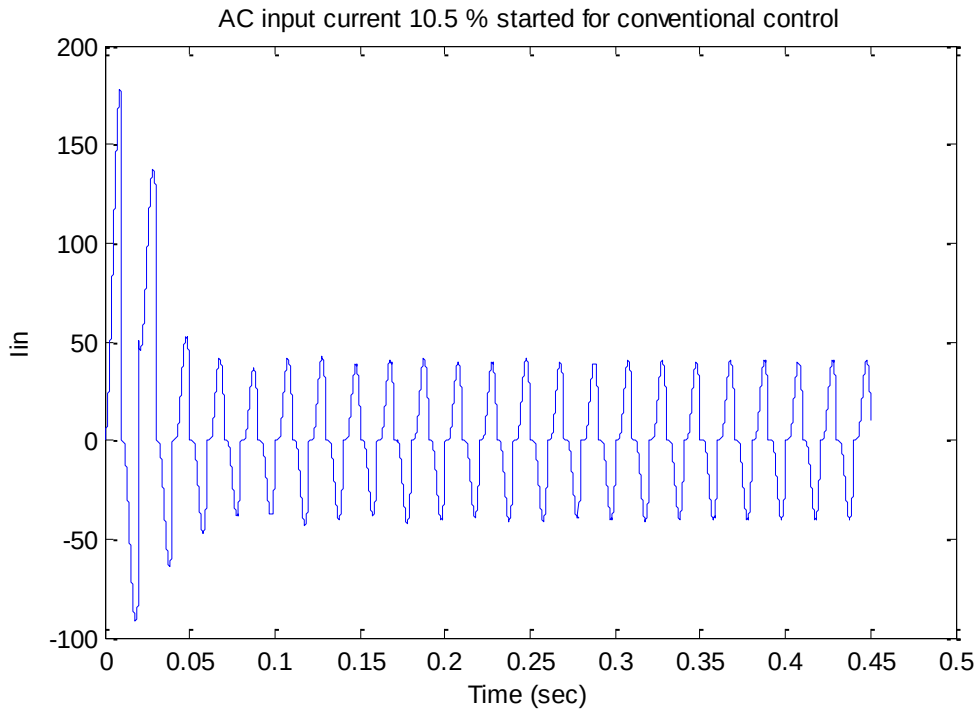

Figure 4.11: AC input current observed from the Li-ion battery charging simulation using the conventional controlled (PI) boost converter (current in ampere and time in sec).

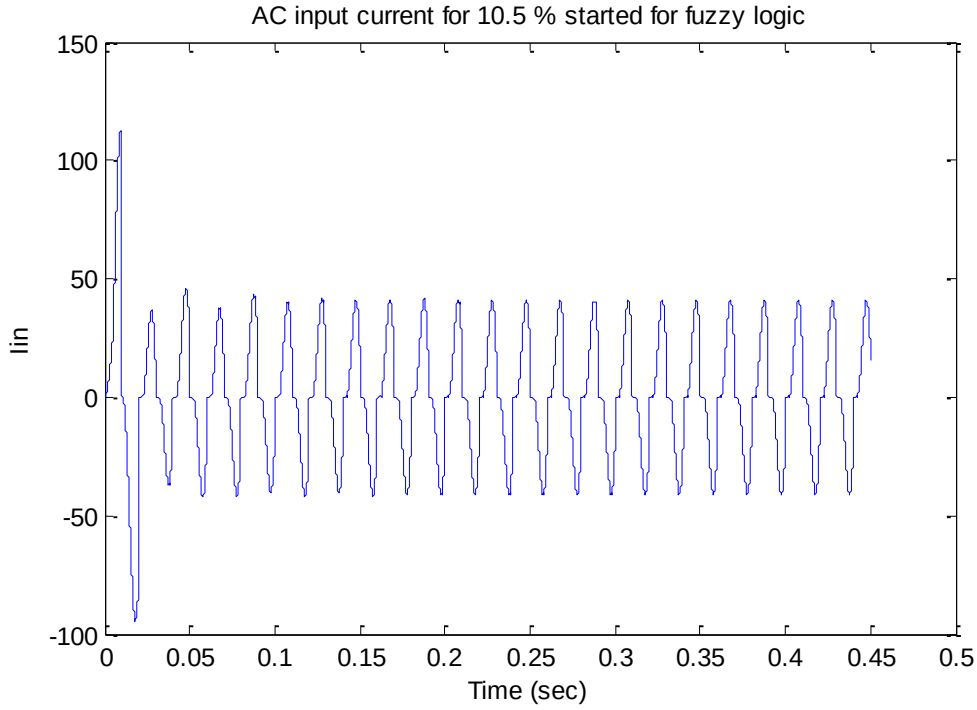

Figure 4.12: AC input current observed from the Li-ion battery charging simulation using the fuzzy-logic controlled boost converter (current in ampere and time in sec).

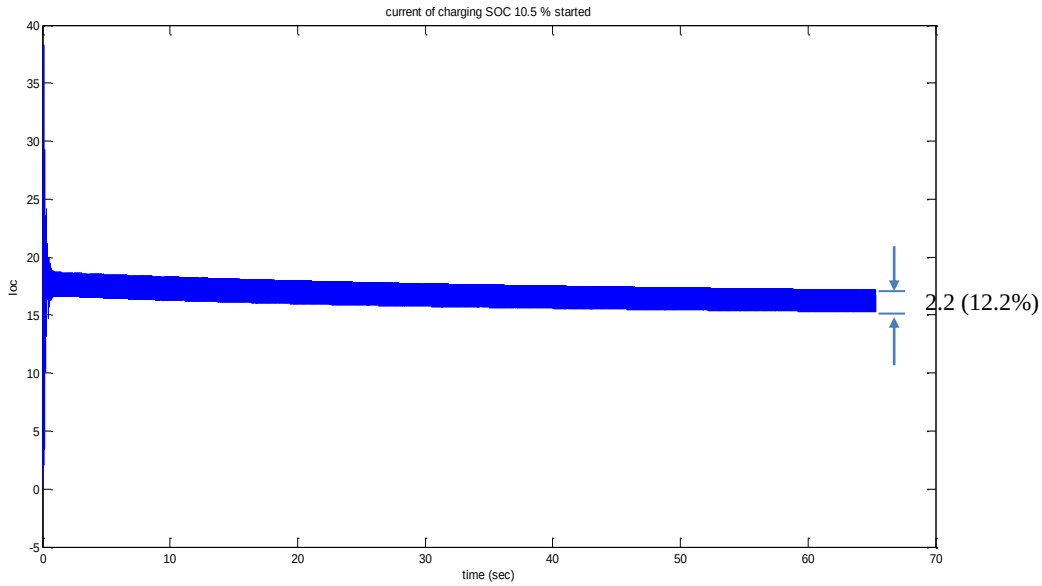

Figure 4.13: Charging current obtained for PI control from the simulation for the case of 10.5% initial battery SOC (current in ampere and time in sec).

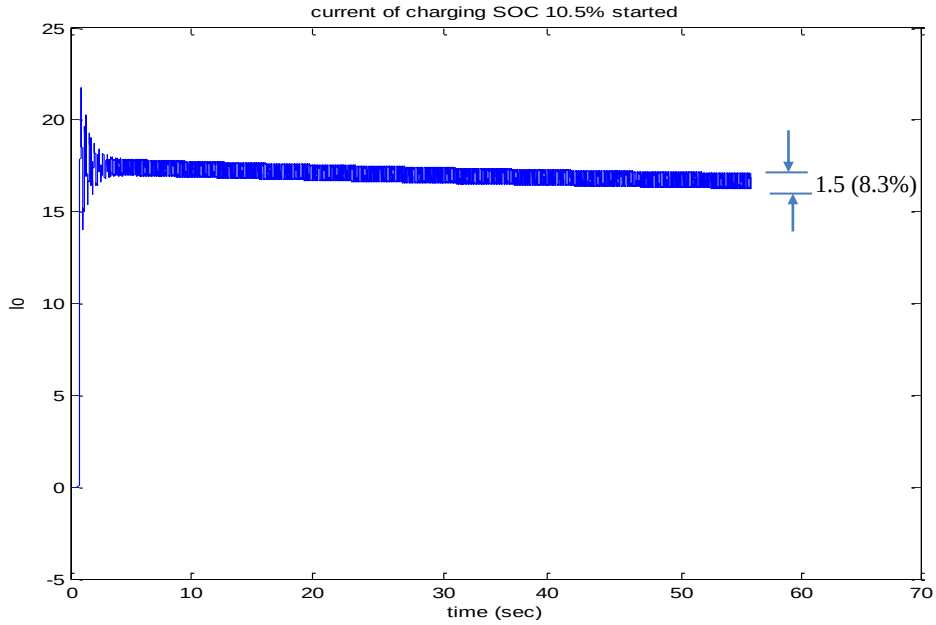

Figure 4.14: Charging current obtained for fuzzy logic control from the simulation for the case of 10.5% initial battery SOC (current in ampere and time in sec).

For the case of 10.5% initial battery SOC observed from Figure 4.13 as showed above (at PI controller) the current performance has over current reach to 38A meaning 2.1 times from steady state charging current that drawing 18A constant current, this charging current has 2.2 ripple current (12.2% charging current).

Conversely, at fuzzy logic controller above the over current (showed in Figure 4.14) reach to 22A meaning 1.2 times steady state charging current that drawing 18A constant current. This charging current has 1.5 ripple current (8.3% from charging current). The ripple current less than standard value 1.875A (10.4%) for 125Ah that proposed in this project. Battery manufacturers have specified that more than about 1.5 A rms of ripple for every 100Ah of battery capacity will effect on battery [51].

The battery voltage during the start of the charging process is 220V which is the same as the RMS voltage of the AC supply. Hence, the duty cycle obtained from the controller was very small (near to zero) due to the converter not required to boost the input voltage. Another observation from the simulation is that the battery voltage increases at a higher rate during the start of the charging process as compared with the later part of the simulations shown by the voltage convexity shape illustrated in Figure 4.15 and Figure 4.16. In Figure 4.17 below (for PI controller) observed the over voltage in battery charging is 0.4V, and voltage charge until 226.9V (shown in Figure 4.15 below). In the other hand, (for fuzzy logic controller) observed from Figure 4.18 the over voltage in battery charging is 0.2V represent half value in PI controller, and voltage charge until 227.1V (shown in Figure 4.16 below). The battery SOC was seen to increase during the simulation which proves that the designed fuzzy-logic and PI controlled boost converter are charging the battery as shown in Figure 4.19.

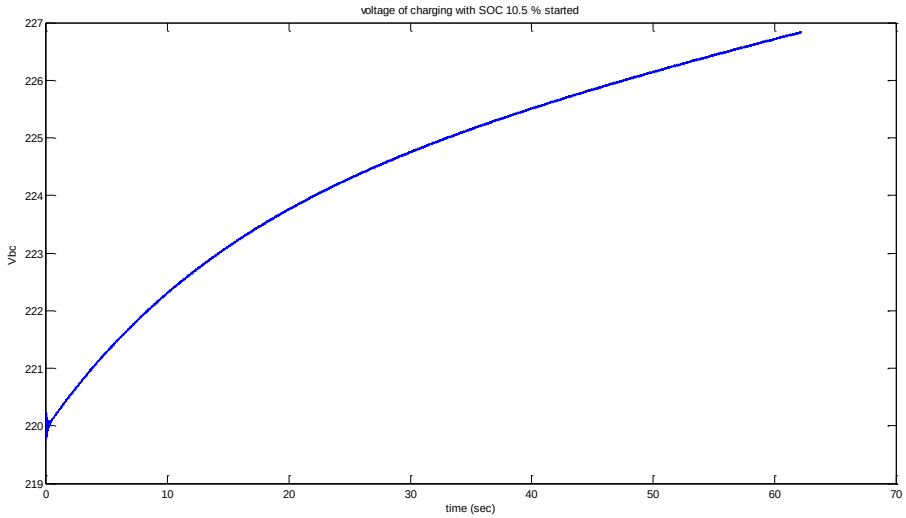

Figure 4.15: Voltage of the battery for PI control during the charging process for the case of 10.5% initial battery SOC(voltage in Volt and time in sec).

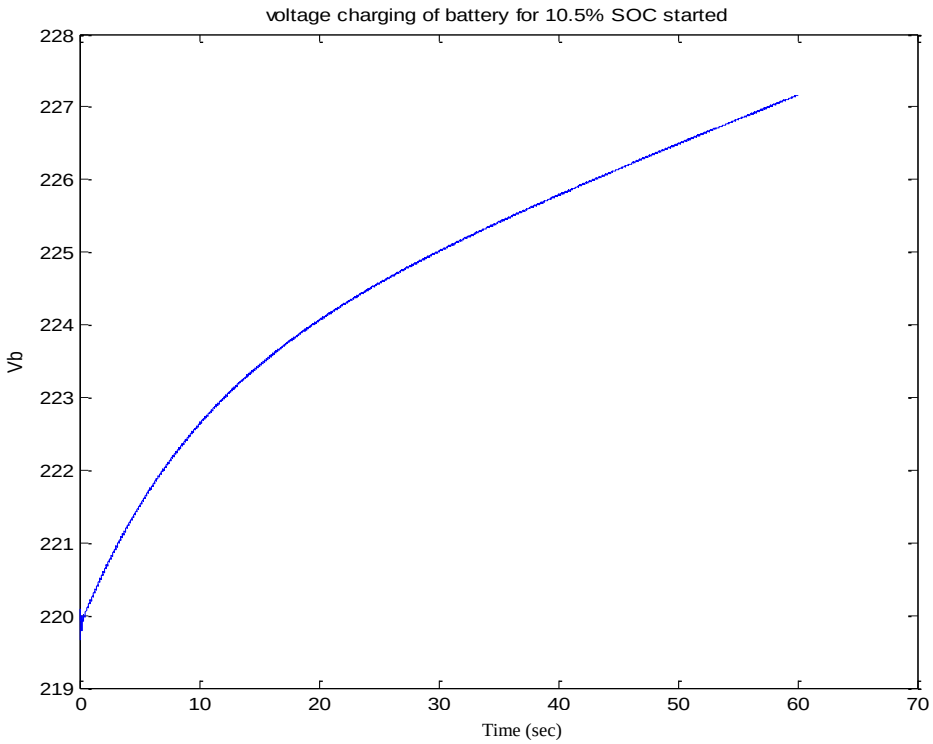

Figure 4.16: Voltage of the battery for fuzzy logic control during the charging process for the case of 10.5% initial battery SOC(voltage in Volt and time in sec)

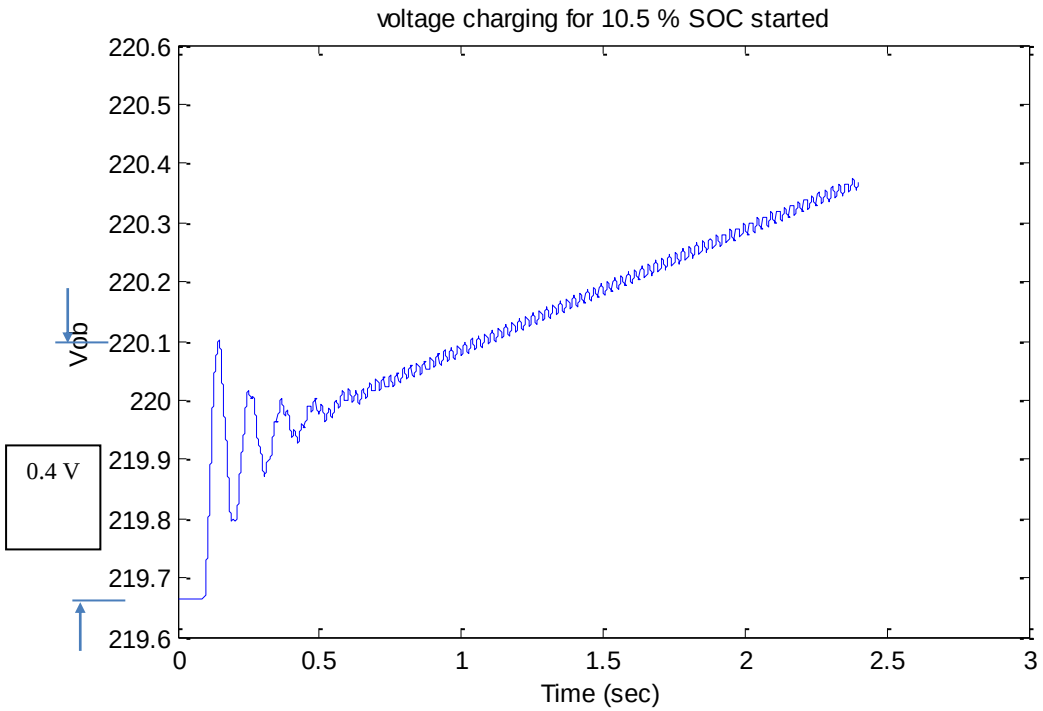

Figure 4.17: For short time voltage of the battery for PI control during the charging process for the case of 10.5% initial battery SOC to show overvoltage (voltage in Volt and time in sec)

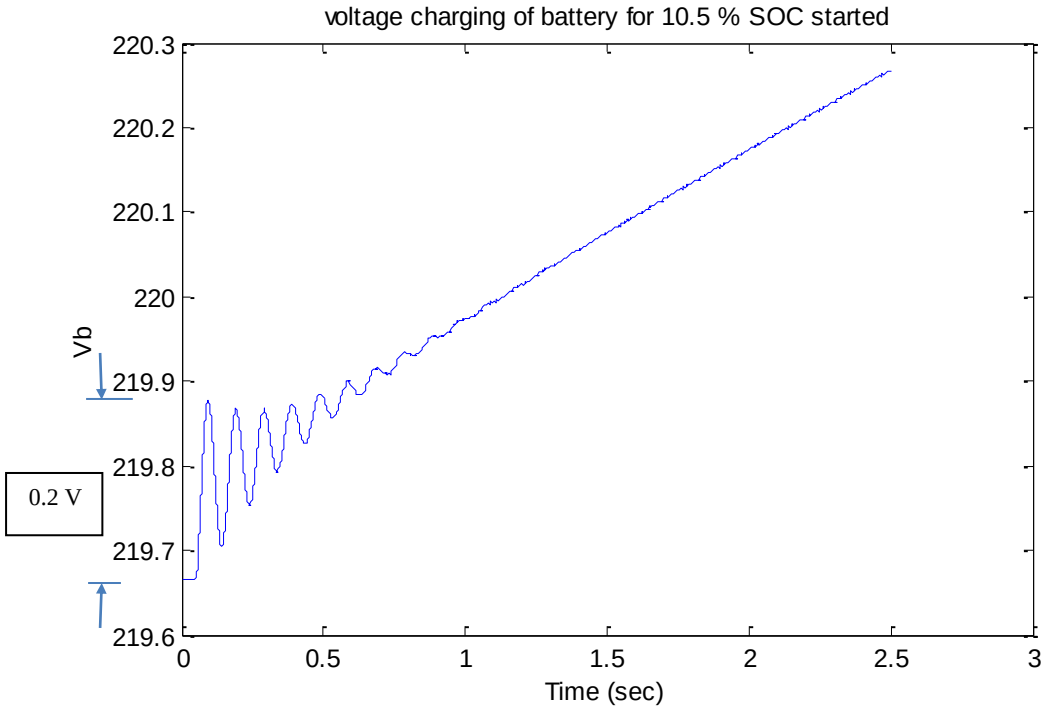

Figure 4.18: For short time voltage of the battery for fuzzy logic control during the charging process for the case of 10.5% initial battery SOC to show overvoltage (voltage in Volt and time in sec).

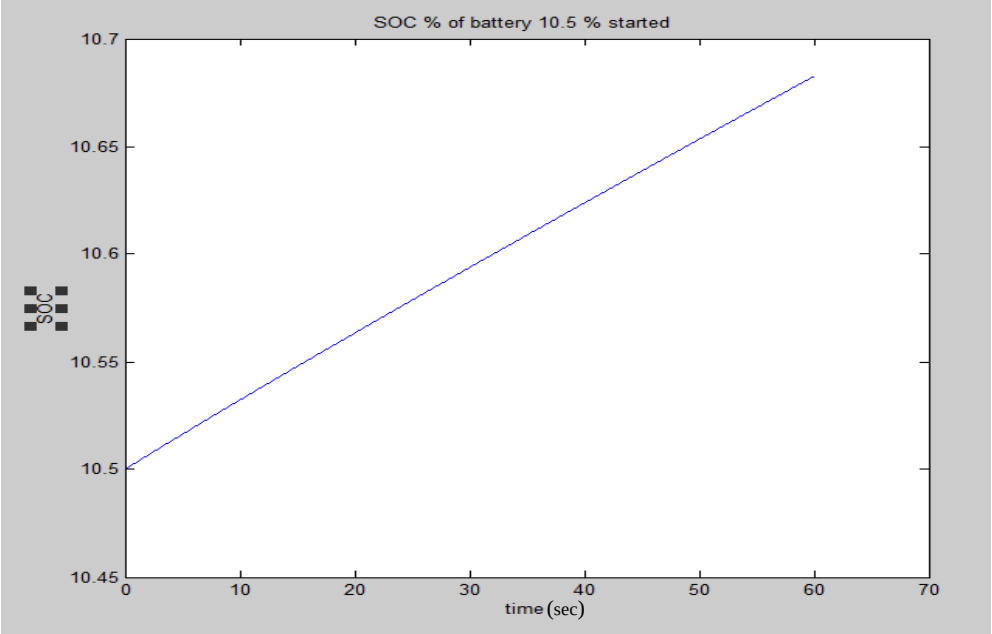

Figure 4.19: SOC of battery during the charging process for the case of 10.5% initial battery SOC.

The simulation was repeated with the initial battery SOC increased to 12.5%. In PI controller observed from Figure 4.20 below that showed below the current performance has over current reach to 59A meaning 3.2 times from steady state charging current that drawing 18A constant current, this charging current has 2.5 ripple current (13.8% charging current). Conversely, at fuzzy logic controller the over current (showed in Figure 4.21 below) reach to 32A meaning 1.7 times from steady state charging current that drawing 18A constant current. This charging current has 1.5 ripple current (8.3% from charging current) similar to the case of 10.5% initial battery SOC.

The battery voltage was observed to increase from the starting value of 261.25V (show in Figure 4.22 below) until reach to 267.8V in case PI controller, but in fuzzy logic controller the voltage charge until 267.9V as observed from Figure 4.23 below, and consequently the battery SOC was observed to increase from 12.5% during the simulation, as shown in Figures 4.24 below.

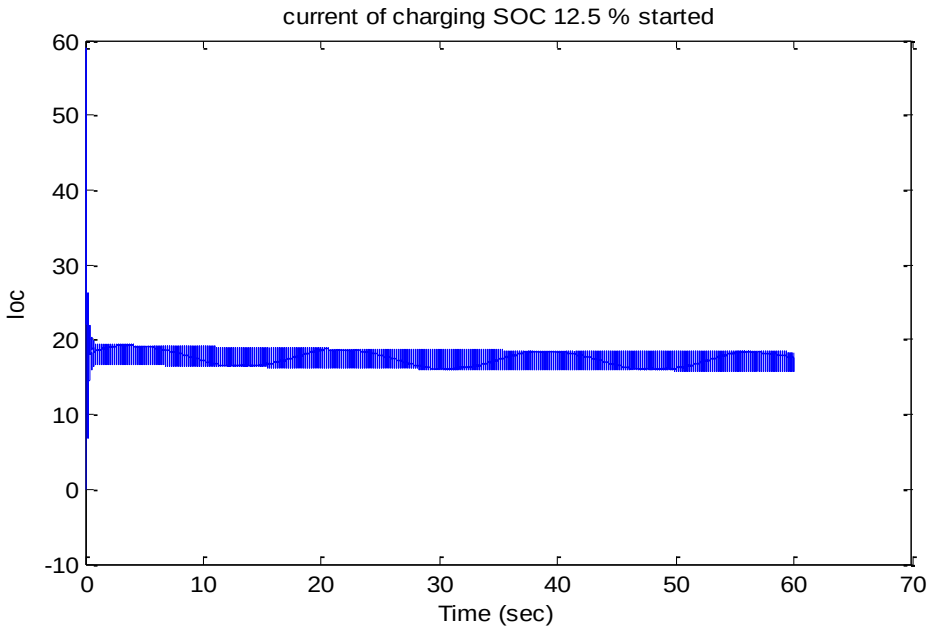

Figure 4.20: Charging current obtained for PI control from the simulation for the case of 12.5% initial battery SOC (current in ampere and time in sec)

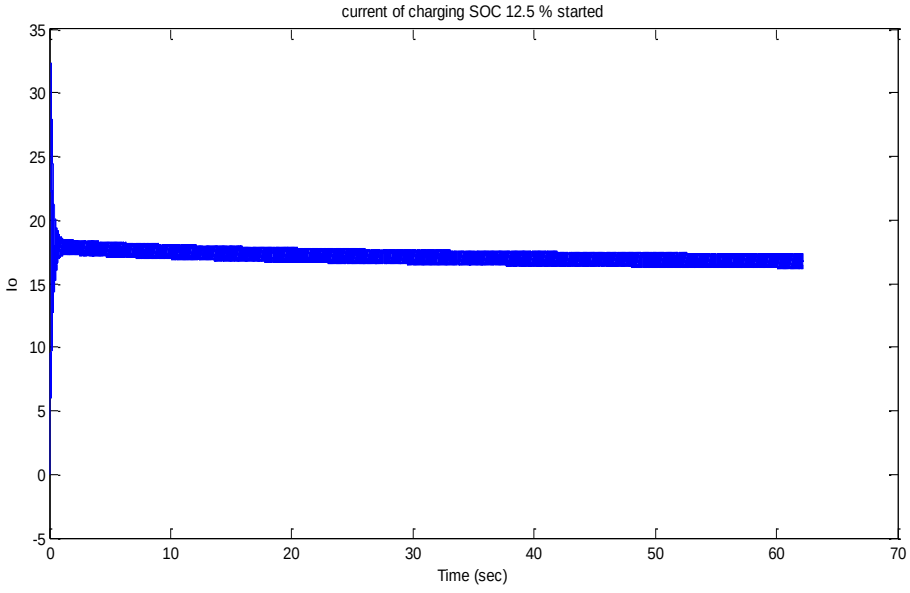

Figure 4.21: Charging current obtained for fuzzy logic control from the simulation for the case of 12.5 % initial battery SOC (current in ampere and time in sec)

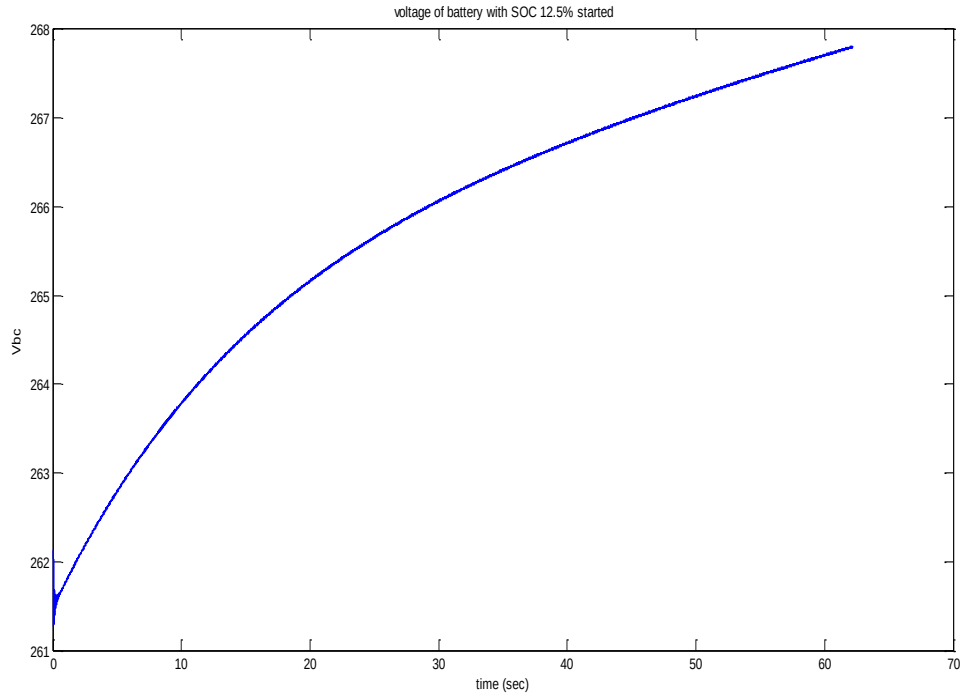

Figure 4.22: Voltage of the battery for PI control during the charging process for the case of 12.5% initial battery SOC(voltage in Volt and time in sec)

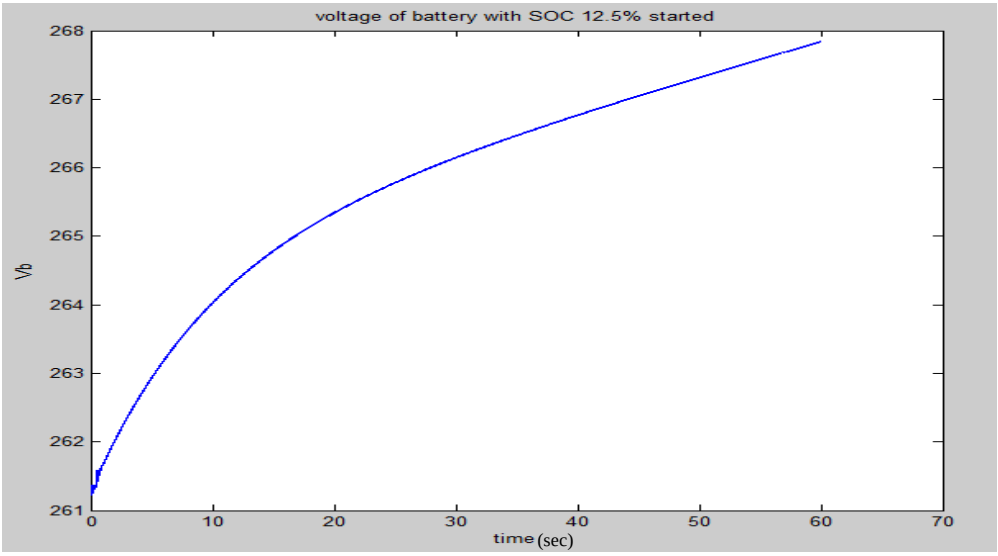

Figure 4.23: Voltage of the battery for fuzzy logic control during the charging process for the case of 12.5% initial battery SOC (voltage in Volt and time in sec)

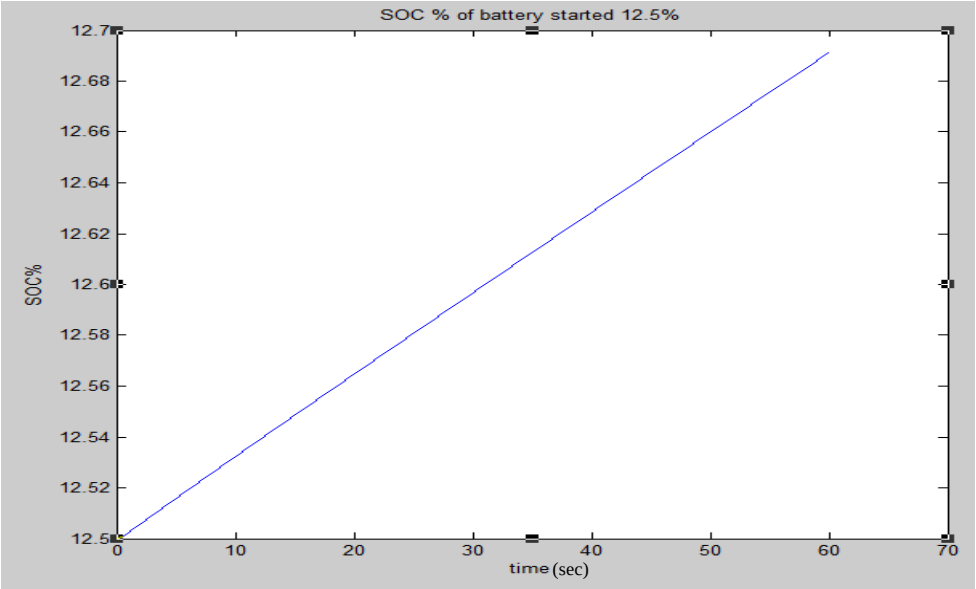

Figure 4.24: SOC of battery during the charging process for the case of 12.5% initial battery SOC.

In case initial SOC is 17%, the over current charging reach to 90A showed below in Figure 4.25 (at PI controller) that represent 5 times from steady state of charging current that maintain on 18A, this charging current has 2.2 ripple current (12.2 % from charging current. In the other hand at fuzzy logic test, the over current is 27A (represent 1.5 times from steady state of charging current), charging current stabilize on 18A that shows in Figure 4.26.

In PI test, the initial battery voltage 319V charges until 324V (shown in Figure 4.27). But in fuzzy logic test, the battery voltage charges from 319V until reach to 324.8V observed within 60 sec that show in Figure 4.28.

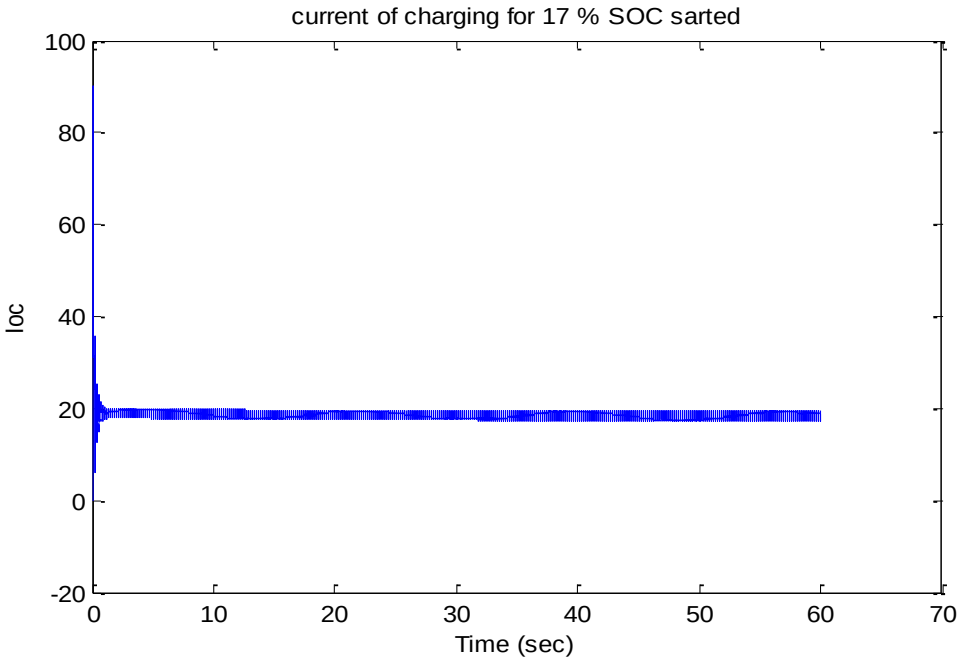

Figure 4.25: Charging current obtained for PI control from the simulation for the case of 17% initial battery SOC.

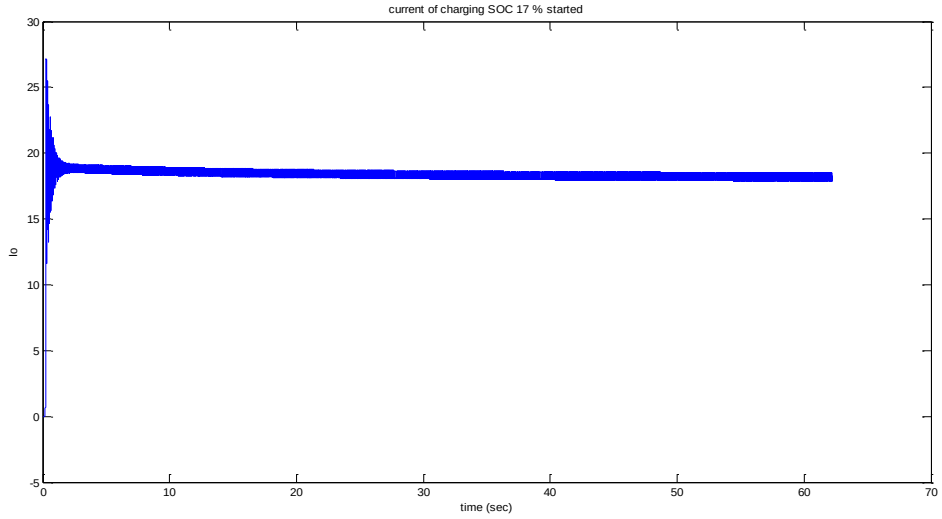

Figure 4.26: Charging current obtained for fuzzy logic control from the simulation for the case of 17% initial battery SOC.

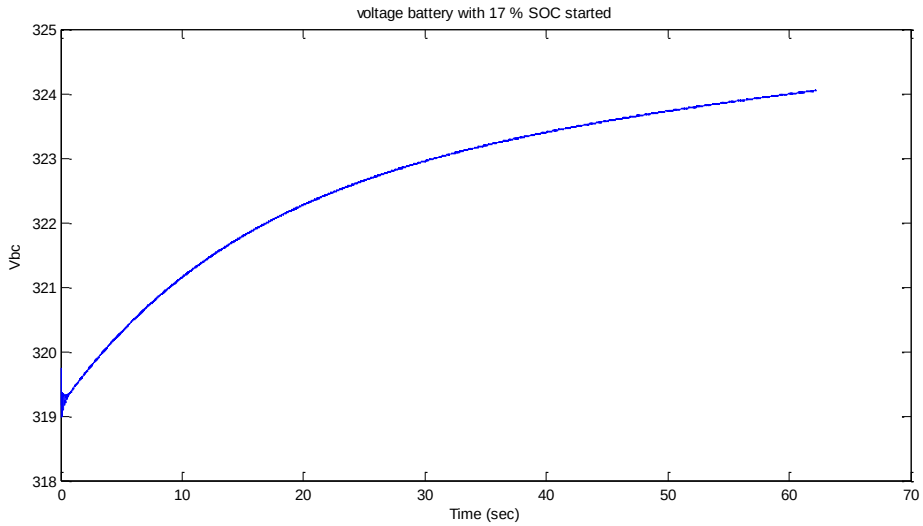

Figure 4.27: Voltage of the battery for PI control during the charging process for the case of 17% initial battery SOC.

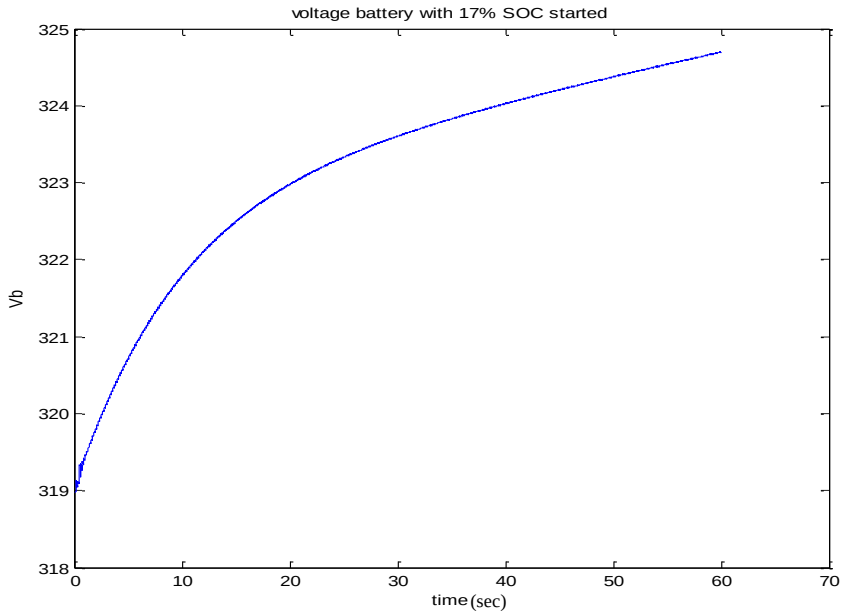

Figure 4.28: Voltage of the battery for fuzzy logic control during the charging process for the case of 17% initial battery SOC.

In case SOC initial from 33%, the charging current steady state decrease to 9.5A with over current 17.9A in PI test (represent 1.88 times constant charging current) that shows in Figure 4.29, the ripple current of charging current decrease to 1.3 (13.6% from charging current). In contrast at fuzzy logic test, the charging current also decrease to 9.5A with over current 17.8A, the ripple current of charging current decrease to 0.75 (meaning 4.1 % from charging current) shows in Figure 4.30.

Then the voltage charge from 396.5V until reach to 399.1V that observed from Figure 4.31 below in PI test. But the voltage charge from 396.5V until reach to 399.25V that observed from Figure 4.32 below in fuzzy logic test.

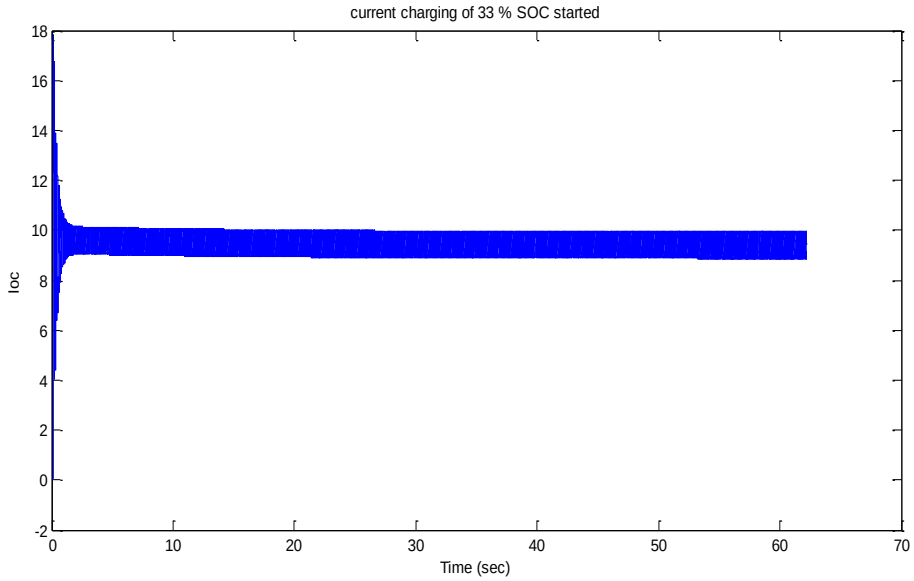

Figure 4.29: Charging current obtained in PI control from the simulation for the case of 33% initial battery SOC.

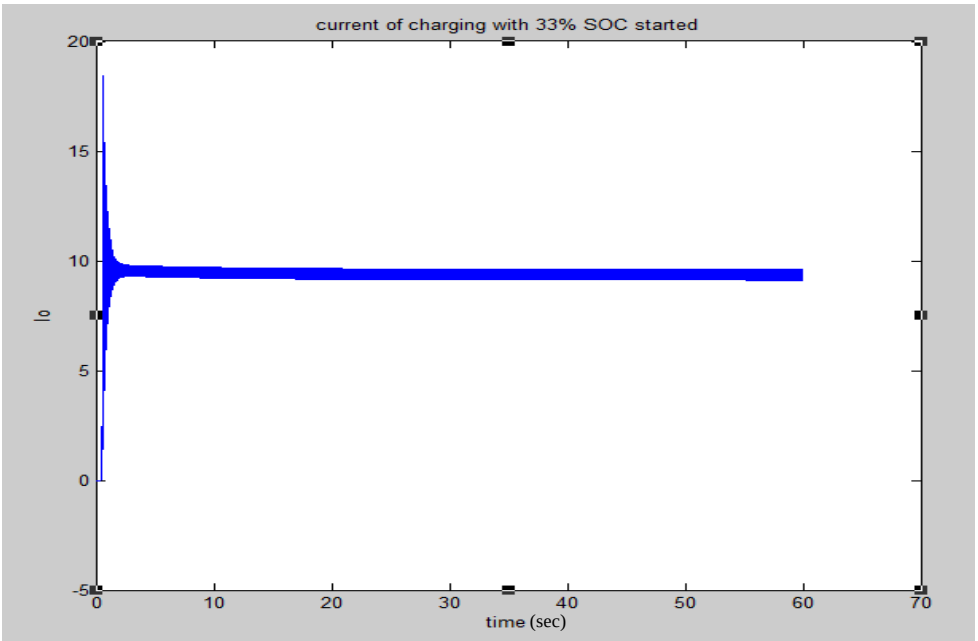

Figure 4.30: Charging current obtained fuzzy logic control from the simulation for the case of 33% initial battery SOC.

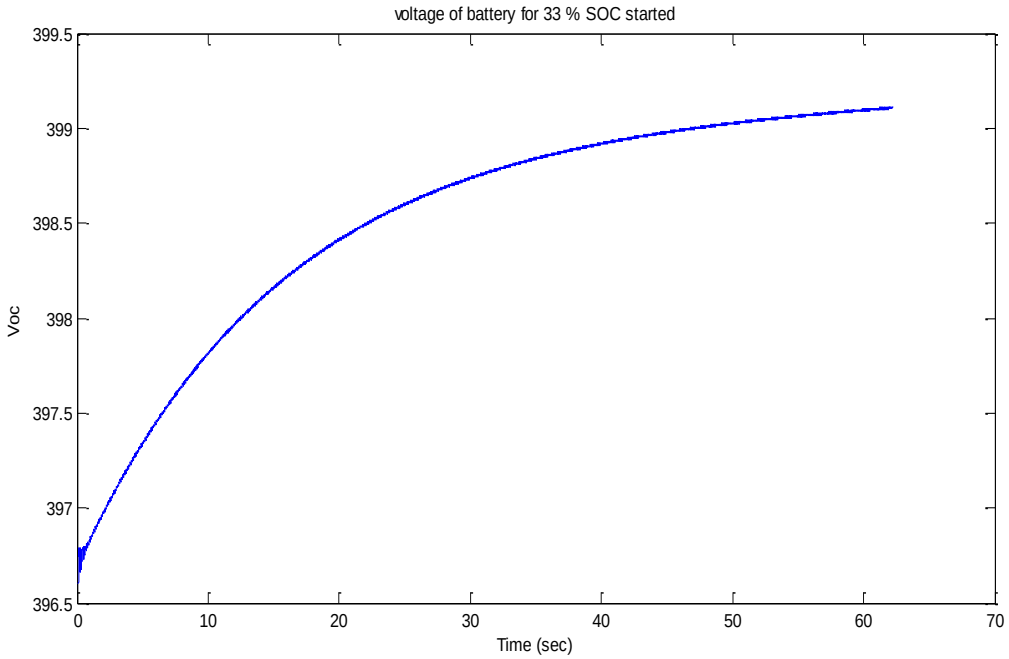

Figure 4.31: Voltage of the battery for PI control during the charging process for the case of 33% initial battery SOC.

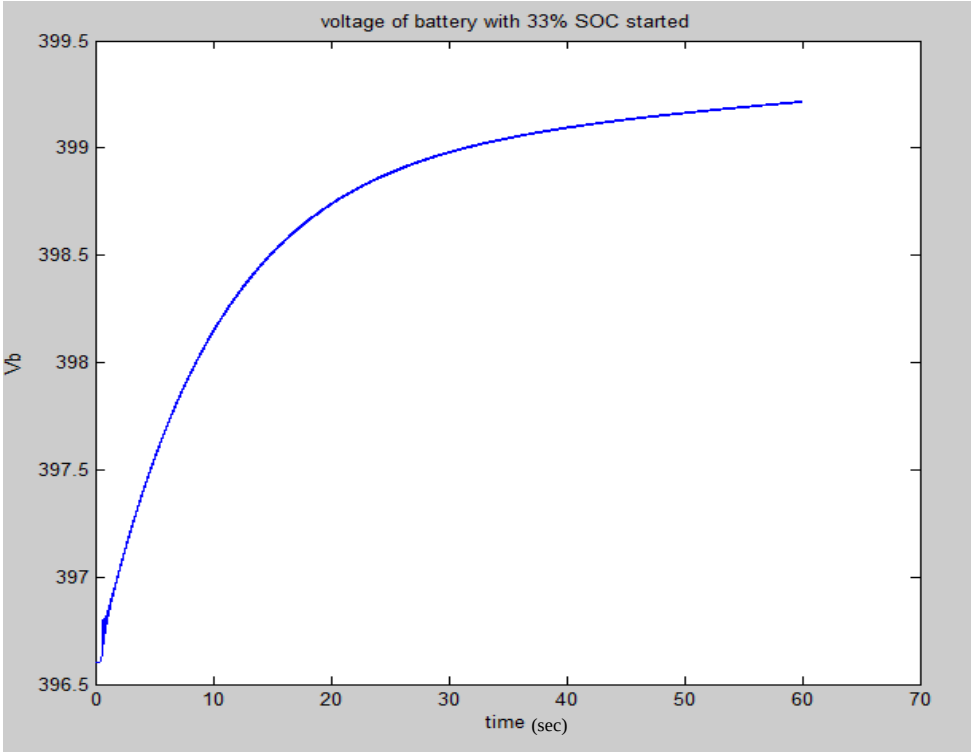

Figure 4.32: Voltage of the battery for fuzzy logic control during the charging process for the case of 33% initial battery SOC.

In The fuzzy-logic controller was designed such that when the voltage of the battery reaches 395V during the charging process, the current will decrease until it reaches zero at which the battery voltage should reach 422V which is the maximum value of the battery voltage, corresponding to 95% of battery SOC. This is the second stage of the charging process in which the charging system transfers to the constant voltage charging strategy. This process is achieved by controlling the duty cycle of the boost converter depending on the battery voltage and SOC based on the fuzzy rules explained in Section 3.6 to ensure safe charging of the battery.

In case SOC initial 39.5% the over current reduce (at PI test) to 16.1A (represent 1.9 times from charging current steady state), this charging current reduce to 8.5A due to The charging current is decrease when the battery voltage is above 395V shown in Figure 4.33, this charging current has 1.1 ripple current (represent 12.9% from charging current value). In fuzzy logic test the over current is 15.9A (represent 1.87 times charging current), this charging current also 8.5A, this current has 0.5 ripple current (5.8% from charging current) shown in Figure 4.34.

And observed from battery voltage performance in Figure 4.35 and Figure 4.36 (in PI test and fuzzy logic test respectively) the voltage increase very slowly seems constant for same time 60 sec in all cases. The voltage charge from 410.1V until 412.3V for IP test and the voltage charge from 410.1V until 412.45V (shown in Figure 4.35 and Figure 4.36 respectively). This increasing in voltage will continues with increase of SOC until the voltage of battery reach to 422V and stop simulation.

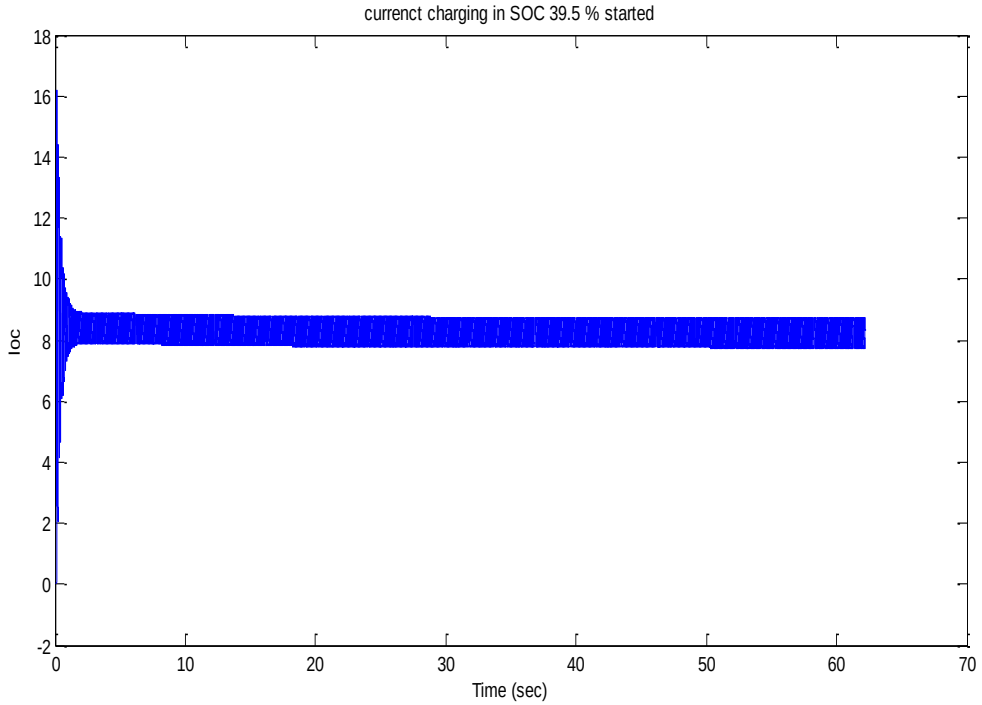

Figure 4.33: Charging current obtained for PI control from the simulation for the case of 39.5% initial battery SOC.

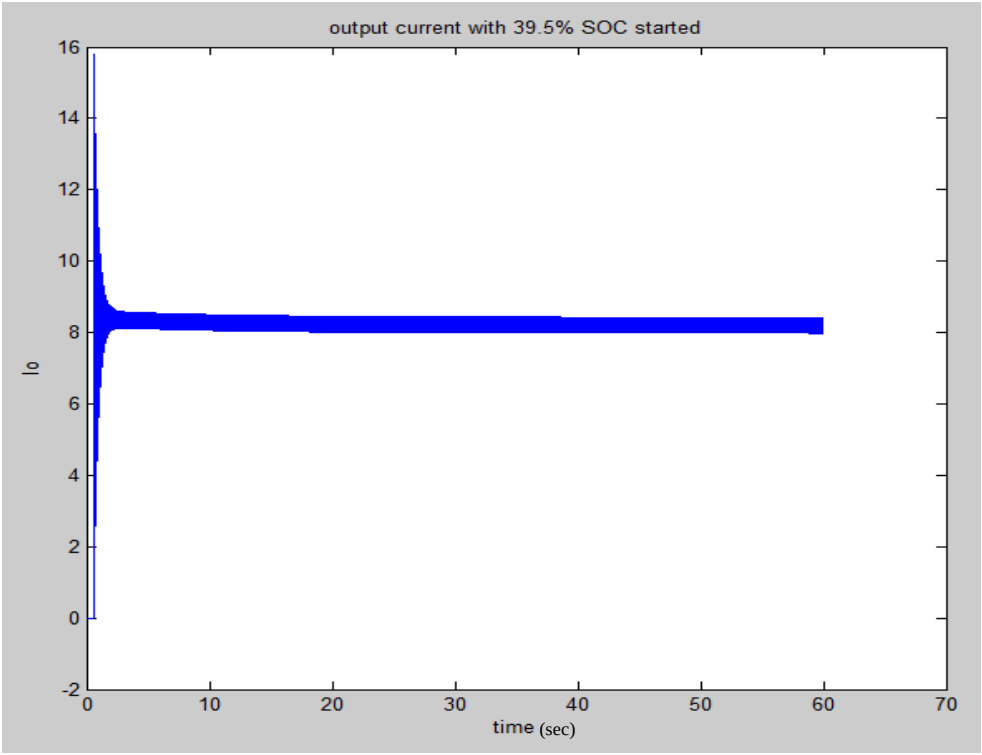

Figure 4.34: Charging current obtained for fuzzy logic control from the simulation for the case of 39.5% initial battery SOC.

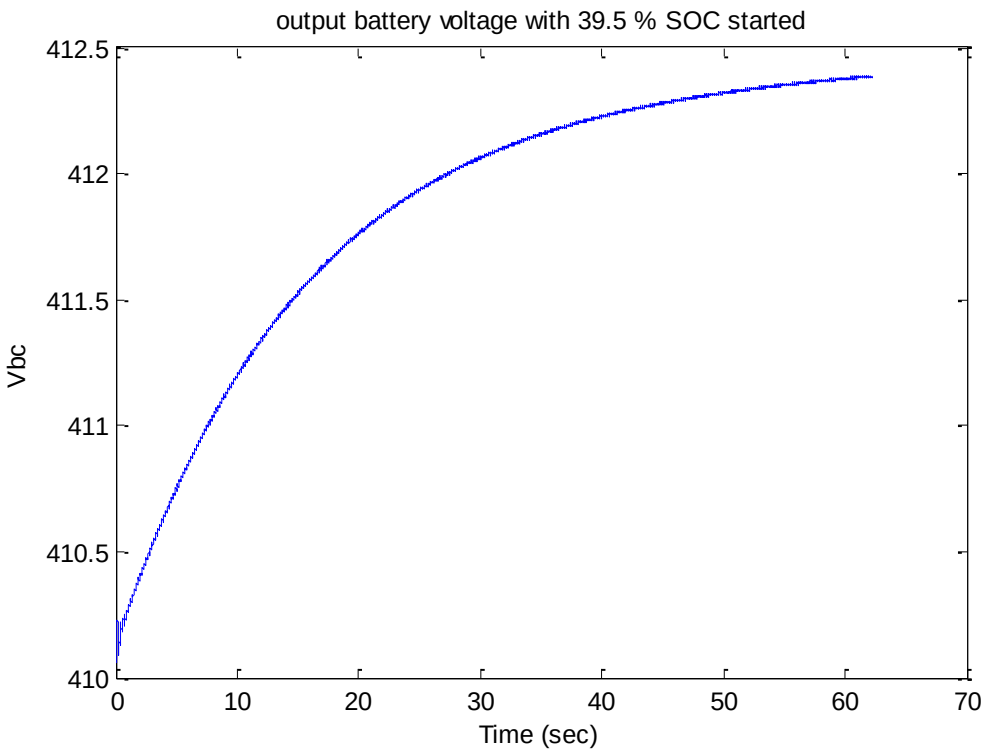

Figure 4.35: Voltage of the battery for PI control during the charging process for the case of 39.5% initial battery SOC.

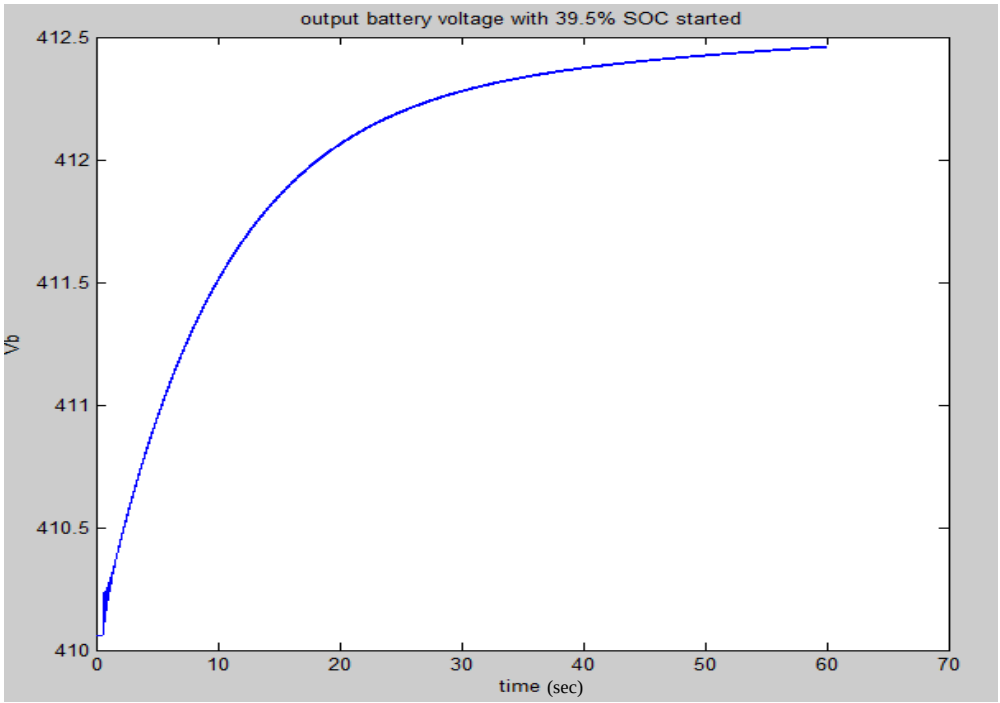

Figure 4.36: Voltage of the battery for fuzzy logic control during the charging process for the case of 39.5% initial battery SOC.

4.8 Summary

The simulation results shows Sugeno fuzzy logic has better performance with respect to PI conventional control when using to control charging phase shifted semi brigdeless converter topology, so the table 4.1 below show to comparison between them. The ripple current 1.5 (8.3%) less than standard value 1.875A (10.4%) for 125Ah that proposed in this project. Battery manufacturers have specified that more than about 1.5 A rms of ripple for every 100Ah of battery capacity will effect on battery [51].

Table 4.1 Comparing PI control with Sugeno fuzzy logic control results

No	Items	PI (conventional controller)	Sugeno fuzzy logic controller
1	Maximum ripple current	2.5 (13.8 %)	1.5 (8.3%)
2	Input over current	170A (4.25 times steady state value)	110A (2.75 times steady state value)
3	Output over current	17.9A- 90A (1.88 - 5 times steady state value)	22A – 27A (1.2 – 1.5times steady state value)
4	Output over voltage	0.4V	0.2V
5	Transit time	0.04 sec	0.02 sec
6	Extra sources	Need two extra sources	No need

CHAPTER 5

CONCLUSION AND RECOMMENDATIONS FOR FUTURE WORK

5.1 Introduction

This dissertation focused on the design of a Sugeno fuzzy logic controller to control the phase shifted semi-bridgeless boost converter that converts a single-phase AC supply from a residential power socket to DC output voltage for an active load represented by a Lithium-ion battery of an electrical vehicle. Chapter 2 was presented the advantages of the Lithium-ion battery as compared to other types of battery.The different types of converter topology employed for battery charging was also presented together with the advantages of using fuzzy logic to control the operation of the converters.Chapter 3 explained the methodology employed to design the Sugeno fuzzy logic controllers for the phase shifted semi-bridgeless boost converter. To prove the performance of the designed controllers, the boost converter system was simulated for charging a battery load for the Sugeno fuzzy-logic controller with comparing with conventional controller as presented in Chapter 4. In this chapter, the conclusions of the work are presented and recommendations for future workare also proposed.

5.2 Conclusions of the Work

In short, based on the objectives of the dessertion and the results that presented in Chapter 4, literature has shown that charging of Li-ion batteries normally employs a two-stage converter [25]. However, this project proposes controller to use of a single-stage converter for Li-ion battery charging, that is employing the phase shifted semi bridgless boost converter topology.This is because the chosen converter has fairly lower cost (due to it having only two MOSFETs). The home unit charger is very important to exploit the time at night to charge the Li-ion battery of an eletrical

vehicle especially with increased interest in the use of EV to replace conventional vehicles. Therefore, the designed converter was chosen to convert a single-phase AC supply into DC voltage for the battery charging application.

First part from results showed conventional controller to control charging prosess for phase shfited semi bridgeless boost converter to compare with fuzzy logic. Concluded the input current has over current started around 4.15 times steady state input current with starting DC charging current 1.88 to 5 times of steady state current, but transit current take short time around 0.04 sec. and output current has 12.2% ripple current.

The second part of the results were presented for the case of empolying the designed Sugeno fuzzy-logic controled phase shifted smi-bridgless boost converter to charge a Li-ion battery. Due to the increase in battery voltage during the charging process until it reaches the desired voltage, therefore the controller must increase the duty cycle from zero to 0.75. The charging strategy employed is to keep the charging current constant while increasing of the battery voltage. This process was achieved using a Sugeno fuzzy-logic controller which allowed the output of the fuzzy system to be dependent on the input of the fuzzy system, i.e. the battery SOC, through a linear function. The results presented had showed that the designed converter system was able to charge the 108-cell Li-ion battery from a starting voltage of 220V (corresponding to 2V/cell) until its fully charged voltage of 422V (corresponding to 3.9V/cell). As shown in the results the starting current is 2.75 times input current and 1.5 times output charging current that repersented low over current with respect to conventioanl current, then the fuzzy-logic controller was able to maintain the charging current to be constant at 18A (with 8.3% ripple current) during the charging process from an intial battery voltage of 220V until the battery reached a voltage of 395V. Then, the designed controller switched into the constant voltage mode in which the charging current was shown to decrease while the battery voltage increased from 395V to 422V before stopping the charging process.In the simulation results presented, the lowest initial battery voltage was set to 220V which is the same as the input AC supply RMS voltage. If the battery is required to be charged from an initial voltage of lower than the input AC supply voltage, then a buck converter must

be connected in parallel to the designed phase shifted semi-bridgeless boost converter.

5.3 Recommendations for Future Work

5.3.1 Hardware implementation of the designed system proposed

The simulation results presented has shown the efficacy of design. However, to validate the simulation results, hardware implementation of the designed fuzzy-logic controlled boost converter is recommended to extend the project. This will require selection of suitable type of MOSFETs and diodes together with the fabrication of the converter on the PCB board together with heat sinks to dissipate the heat generated from the converter. The fuzzy logic controller must be programmed on separate DSP chips based on the Mamdani and Sugeno fuzzy logic techniques.

5.3.2 Using genetic algorithm (GA) to control the converter

The development of membership functions and fuzzy rules to control the converter require extensive user understanding of the converter operation for the specific loads. The best results cannot be achieved because of the assumptions made in the fuzzy rules. Hence, a self-learning genetic algorithm (GA) technique is recommended to control the converter. It is common method to tune the fuzzy logic controller by using GA. This method provides complete design of the main components of fuzzy controllers, membership functions and the rule sets for input and output of the fuzzy logic system, leading to high performance controllers which are totally computer-designed.

LIST OF REFERENCES

[1] J. Van Mierlo, *et al.*, "Which energy source for road transport in the future? A comparison of battery, hybrid and fuel cell vehicles," *Energy Conversion and Management*, vol. 47, pp. 2748-2760, 2006.

[2] Y.-S. Lee and M.-W. Cheng, "Intelligent control battery equalization for series connected lithium-ion battery strings," *Industrial Electronics, IEEE Transactions on*, vol. 52, pp. 1297-1307, 2005.

[3] Y.-S. Lee and C.-W. Jao, "Fuzzy controlled lithium-ion battery equalization with state-of-charge estimator," in *Systems, Man and Cybernetics, 2003. IEEE International Conference on*, 2003, pp. 4431-4438.

[4] F. Musavi, *et al.*, "A phase shifted semi-bridgeless boost power factor corrected converter for plug in hybrid electric vehicle battery chargers," in *Applied Power Electronics Conference and Exposition (APEC), 2011 Twenty-Sixth Annual IEEE*, 2011, pp. 821-828.

[5] L. Petersen and M. Andersen, "Two-stage power factor corrected power supplies: The low component-stress approach," in *Applied Power Electronics Conference and Exposition, 2002. APEC 2002. Seventeenth Annual IEEE*, 2002, pp. 1195-1201.

[6] S. J. Gerssen-Gondelach and A. P. Faaij, "Performance of batteries for electric vehicles on short and longer term," *Journal of power sources*, vol. 212, pp. 111-129, 2012.

[7] OECD/ITF. (2010, 5/11/2011). *Reducing Transport Greenhouse Gas Emissions. Trends and Data*. Available: http:// www.internationaltransportforum.org/Pub/pdf/10GHGTrends.pdf. [Accessed 25 April 2013]

[8] M. Yilmaz and P. Krein, "Review of battery charger topologies, charging power levels and infrastructure for plug-in electric and hybrid vehicles," *on power electronics, vol.28, no 5May* 2013.

[9] J. P. M. Figueiredo, *et al.*, "A review of single-phase PFC topologies based on the boost converter," in *Industry Applications (INDUSCON), 2010 9th IEEE/IAS International Conference on*, 2010, pp. 1-6.

[10] P. T. K. Murat Yilma, "Review of Integrated Charging Methods for Plug-In Electric and Hybrid Vehicles," presented at the International Conference on Vehicular Electronics and Safety, Istanbul, Turkey, 2012.

[11] K. Chau and Y. Wong, "Overview of power management in hybrid electric vehicles," *Energy Conversion and Management*, vol. 43, pp. 1953-1968, 2002.

[12] A. Fuhs, *Hybrid Vehicles: and the Future of Personal Transportation*: CRC Press, 2008.

[13] B. G. Pollet, *et al.*, "Current status of hybrid, battery and fuel cell electric vehicles: From electrochemistry to market prospects," *Electrochimica Acta*, vol. 84, pp. 235-249, 2012.

[14] M. R. Palacin, "Recent advances in rechargeable battery materials: a chemist's perspective," *Chemical Society Reviews*, vol. 38, pp. 2565-2575, 2009.

[15] S. F. Tie and C. W. Tan, "A review of energy sources and energy management system in electric vehicles," *Renewable and Sustainable Energy Reviews*, vol. 20, pp. 82-102, 2013.

[16] J. J. Kopera, "Inside the nickel metal Hydride battery," *Cobasys, MI*, 2004.

[17] C.-H. Dustmann, "Advances in ZEBRA batteries," *Journal of power sources*, vol. 127, pp. 85-92, 2004.

[18] J. Sudworth, "The sodium/nickel chloride (ZEBRA) battery," *Journal of power sources*, vol. 100, pp. 149-163, 2001.

[19] C. Kallfab, *et al.*, "Short-circuit and overcharge behaviour of some lithium ion batteries," in *Systems, Signals and Devices (SSD), 2012 9th International Multi-Conference on*, 2012, pp. 1-5.

[20] F. Tredeau and Z. Salameh, "Evaluation of Lithium iron phosphate batteries for electric vehicles application," in *Vehicle Power and Propulsion Conference, 2009. VPPC'09. IEEE*, 2009, pp. 1266-1270.

[21] J.-S. Moon, *et al.*, "An efficient battery charging algorithm based on state-of-charge estimation for electric vehicle," in *Electrical Machines and Systems (ICEMS), 2011 International Conference on*, 2011, pp. 1-6.

[22] N. H. Kutkut, "A modular nondissipative current diverter for EV battery charge equalization," in *Applied Power Electronics Conference and*

Exposition, 1998. APEC'98. Conference Proceedings 1998., Thirteenth Annual, 1998, pp. 686-690.

[23] A. Manenti, *et al.*, "A new BMS architecture based on cell redundancy," *Industrial Electronics, IEEE Transactions on*, vol. 58, pp. 4314-4322, 2011.

[24] W.-S. Jwo and W.-L. Chien, "Design and implementation of a charge equalization using positive/negative pulse charger," in *Industry Applications Conference, 2007. 42nd IAS Annual Meeting. Conference Record of the 2007 IEEE*, 2007, pp. 1076-1081.

[25] M. Brandl, *et al.*, "Batteries and battery management systems for electric vehicles," in *Proceedings of the Conference on Design, Automation and Test in Europe*, 2012, pp. 971-976.

[26] F. Musavi, *et al.*, "Efficiency evaluation of single-phase solutions for AC-DC PFC boost converters for plug-in-Hybrid electric vehicle battery chargers," in *Vehicle Power and Propulsion Conference (VPPC), 2010 IEEE*, 2010, pp. 1-6.

[27] F. Musavi, *et al.*, "Energy efficiency in plug-in hybrid electric vehicle chargers: evaluation and comparison of front end ac-dc topologies," in *Energy Conversion Congress and Exposition (ECCE), 2011 IEEE*, 2011, pp. 273-280.

[28] N. Mi, *et al.*, "A novel economical single stage battery charger with power factor correction," in *Applied Power Electronics Conference and Exposition, 2003. APEC'03. Eighteenth Annual IEEE*, 2003, pp. 760-763.

[29] F. Musavi, *et al.*, "A high-performance single-phase AC-DC power factor corrected boost converter for plug in hybrid electric vehicle battery chargers," in *Energy Conversion Congress and Exposition (ECCE), 2010 IEEE*, 2010, pp. 3588-3595.

[30] G. Schauer and R. Garcia-Valle, "Electrical Vehicles Activities Around the World," in *Electric Vehicle Integration into Modern Power Networks*, ed: Springer, 2013, pp. 273-319.

[31] M. Milanovic, *et al.*, "Battery charger based on double-buck and boost converter," in *Industrial Electronics, 1999. ISIE'99. Proceedings of the IEEE International Symposium on*, 1999, pp. 747-752.

[32] M. Pahlevaninezhad, *et al.*, "A load adaptive control approach for a zero-voltage-switching DC/DC converter used for electric vehicles," *Industrial Electronics, IEEE Transactions on*, vol. 59, pp. 920-933, 2012.

[33] S. Li and K. Nam, "Design and analysis of a DC-DC converter for EVs battery charger," in *Power Electronics and Motion Control Conference (IPEMC), 2012 7th International*, 2012, pp. 2981-2986.

[34] R. Wai and K. Jheng, "High-Efficiency Single-Input Multiple-Output DC-DC Converter," *power Electronics, IEEE Transactions on*, vol. 28, pp. 886-898, 2013.

[35] V. Chandrasekar, *et al.*, "Design and implementation of a digital automatic high frequency battery charger for HEV application," in *Electric Vehicle Conference (IEVC), 2012 IEEE International*, 2012, pp. 1-6.

[36] M.-S. Huang, *et al.*, "An Electrolytic capacitor-less and single-stage controlled three-phase isolated battery charger with wide-range output voltage for EV applications," in *Energy Conversion Congress and Exposition (ECCE), 2012 IEEE*, 2012, pp. 4217-4222.

[37] H. Makkonen, *et al.*, "Concept of battery charging and discharging in automotive applications," in *Power Electronics Electrical Drives Automation and Motion (SPEEDAM), 2010 International Symposium on*, 2010, pp. 1664-1669.

[38] L. Ma, *et al.*, "An integrated multifunction DC/DC converter for PV generation systems," in *Industrial Electronics (ISIE), 2010 IEEE International Symposium on*, 2010, pp. 2205-2210.

[39] F. Musavi, *et al.*, "A cost effective high-performance smart battery charger for Off-road and neighborhood EVs," in *Transportation Electrification Conference and Expo (ITEC), 2012 IEEE*, 2012, pp. 1-6.

[40] M. Elias, *et al.*, "Design of smart charger for series Lithium-Ion batteries," in *Power Electronics and Drives Systems, 2005. PEDS 2005. International Conference on*, 2005, pp. 1485-1490.

[41] P. Ionescu, *et al.*, "Intelligent charger with fuzzy logic," in *Signals, Circuits and Systems, 2003. SCS 2003. International Symposium on*, 2003, pp. 101-104.

[42] C. E. Lyn, *et al.*, "DSP-based fuzzy logic controller for a battery charger," in *TENCON'02. Proceedings. 2002 IEEE Region 10 Conference on Computers, Communications, Control and Power Engineering*, 2002, pp. 1512-1515.

[43] M.-W. Cheng, *et al.*, "Fuzzy controlled fast charging system for lithium-ion batteries," in *Power Electronics and Drive Systems, 2009. PEDS 2009. International Conference on*, 2009, pp. 1498-1503.

[44] G.-C. Hsieh, *et al.*, "Fuzzy-controlled Li-ion battery charge system with active state-of-charge controller," *Industrial Electronics, IEEE Transactions on*, vol. 48, pp. 585-593, 2001.

[45] F.-J. Lin, *et al.*, "DSP-based probabilistic fuzzy neural network control for Li-ion battery charger," *Power Electronics, IEEE Transactions on*, vol. 27, pp. 3782-3794, 2012.

[46] A. R. P. Robat and F. R. Salmasi, "State of charge estimation for batteries in HEV using locally linear model tree (LOLIMOT)," in *Electrical Machines and Systems, 2007. ICEMS. International Conference on*, 2007, pp. 2041-2045.

[47] Y.-H. Liu, *et al.*, "An FPGA-based lithium-ion battery charger system," in *TENCON 2004. 2004 IEEE Region 10 Conference*, 2004, pp. 435-438.

[48] I. Pazdera, *et al.*, "Battery System of Electric Airplane VUT 051 RAY," *ECS Transactions*, vol. 40, pp. 267-273, 2012.

[49] p. batteries. (2013, 10/2/2013). *NCR18650A 3.1Ah LITHIUM ION*. Available: http://www.panasonic.com/industrial/batteries-oem/[Accessed 17 April 2013]

[50] K. S. Ng, *et al.*, "Enhanced coulomb counting method for estimating state-of-charge and state-of-health of lithium-ion batteries," *Applied energy*, vol. 86, pp. 1506-1511, 2009.

[51] J. McDowall, et al., "Maintaining the health of stationary battery systems," in Power Engineering Society Summer Meeting, 2001, 2001, pp. 1817-1819.

APPENDICES

Appendix A

- **Rules of Sugeno fuzzy logic control**

- 1. If (Vb is charge) and (SOC is 1) then (output1 is 1) (1)
- 2. If (Vb is charge) and (SOC is 2) then (output1 is 2) (1)
- 3. If (Vb is charge) and (SOC is 3) then (output1 is 3) (1)
- 4. If (Vb is charge) and (SOC is 4) then (output1 is 4) (1)
- 5. If (Vb is charge) and (SOC is 6) then (output1 is 5) (1)
- 6. If (Vb is charge) and (SOC is 7) then (output1 is 6) (1)
- 7. If (Vb is charge) and (SOC is 8) then (output1 is 5) (1)
- 8. If (Vb is charge) and (SOC is 9) then (output1 is 7) (1)
- 9. If (Vb is charge) and (SOC is 10) then (output1 is 8) (1)
- 10. If (Vb is charge) and (SOC is 11) then (output1 is 9) (1)
- 11. If (Vb is charge) and (SOC is 12) then (output1 is 10) (1)
- 12. If (Vb is charge) and (SOC is 13) then (output1 is 11) (1)
- 13. If (Vb is charge) and (SOC is 14) then (output1 is 12) (1)
- 14. If (Vb is charge) and (SOC is 15) then (output1 is 10) (1)
- 15. If (Vb is charge) and (SOC is 16) then (output1 is 11) (1)
- 16. If (Vb is charge) and (SOC is 17) then (output1 is 10) (1)
- 17. If (Vb is charge) and (SOC is 18) then (output1 is 9) (1)
- 18. If (Vb is charge) and (SOC is 19) then (output1 is 13) (1)
- 19. If (Vb is charge) and (SOC is 5) then (output1 is 14) (1)
- 20. If (Vb is charge) and (SOC is 20) then (output1 is 15) (1)
- 21. If (Vb is full) and (SOC is 20) then (output1 is 15) (1)
- 22. If (Vb is full) and (SOC is 19) then (output1 is 14) (1)
- 23. If (Vb is full) and (SOC is 18) then (output1 is 13) (1)
- 24. If (Vb is full) and (SOC is 17) then (output1 is 12) (1)
- 25. If (Vb is full) and (SOC is 16) then (output1 is 11) (1)
- 26. If (Vb is full) and (SOC is 15) then (output1 is 10) (1)
- 27. If (Vb is full) and (SOC is 14) then (output1 is 9) (1)
- 28. If (Vb is full) and (SOC is 13) then (output1 is 8) (1)
- 29. If (Vb is full) and (SOC is 12) then (output1 is 7) (1)
- 30. If (Vb is full) and (SOC is 11) then (output1 is 6) (1)
- 31. If (Vb is full) and (SOC is 10) then (output1 is 5) (1)
- 32. If (Vb is full) and (SOC is 9) then (output1 is 4) (1)
- 33. If (Vb is full) and (SOC is 8) then (output1 is 4) (1)
- 34. If (Vb is full) and (SOC is 7) then (output1 is 3) (1)
- 35. If (Vb is full) and (SOC is 6) then (output1 is 2) (1)
- 36. If (Vb is full) and (SOC is 5) then (output1 is 2) (1)
- 37. If (Vb is full) and (SOC is 4) then (output1 is 4) (1)

- 38. If (Vb is full) and (SOC is 3) then (output1 is 6) (1)
- 39. If (Vb is full) and (SOC is 2) then (output1 is 1) (1)
- 40. If (Vb is full) and (SOC is 1) then (output1 is 1) (1)